POLISH MARITIME RESEARCH
No 3(61)   2009   Vol 16

CONTENTS

Editorial

POLISH MARITIME RESEARCH is a scientific journal of worldwide circulation. The journal appears as a quarterly four times a year. The first issue of it was published in September 1994. Its main aim is to present original, innovative scientific ideas and Research & Development achievements in the field of :

Engineering, **Computing & Technology**, **Mechanical Engineering**,

which could find applications in the broad domain of maritime economy. Hence there are published papers which concern methods of the designing, manufacturing and operating processes of such technical objects and devices as : ships, port equipment, ocean engineering units, underwater vehicles and equipment as well as harbour facilities, with accounting for marine environment protection.
The Editors of POLISH MARITIME RESEARCH make also efforts to present problems dealing with education of engineers and scientific and teaching personnel. As a rule, the basic papers are supplemented by information on conferences , important scientific events as well as cooperation in carrying out international scientific research projects.

Scientific Board

On the modeling of car passenger ferryship design parameters with respect to selected sea-keeping qualities and additional resistance in waves

Tomasz Cepowski, Assoc. Prof.
Szczecin Maritime University

ABSTRACT

This paper presents the modeling of car passenger ferryship design parameters with respect to such design criteria as selected sea-keeping qualities and additional resistance in waves. In the first part of the investigations approximations of selected statistical parameters of design criteria of ferryship were elaborated with respect to ship design parameters. The approximation functions were obtained with the use of artificial neural networks. In the second part of the investigations design solutions were searched for by applying the single- and multi-criterial optimization methods. The multi-criterial optimization was performed by using Pareto method. Such approach made it possible to present solutions in such form as to allow decision makers (shipowner, designer) to select solutions the most favourable in each individual case.

Keywords: sea-keeping qualities; roll-on - roll-off ferryship; rolling; motion sickness index; lateral accelerations, additional resistance in waves; ship design parameters; modeling; artificial neural networks; optimization; Pareto method

INTRODUCTION

In ship design process design solutions which fulfil both economic criteria and technical limitations are searched for. Economic criteria are consisted of a set of requirements imposed by shipowner, among which a suitable internal capacity and service speed of the ship can be numbered, that significantly influences operational profitability of the ship sailing on a given shipping line. Obtaining the assumed service speed by the ship depends a.o. on parameters and operational conditions of propulsion system as well as value of total hull resistance to motion. Since total resistance of ship hull consists of a.o. additional resistance in waves associated with ship sailing in heavy weather conditions, the additional resistance can be used as a design criterion for certain types of ships.

And, technical limitations are consisted of a.o. appropriate stability, unsinkability or hull structural strength. For certain types of ships insensibility to weather conditions, i.e. the so-called good sea-keeping qualities are more and more often used as a design criterion. In such case among sea-keeping qualities wave effects can be numbered in the form of rolling and secondary wave effects (resulting from waving and rolling) to which a.o. accelerations, slamming, shipping of water on the deck and sickness motion index, belong.

The presented investigations were aimed at determination of optimum values of ship design parameters with respect to assumed economic criteria and technical limitations. The investigations were performed on the example of

preliminary design of a car passenger ferry ship. The type of ship is characteristic of specific operational and design problems such as internal capacity, stability (unsinkability), speed or insensibility to weather conditions. Therefore for the ship in question selected sea-keeping qualities and additional resistance in waves at a given ship capacity were assumed to be design criteria. In the first phase of the investigations approximation functions of the above mentioned criteria were determined on the basis of main geometrical parameters of ship hull. In the second phase values of the design parameters were determined for which the assumed design task were characterized by the best merits as regards the assumed criteria.

METHOD

The following design task was formulated in the investigations: to find the vector of independent variables, $X = X(X_1, X_2, \ldots X_n)$, which minimizes or maximizes functions of partial targets under limitations given for car passenger ferry ship sailing in heavy weather conditions.

The following data were assumed:
- independent variables: L/B, B/d, CB, CWL, where: L, B, d - ship length, breadth and draught, CB - block coefficient of hull underwater part, CWL - waterplane coefficient;
- limitations:
  - theoretical volumetric displacement V = 17500 m^3
  - L/B ratio within the range of 5.17 ÷ 7.64
  - B/d ratio within the range of 3.22 ÷ 4.46

- CB within the range of 0.6 ÷ 0.64
- CWL within the range of 0.8 ÷ 0.85
- initial lateral metacentric height GM = 1 m
- ship speed v = 5 kn;
- design criteria:
  - the motion sickness index MSI (acc. ISO 2631/3) [9] for the wave encounter angle β = 120° (in the reference system of: 180° – head wave, 0° – following wave)
  - the additional resistance in waves R for β = 180°
  - the roll angle φ for β = 30°
  - the lateral acceleration on the car deck, at, acc. [11] for β = 30°.

In the investigations was assumed a conventional wave spectrum consisted of wave energy spectral density functions acc. ITTC for waves of the significant heights H = 6 m and characteristic periods T in the range from 6 to 14 s, (Fig.1). This made it possible to eliminate impact of the characteristic period on ship responses and to decrease number of independent variables in the design task.
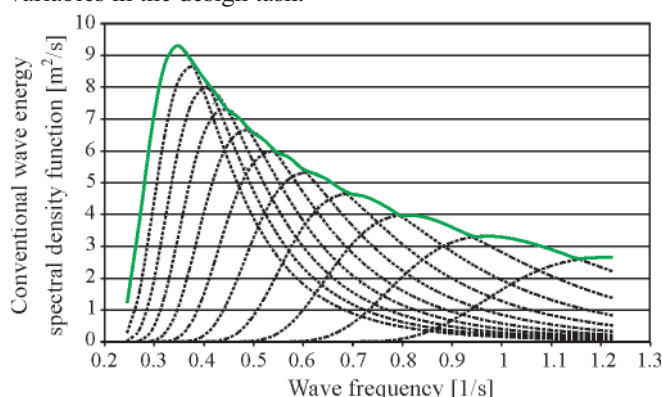
Fig. 1. *Conventional wave energy spectral density function, ITTC spectrum, H = 6 m, T = 6 ÷ 14 s*

In the first phase of the investigations functions of partial targets were determined depending on independent variables.

APPROXIMATION OF DEPENDENT VARIABLES

Functions of partial targets, which are necessary to solve the design task, are to be expressed in the form of analytical functions approximating the assumed dependent variables (i.e.: motion sickness index, additional resistance in waves, roll angles and lateral accelerations). To perform approximations the method presented in Fig. 2 was assumed.
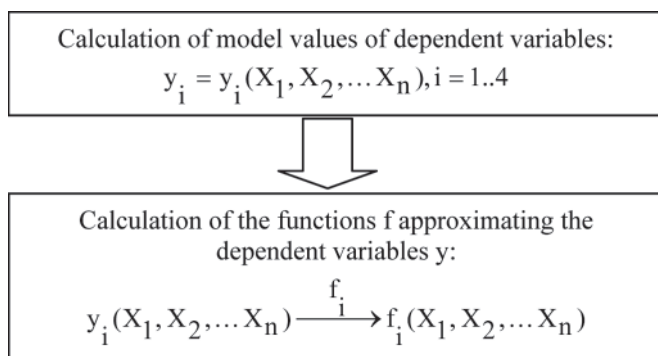
Fig. 2. *Algorithm of approximation of the dependent variables y_i, where: $X_1, X_2, ... X_n$ – independent variables (design parameters), $\hat{y}_i$ – model values of dependent variables, f_i – searched for approximating functions, i=1..4.*

To determine the functions f_i in the equation (1) it is possible to make use of statistical methods or those based on artificial neural networks. The application of artificial neural networks to approximation of unknown relations belongs to mathematical numerical methods dealing with the so-called „artificial intelligence" and finds wider and wider use in shipbuilding [1, 2, 5, 6].

To calculate model values the set of 24 design variants of car passenger ferry ship of different hull forms shown in Tab. 1, was assumed. Model values were presented in the form of irregular wave statistical values of the wave energy spectral density function shown in Fig. 1.

Tab. 1. *Model set of independent and dependent variables appearing in the above assumed parameters of ship motions and waving, where: CB – block coefficient of hull underwater part, CWL – waterplane coefficient, L – ship length, B – ship breadth, d – ship draught, MSI – motion sickness index, a_t – lateral acceleration on car deck, φ – significant amplitude of ship roll angles, R – additional resistance in waves*

Design variants	Independent variables				Dependent variables			
	CB	CWL	L/B	B/d	MSI [%]	φ [°]	a_t [m/s²]	R [kN]
1	0.599	0.809	5.68	3.22	97.20	10.82	1.71	878.50
2	0.599	0.809	6.74	3.84	88.40	9.56	1.76	1150.60
3	0.599	0.809	5.17	4.46	93.90	7.98	1.32	1164.00
4	0.644	0.828	6.17	3.58	91.50	9.61	1.67	856.60
5	0.644	0.828	6.74	3.22	92.30	11.60	1.81	796.40
6	0.644	0.828	5.17	4.46	91.40	7.50	1.31	985.90
7	0.637	0.811	5.71	3.40	88.20	9.62	1.58	712.00
8	0.637	0.811	6.74	3.84	66.80	9.57	1.60	893.00
9	0.637	0.811	5.17	4.46	81.30	6.32	1.33	933.60
10	0.616	0.828	5.17	4.46	79.50	6.27	1.30	1068.10
11	0.616	0.828	6.74	3.22	80.00	8.69	1.82	843.80
12	0.616	0.828	5.96	3.84	79.30	7.66	1.52	970.30
13	0.620	0.831	6.74	3.90	78.20	8.73	1.90	1108.90
14	0.620	0.831	5.96	3.22	92.80	10.51	1.91	852.50
15	0.620	0.831	5.17	4.46	85.80	7.54	1.45	1116.00
16	0.634	0.852	5.57	3.77	80.80	7.84	1.57	956.30
17	0.634	0.852	6.74	3.22	78.70	10.01	1.84	879.10
18	0.634	0.852	5.17	4.46	75.20	6.80	1.35	1106.20
19	0.626	0.850	5.64	3.50	87.30	7.31	1.49	878.90
20	0.626	0.850	6.74	3.22	79.60	9.07	1.69	882.10
21	0.626	0.850	5.17	4.46	79.00	6.30	1.25	1090.00
22	0.610	0.804	6.74	4.04	71.20	5.54	1.55	798.90
23	0.610	0.804	5.96	3.22	90.70	7.96	1.59	595.80
24	0.610	0.804	5.17	4.46	82.40	4.70	1.25	775.50

The values of dependent variables given in Tab. 1 were calculated by means of exact numerical methods with the use of SEAWAY software which is based on planar flow theory. Exactness tests of the software, presented in [4], indicate a high accuracy of calculations. For calculations of additional resistance in waves the Gerritsma-Beukelman method was used [3].

Approximation functions of the dependent variables: MSI, φ, R and a_t were determined by using artificial neural networks and presented analytically in the form of Eqs. (1), (2), (3) and (4):

$$MSI = \frac{\left(\dfrac{1}{1+e^{-(([CB,CWL,CB/CWL,L/B,B/d]\times S+P)\times A-B)}} \times C - \alpha_0 \right) - \alpha_1}{\alpha_2}$$

(1)

where:

MSI   – motion sickness index [%]
L   – ship length
B   – ship breadth
d   – ship draught
CB   – block coefficient of hull underwater part
CWL   – waterplane coefficient
A   – matrix of weight values:

$$\begin{bmatrix} -0.581 & 1.019 & -2.326 & -0.015 & 1.460 & -0.044 \\ 0.379 & -0.268 & -0.469 & -0.021 & 0.310 & -1.453 \\ -0.924 & 0.480 & -1.928 & -1.033 & 1.071 & 0.487 \\ -0.321 & 0.842 & 1.699 & -0.686 & -0.422 & 0.652 \\ -0.283 & -0.254 & 2.564 & 1.254 & 1.030 & 0.340 \end{bmatrix}$$

S – matrix of coefficients:

$$\begin{bmatrix} 22.22 & 0 & 0 & 0 & 0 \\ 0 & 20.83 & 0 & 0 & 0 \\ 0 & 0 & 20.41 & 0 & 0 \\ 0 & 0 & 0 & 0.64 & 0 \\ 0 & 0 & 0 & 0 & 0.81 \end{bmatrix}$$

B   – vector of threshold values: [-1.583 -0.131 -1.882 0.366 0.508 -2.022]
C   – column vector of weight values: [1.15 -0.71 -2.80 1.59 -1.88 1.75]
P   – vector of displacement values: [-13.31 -16.75 -15.02 -3.29 -2.60]
$\alpha_0, \alpha_1, \alpha_2$ – coefficients of the following values: $\alpha_0 = -1.62$, $\alpha_1 = -2.74$, $\alpha_2 = 0.04$

$$R = \frac{\left(\dfrac{1}{1+e^{-(([CWL,CB/CWL,L/B,B/d]\times S+P)\times A-B)}} \times C - \alpha_0 \right) - \alpha_1}{\alpha_2}$$

(2)

where:

R   – additional resistance in waves [kN]
A   – matrix of weight values:

$$\begin{bmatrix} 0.726 & 2.897 & -2.504 & 0.570 & 1.932 & -0.365 & -0.164 \\ 3.661 & -4.110 & 0.244 & 0.431 & 3.790 & 0.275 & -0.070 \\ -1.219 & -0.517 & 1.854 & -0.481 & 0.820 & -0.656 & -0.492 \\ -0.423 & -0.886 & 1.422 & 0.046 & -0.087 & -1.134 & -0.560 \end{bmatrix}$$

S – matrix of coefficients:

$$\begin{bmatrix} 20.83 & 0 & 0 & 0 \\ 0 & 20.41 & 0 & 0 \\ 0 & 0 & 0.64 & 0 \\ 0 & 0 & 0 & 0.81 \end{bmatrix}$$

B   – vector of threshold values: [2.220 -2.108 1.688 -0.967 -0.410 -1.842 0.633]
C   – column vector of weight values: [2.665 2.431 1.836 0.373 -2.001 -2.197 -0.728]
P   – vector of displacement values: [-16.75 -15.02 -3.29 -2.60]
$\alpha_0, \alpha_1, \alpha_2$ – coefficients of the following values: $\alpha_0 = -0.939$, $\alpha_1 = -1.575$, $\alpha_2 = 0.0022$

$$a_t = \frac{\left(\dfrac{1}{1+e^{-(([CB,CWL,CB/CWL,L/B,B/d]\times S+P)\times A-B)}} \times C - \alpha_0 \right) - \alpha_1}{\alpha_2}$$

(3)

where:

a_t – maximum lateral acceleration on the car deck [m/s^2]
A   – matrix of weight values:

$$\begin{bmatrix} -0.874 & 0.408 & 0.046 & 0.313 & 0.001 & 0.863 & -0.096 & 0.041 & 0.368 & 0.265 & 0.732 & -0.753 & -0.471 \\ 1.062 & -0.014 & -0.680 & 0.739 & 0.903 & -0.981 & -0.583 & -0.089 & -0.835 & 0.239 & 0.035 & -0.380 & -0.550 \\ 0.955 & -0.358 & -0.392 & 0.412 & -0.270 & 0.704 & -0.467 & 0.149 & -0.867 & 0.060 & 0.801 & -0.202 & 0.736 \\ -0.755 & 0.616 & -0.266 & 0.527 & 0.320 & 0.507 & -0.968 & -0.821 & 0.870 & 0.378 & 0.261 & -0.480 & -0.089 \\ 0.810 & -0.399 & -0.822 & 0.233 & 0.480 & 0.903 & -0.424 & 0.241 & -0.655 & 0.385 & 0.301 & -0.656 & 0.420 \end{bmatrix}$$

S – matrix of coefficients:

$$\begin{bmatrix} 22.22 & 0 & 0 & 0 & 0 \\ 0 & 21.47 & 0 & 0 & 0 \\ 0 & 0 & 20.41 & 0 & 0 \\ 0 & 0 & 0 & 0.64 & 0 \\ 0 & 0 & 0 & 0 & 0.81 \end{bmatrix}$$

B   – vector of threshold values:
[0.368 -0.043 -0.045 -0.231 -0.109 0.821 -0.289 0.924 0.776 0.683 1.025 -0.397 -0.121]

C   – column vector of weight values:
[-0.923 0.021 -0.562 0.617 0.171 -0.052 0.356 -0.773 0.798 0.786 0.628 1.003 -0.989]

P   – vector of displacement values: [-13.31 -17.48 -15.02 -3.29 -2.60]

α_0, α_1, α_2 – coefficients of the following values: $\alpha_0 = 0.193$, $\alpha_1 = -2.18$, $\alpha_2 = 1.67$

$$\phi = \frac{(([CB,CWL,CB/CWL,B/d] \times S + P) \times A + \mathbf{6.96}) + 1.049}{0.189} \tag{4}$$

where:

ϕ – significant amplitude of roll angles [°]

A   – column vector of weight values: [38.14 -30.37 -33.83 -0.54]

S   – matrix of coefficients:

$$\begin{bmatrix} 22.22 & 0 & 0 & 0 \\ 0 & 20.83 & 0 & 0 \\ 0 & 0 & 20.41 & 0 \\ 0 & 0 & 0 & 0.81 \end{bmatrix}$$

P – vector of displacement values: [-13.31 -16.75 -15.02 -2.60]

In Tab. 2 the above presented networks are described together with their selected statistical parameters. From the above given sheets it results that the functions (1), (2), (3) and (4) are characterized by a simple structure and relatively high accuracy.

Tab. 2. Type, structure and selected statistical parameters of the elaborated neural networks

Variable	Type of network	Structure of neural network	Correlation coefficient R	Root mean square error, RMS, of:	
				learning	testing
MSI	MLP	5x6x1	0.998	2.08	4.29
R	MLP	4x7x1	0.999	11.3	38.67
a_t	MLP	5x13x1	0.998	0.12	0.07
ϕ	linear	4x1	0.984	0.65	0.25

SELECTION OF OPTIMUM DESIGN PARAMETERS OF SHIP HULL

In this part of the experiment hull form parameters of car passenger ferry ship were searched for with respect to the assumed criteria, i.e.:

- maximum of MSI
- minimum of the additional resistance in waves, R
- minimum of the acceleration on the car deck, a_t
- minimum of the roll angle ϕ.

The functions (1), (2), (3), (4) were used to solve the problem. To find a design solution which satisfies the assumed criteria the single- and multi-criterial optimization methods were applied.

SINGLE-CRITERIAL OPTIMIZATION

In this part of the investigations minimum values of the functions (1), (2), (3) and (4) were determined. In the first phase the GRG2 (Generalized Reduced Gradient) program of linear optimization was used [7]. The results are presented in Tab. 3 and Fig. 3 and 4.

The main disadvantage of optimization methods of both kinds (single- and multi-criterial) is that they provide only information on location of an optimum point. They do not give information on shape of objective function and it is not certain whether the achieved optimum solution is global [3]. Hence in the next phase of the investigations a set of all possible design solutions was determined and the results were analyzed against the assumed criteria. To the calculations the following increments of the design parameters were assumed:

- $\Delta L/B$ = 0.01 m
- $\Delta B/d$ = 0.01 m
- ΔCB = 0.01
- ΔCWL = 0.01.

Tab. 3. Optimum design solutions with respect to the assumed criteria

Variant	CB	CWL	L/B	B/D	MSI [%]	R [kN]	φ [°]	a_t [m/s²]	Criterion
A	0.636	0.804	6.74	4.46	53.7	1141.9	4.32	1.49	min. of MSI
B	0.617	0.804	6.15	3.22	88.1	551.30	8.29	1.59	min. of R
C	0.599	0.852	6.74	4.46	97.2	1164.2	0.26	1.67	min. of φ
D	0.650	0.800	5.17	4.46	97.2	1164.2	2.11	1.19	min. of a_t
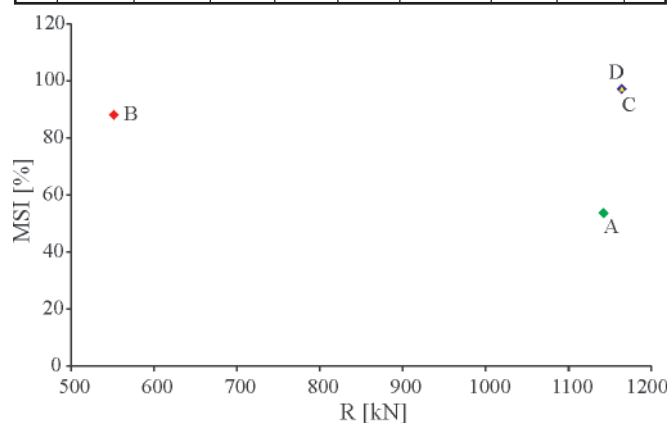
Fig. 3. Comparison of the design solutions with respect to the additional resistance in waves, R, and the motion sickness index MSI
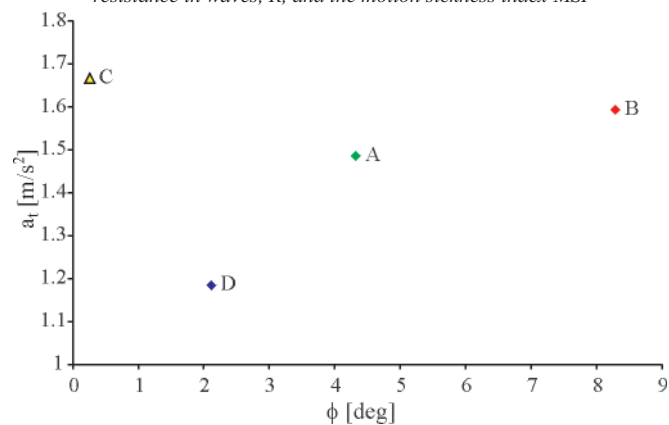
Fig. 4. Comparison of the design solutions with respect to the roll angle φ and the lateral acceleration a_t

The analysis results are illustrated in Fig. 5 through 11. In Fig. 5, 7, 9, 11 are presented the sets of minimum values of the variables (design criteria) dependent on a given criterion. From the sets merits of the design solutions result with respect to the assumed criteria. For instance from Fig. 5 it results that the design solutions characterized by small values of MSI index are also characteristic of large values of additional resistance and small values of roll angles and lateral accelerations. And, the design solutions characterized by large values of MSI index are also characteristic of a.o. small values of mean additional resistance in waves. In Fig. 6, 8, 10, 12 values of design parameters are presented depending on selected design criteria. On the basis of both groups of the diagrams the car passenger ferryship design parameters which satisfy decision maker with respect to assumed criteria, can be determined.
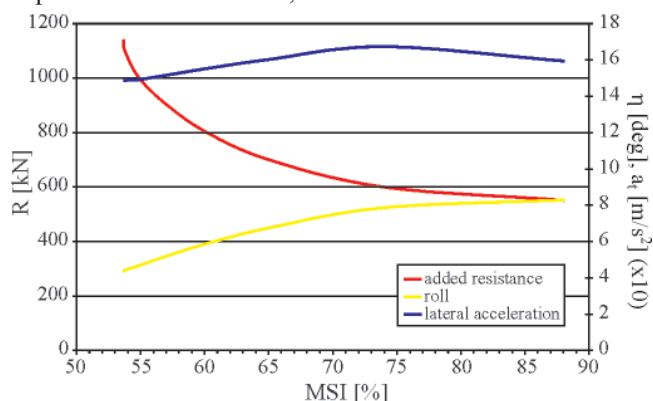
Fig. 5. Minimum values of dependent variables within the range of MSI = 53 ÷ 88 %
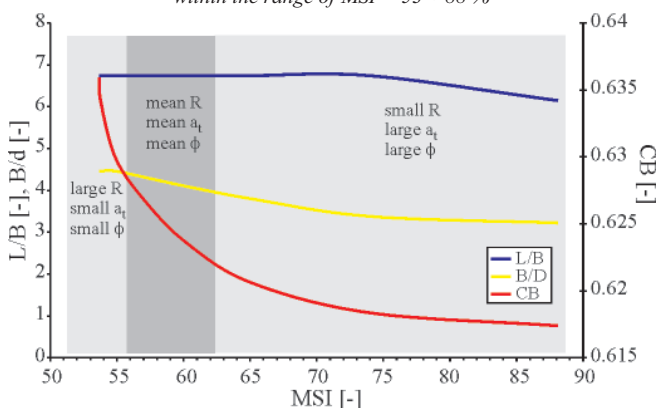
Fig. 6. Values of design prameters in function of MSI index, CWL = 0.80
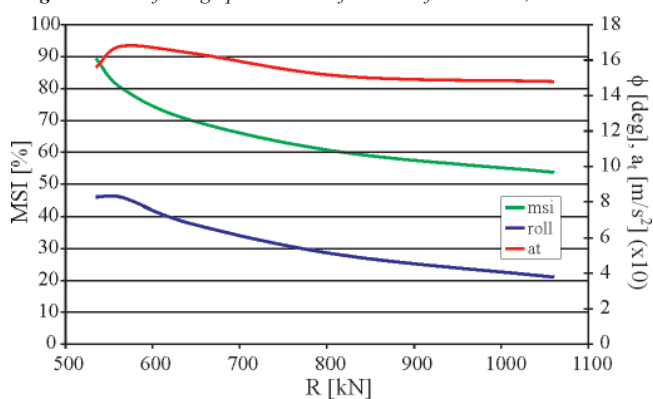
Fig. 7. Minimum values of dependent variables within the range of R = 530 ÷ 1060 kN
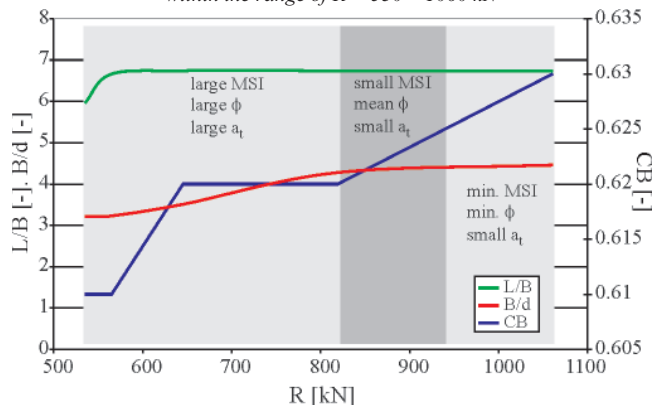
Fig. 8. Values of design parameters in function of the additional resistance in waves R, CWL = 0.80
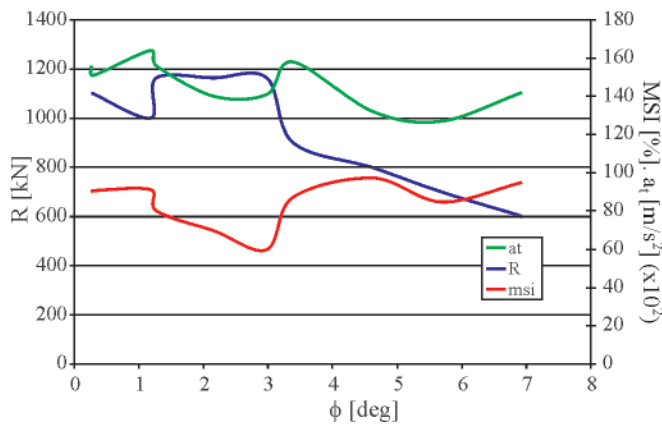
Fig. 9. *Minimum values of dependent variables within the range of φ = 0.26 ÷ 6.93°*
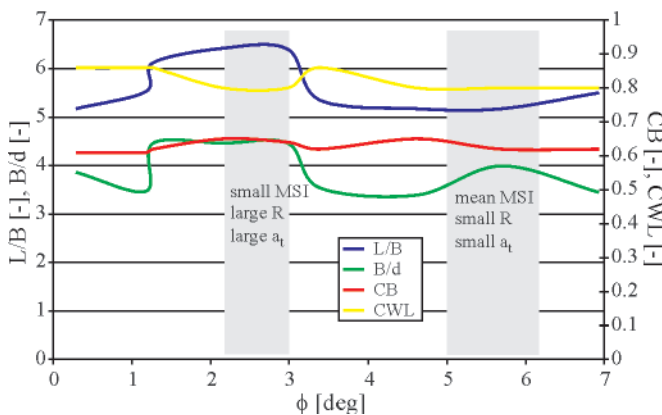
Fig. 10. *Values of design parameters in function of the roll angle φ*
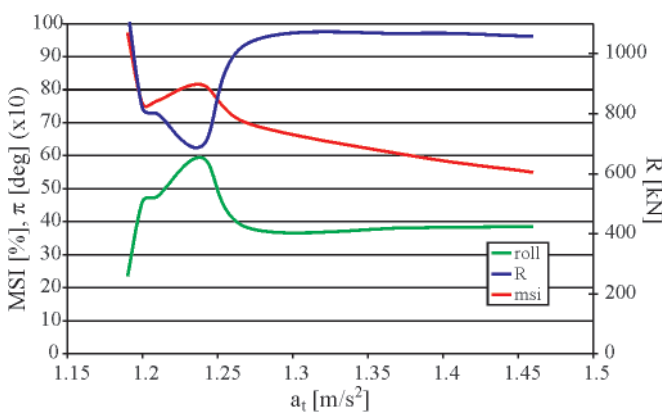
Fig. 11. *Minimum values of dependent variables within the range of a_t = 1.19 ÷ 1.46 m/s²*
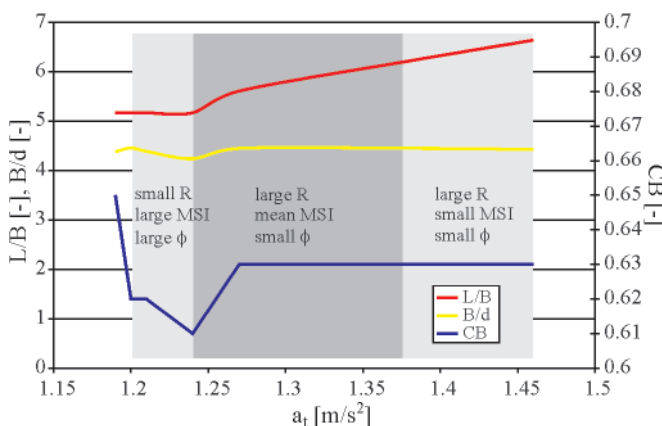
Fig. 12. *Values of design parameters in function of the lateral acceleration a_t, CWL = 0.80*

MULTI-CRITERIAL OPTIMIZATION

The next step in the investigations was an attempt of using the mult-criterial optimization methods in order to determine an optimum design solution of ro-ro ferry ship. In such case the notion of optimum solution is not simple as in the case when one does not accept to compare different criteria to each other and then must propose such definition of optimality which respects integrity of each of the criteria [5]. In order to select an optimum solution in the analyzed case when sets of partial solutions do not have any common part, it is necessary to find an acceptable compromise between partial targets. Importance of particular partial targets can be expressed by means of the weight coefficient [3] and hence obtained design solutions depend on values of the weights. In such case a verdict is automatically given and relations between partial solutions are unknown. This is disadvantageous as decision maker has no possibility to assess all variants (or only a part of them) before a verdict is given.

In the case of the ship hull parametric modeling for the offer design purposes it is sometimes important to know influence of partial criteria on design solutions. Then in the offer design its merits can be proposed from the point of view of different criteria and decision maker (shipowner) is able to choose the best variant from his point of view. Therefore in the assumed design task the notion of optimality in the sense of Pareto was used. The Pareto optimality concept does not provide any indications as to making choice of a final solution (out of P-optimum ones) . Decision on choice of optimum solution has to be taken by decision maker himself [5].

The optimality condition in the Pareto sense can be presented as follows: *the vector x will be consider (partly) smaller than the vector y, if and only if the relation [5] is satisfied:*

$$(\forall i)(x_i \leq y_i) \wedge (\exists i)(x_i \leq y_i) \tag{5}$$

Then it is also said that the vector y is dominated by the vector x. If a given vector is not dominated by no other one then it is called the non-dominated vector. By analyzing Fig. 3 one can state that the solutions A and B are not dominated and the solutions C and D are dominated by the solutions A and B (with respect to MSI index and additional resistance R). And, from Fig. 4 results that the soultions A and B are dominated by the solution D with respect to the criteria of the roll angle φ and lateral acceleration a_t. From the fact it results that in the assumed design task no single optimum solution with respect to all the criteria can be obtained but only the set of four solutions which are not mutually dominated, and any decision on choice of a solution is compromise.

In Fig. 13 is presented the set of values of the dependent variables of all the optimum solutions - in the sense of Pareto - (i.e. those non-dominated) of the considered design task. The set is presented in function of the MSI index. As it turned out, in the obtained design solution the dependent variables achieved the following values:
• the motion sickness index, MSI = 55 ÷ 90 %
• the additional resistance in waves, R = 614 ÷1164 kN
• the significant amplitude of roll angles φ = 0.26 ÷ 8.91°
• the lateral accelerations a_t = 1.22 ÷ 1.91 m/s².

From the above given set optimum solutions can be selected with respect to arbitrary assumed criteria. In Tab. 4, 5 and 6 are presented example design solutions with respect to:

- all the criteria which achieve maximum mean values, i.e.: MSI < 85.5%, R < 889 kN, ϕ < 4.59°, a_t < 1.57 m/s² (Tab. 4)
- MSI and R values smaller than mean ones, as well as ϕ and a_t values greater than mean ones, i.e.: MSI < 78%, R < 730 kN, ϕ < 7°, a_t < 1.7 m/s² (Tab. 5)
- ϕ and a_t values smaller than mean ones and MSI and R values greater than mean ones, i.e.: MSI < 90%, R < 1165 kN, ϕ < 2°, a_t < 1.39 m/s² (Tab. 6).
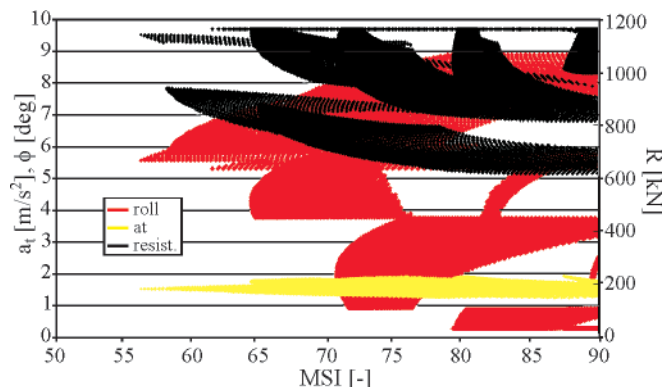
Fig. 13. *The set of all optimum design solutions in the sense of Pareto, MSI = 55 ÷ 90 %, R = 614 ÷1164 kN, f = 0.26 ÷ 8.91°, a_t = 1.22 ÷ 1.91 m/s²*

Tab. 4. *Optimum design solutions in the sense of Pareto, MSI < 85.5%, R < 889 kN, ϕ < 4.59°, a_t < 1.57 m/s²*

CB [-]	CWL [-]	L/B [-]	B/D [-]	MSI [%]	R [kN]	ϕ [°]	a_t [m/s²]
0.63	0.87	5.32	3.57	85.46	883.65	2.97	1.59
0.63	0.87	5.34	3.57	85.14	883.48	2.97	1.59
0.63	0.87	5.36	3.57	84.83	883.34	2.97	1.59
0.63	0.87	5.34	3.59	84.67	887.48	2.92	1.59
0.63	0.87	5.36	3.59	84.36	887.36	2.92	1.59
0.63	0.87	5.38	3.59	84.06	887.28	2.92	1.59

Tab. 5. *Optimum design solutions in the sense of Pareto, MSI < 78%, R < 730kN, ϕ < 7° a_t 1.7 m/s²*

CB [-]	CWL [-]	L/B [-]	B/D [-]	MSI [%]	R [kN]	ϕ [°]	a_t [m/s²]
0.62	0.81	5.5	4.07	77.81	728.99	6.98	1.35
0.62	0.81	5.52	4.07	77.51	728.99	6.98	1.36
0.62	0.81	5.54	4.07	77.22	729.05	6.98	1.36
0.62	0.81	5.56	4.07	76.93	729.16	6.98	1.36
0.62	0.81	5.58	4.07	76.64	729.32	6.98	1.37
0.62	0.81	5.6	4.07	76.36	729.54	6.98	1.37
0.62	0.81	5.62	4.07	76.08	729.8	6.98	1.38

Tab. 6. *Optimum design solutions in the sense of Pareto, MSI < 90%, R < 1165 kN, ϕ < 2°, a_t < 1.39 m/s²*

CB [-]	CWL [-]	L/B [-]	B/D [-]	MSI [%]	R [kN]	ϕ [°]	a_t [m/s²]
0.61	0.85	5.18	4.45	89.7	1164.2	1.92	1.39
0.61	0.85	5.18	4.47	89.68	1164.2	1.87	1.39
0.61	0.85	5.2	4.47	89.67	1164.2	1.87	1.39

CONCLUSIONS

- Both economic criteria and technical limitations constitute important factors in the process of single- and multi-criterial design optimization. To perform such optimization ship designers should be equipped with suitable tools in the form of calculation methods. Determination of additional hull resistance in waves or ship sea-keeping qualities by means of the presently used design algorithms is excessively complicated as to make it possible to perform optimization successfully. This results from various causes but the most important is that simple and simultaneously exact relations between hull form parameters and ship behaviour in waves are lacking. To predict ship responses in waves is only possible by using exact numerical methods for a given ship hull form.

- A method which makes it possible to solve the problem is presented in this work. To approximate additional resistance in waves and selected sea-keeping qualities, artificial neural networks were used. Despite relatively low number of model variants and wide range of ship hull parameters the obtained approximations are characterized by high accuracy and simple structure.

- The presented approximations may be applied to design analyses (e.g. such as in [2]) or as objective functions in various optimization methods of ship design parameters. In this paper an example of single- and multi- criterial optimization of car passenger ferry ship design parameters is presented. In the first phase ranges of optimum design parameters with respect to the assumed criteria taken into account separately, were determined. In the second phase sets of design solutions optimum in the sense of Pareto, were determined. In each of the phases the solutions were presented in such form as to give a decision maker (ship operator, designer) possibility to select variants most favourable to him.

BIBLIOGRAPHY

1. Cepowski T.: *Approximation of pitching motion of S-175 containership in irregular waves on the basis of ship's service parameters*. Polish Maritime Research, No. 1(47), Vol. 13, 2006
2. Cepowski T.: *Approximation of the index for assessing ships sea-keeping performance on the basis of ship design parameters*. Polish Maritime Research, No. 3(53), Vol. 14, 2007
3. Chądzyński W.: *Elements of contemporary design methods of floating objects* (in Polish). Scientific Reports of Szczecin University of Technology, Department of Ocean Engineering and Marine System Design, Szczecin 2001
4. Gerritsma, J. and Beukelman, W.: *Analysis of the Resistance Increase in Waves of a Fast Cargo-ship*. International Shipbuilding Progress, 18(217), 1972.

5. Goldberg D.E.: *Genetic Algorithms in Search, Optimization, and Machine Learning*. Publication of Pearson Education, Inc, 1989

6. Journée J.M.J.: *Verification and Validation of Ship Motions Program SEAWAY*. Report1213a, Delft University of Technology, The Netherlands, 2001.

7. Lasdon, L.S., Waren, A.D.: *Generalized reduced gradient software for linearly and nonlinearly constrained problems*. [in]: Greenberg, H.J., (Ed.) Design and Implementation of Optimization Software. Sijthoff and Noordhoff, Holland, 1978

8. Mesbashi E., Bertram V.: *Empirical Design Formulae Using Artificial Neural Nets.* 1st International EuroConference on Computer Applications and Information Technology in the Maritime Industries, COMPIT'2000, Potsdam 2000

9. Riola J.M., M.Garcia de Arboleya: *Habitability and personal space in sea-keeping behaviour.* Journal of Maritime Research, Vol. III, No. 1, 2006

10. Szelangiewicz T., Cepowski T.: *Application of artificial neural networks to investigation of ship sea-keeping ability*, Part 1, Polish Maritime Research, Vol.8, No. 3, September 2001

11. Szozda Z.: *A Concept of Ship Stability Criteria Based on Cargo Shift Caused by Rolling due to Gust*. Zeszyty Naukowe (Scientific Bulletins) No. 2 (74), Maritime University of Szczecin, 2004

CONTACT WITH THE AUTHOR
Tomasz Cepowski, Assoc. Prof.
Institute of Marine Navigation,
Maritime University of Szczecin
Wały Chrobrego 1/2
70-500 Szczecin, POLAND
e-mail : cepowski@am.szczecin.pl

An experimental and numerical study of the vortices generated by hydrofoils

J. A. Szantyr, Prof.
R. Biernacki, Ph. D.
P. Flaszyński, Ph. D.
Gdansk University of Technology
P. Dymarski, Ph. D.
M. Kraskowski, M. Sc.
Ship Design and Research Centre CTO SA

ABSTRACT

The article presents the results of the research project concerning the process of formation of the tip vortices shed from hydrofoils of different geometry in different flow conditions. Three hydrofoils resembling the contemporary marine propeller blades have been selected for the study. The experimental part of the project consisted of the LDA measurements of the velocity field in three cross-sections of the vortex generated by the hydrofoils in the cavitation tunnel. The numerical part of the project consisted of calculations of the corresponding velocity field by means of three computer codes and several selected turbulence models. The comparative analysis of the experimental and numerical results, leading to the assessment of the accuracy of the numerical methods, is included.

Keywords: marine propulsors; vortex generation; numerical methods; experimental techniques

INTRODUCTION

One of the most important problems in the advanced design of marine propulsors is the possibly accurate determination of the concentrated vortex structures generated by the lifting foils forming the propulsor. These vortex structures usually lead to formation of the cavitating kernels, which are responsible for the cavitation erosion of the propulsor and the rudder, for the generation of pressure pulses leading to vibration of the ship structure and for the emission of intensive hydro-acoustic signals. Development of the methods for the accurate prediction of the above described phenomena at the design stage would lead to the complete elimination of their negative consequences or at least to limiting them to the acceptable levels.

The rapidly developing methods of the Computational Fluid Mechanics are generally regarded as unable to predict accurately the intensity of the concentrated vortex structures generated by lifting foils, hence they are also unable to predict correctly the conditions for cavitation inception in these vortex structures. It is believed that the structures of the discrete representation of the fluid domain typically employed in these methods are unsuited for the cases with high velocity secondary transverse flows and that the standard turbulence models are developed and calibrated mostly for typical flat plate boundary layers, differing significantly from the vortex dominated flows. The objective of the research project presented in this paper is to develop the rules for generation of the discrete meshes especially suited for vortex dominated flows and to select the turbulence models especially effective in such flows.

This objective is achieved by the combined experimental and numerical research. Three variants of the hydrofoil were selected for the project. Their outline and section profiles resemble those of the typical contemporary marine propeller blades. The radial distribution of pitch typical for a propeller blade was reduced to zero, thus producing the foil with standard distribution of the hydrodynamic loading along the span, denoted N for neutral. As the distribution of the hydrodynamic loading along the span of the foil may influence significantly the process of formation of the tip vortices, two more foils were designed: one with positive linear twist along the span, denoted L for loaded, and another with negative twist along the span, denoted U for unloaded. The absolute value of the twist angle in both cases was equal to 2.5 degrees at the tip, corresponding to the typical values for marine propeller blades. The details of the experimental and numerical parts of the project are described below, with the following comparative analysis of the experimental and numerical results.

EXPERIMENTAL MEASUREMENTS OF THE VELOCITY FIELD AROUND THE CONCENTRATED VORTICES

The comprehensive descriptions of the experiments with three hydrofoil models are presented in [1, 2, 3]. All three hydrofoil models were manufactured in aluminum alloy using the numerically controlled milling machine, which ensured high accuracy (Fig. 1). The span of the hydrofoil models was selected equal to 400 mm, which located the trailing tip

vortex approximately in the centre of the measuring section of the cavitation tunnel of CTO S.A. The hydrofoils were installed in the measuring section of the cavitation tunnel. Using the dynamometer, which enabled both measurements of the lift and drag forces and the accurate setting of the angle of attack (Fig. 2). The nominal velocity of flow in the tunnel was set to 4.0 [m/s], which ensured the turbulent flow over the hydrofoil.

Fig. 1. The model of the hydrofoil N manufactured in aluminum alloy using the numerically controlled milling machine
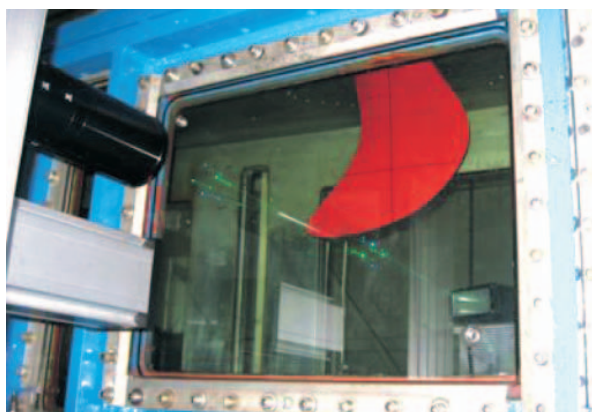
Fig. 2. The model of the hydrofoil fixed in the measuring section of the cavitation tunnel at CTO S. A.
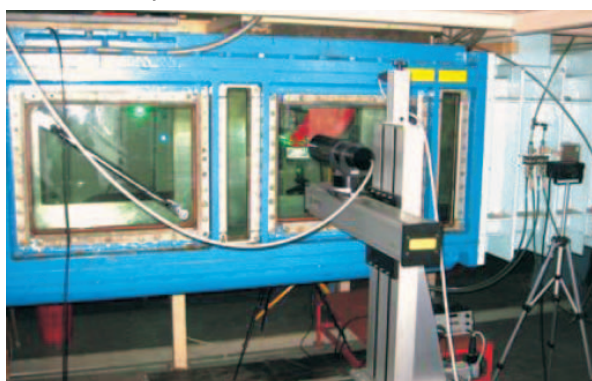
Fig. 3. The laser Doppler anemometer (LDA) ready for measurements of the velocity field around the vortex behind the hydrofoil

Each of the three hydrofoils was in turn set at three angles of attack: +2.5; 0.0 and –2.5 degrees. These values correspond to the typical range of variation of the angle of attack encountered on marine propellers. The measurements of the velocity field behind the hydrofoils were conducted by the laser Doppler anemometer (LDA – Fig. 3). The LDA system was capable of measuring two velocity component simultaneously: the axial component u and the transverse (vertical) component v. The measurements were conducted in three surfaces perpendicular to the vortex axis, located at 10 mm, 70 mm and 300 mm behind

the hydrofoil (Fig. 5). Apart from the velocity field, the variation of the lift and drag forces on the hydrofoils as the functions of the angle of attack were also measured.

NUMERICAL PREDICTION OF THE VELOCITY FIELD AROUND THE CONCENTRATED VORTICES

The comprehensive details of the numerical prediction of the velocity field in the vortex wake behind the hydrofoils are described in [1, 2, 4, 5]. Three numerical codes were used: the commercial programs Fluent and Comet and an indigenous program Solaga developed at CTO S.A. All three programs are based on the Reynolds Averaged Navier Stokes Equations, converted into algebraic equations by means of the Finite Volume Method. The computational domain had the same cross-section as the cavitation tunnel, i.e. 800 x 800 mm and it extended 1500 mm in front of the hydrofoil axis and 3000 mm behind the hydrofoil axis. This domain was divided into the block-structured grid having approximately 1.250.000 finite volumes – see Fig. 1. The size of the smallest finite volumes close to the hydrofoil surface was approximately 0.02 mm. The following turbulence models were used in calculations:

- In the program Fluent 6.3, using the scheme MUSCL (Monotone Upstream-Centered Schemes for Conservation Laws) for the convection terms of the transport equations:
  - Spalart-Allmaras
  - k-epsilon RNG
  - k-omega SST
  - Reynolds Stress Model (RSM)
- In the program Comet:
  - k-epsilon
  - k-omega
  - k-omega SST
- In the program Solaga – Spalart-Allmaras
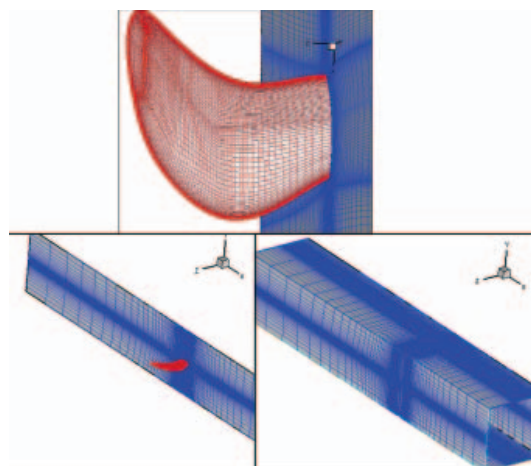
Fig. 4. The discrete mesh for numerical calculations on the hydrofoils surface (top) and on the external surfaces of the flow domain (bottom)
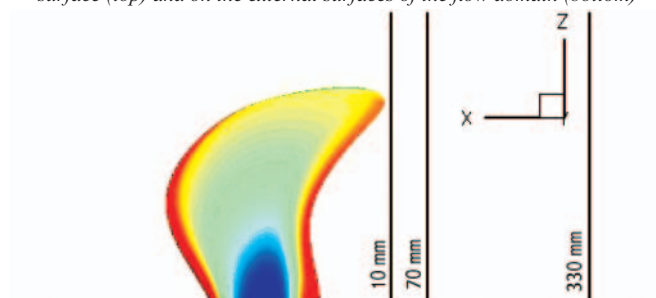
Fig. 5. The location of the three control surfaces both for measurements and calculations of the velocity field behind the hydrofoil

The calculations reproduced the experimental conditions as closely as possible and they concentrated on determination of the axial and transverse (vertical) velocity components in the three cross-section of the vortex wake, respectively 10 mm, 70 mm and 300 mm behind the hydrofoil trailing edge, as shown in Fig. 5.

COMPARISON OF THE EXPERIMENTAL AND NUMERICAL RESULTS

The results selected for comparison refer to two cross-sections of the vortex wake, namely 10 mm and 70 mm behind the hydrofoil. At both sections, the results are presented for

Fluent (k-omega SST)

Fluent (RSM)

Comet (k-epsilon)

Comet (k-omega SST)
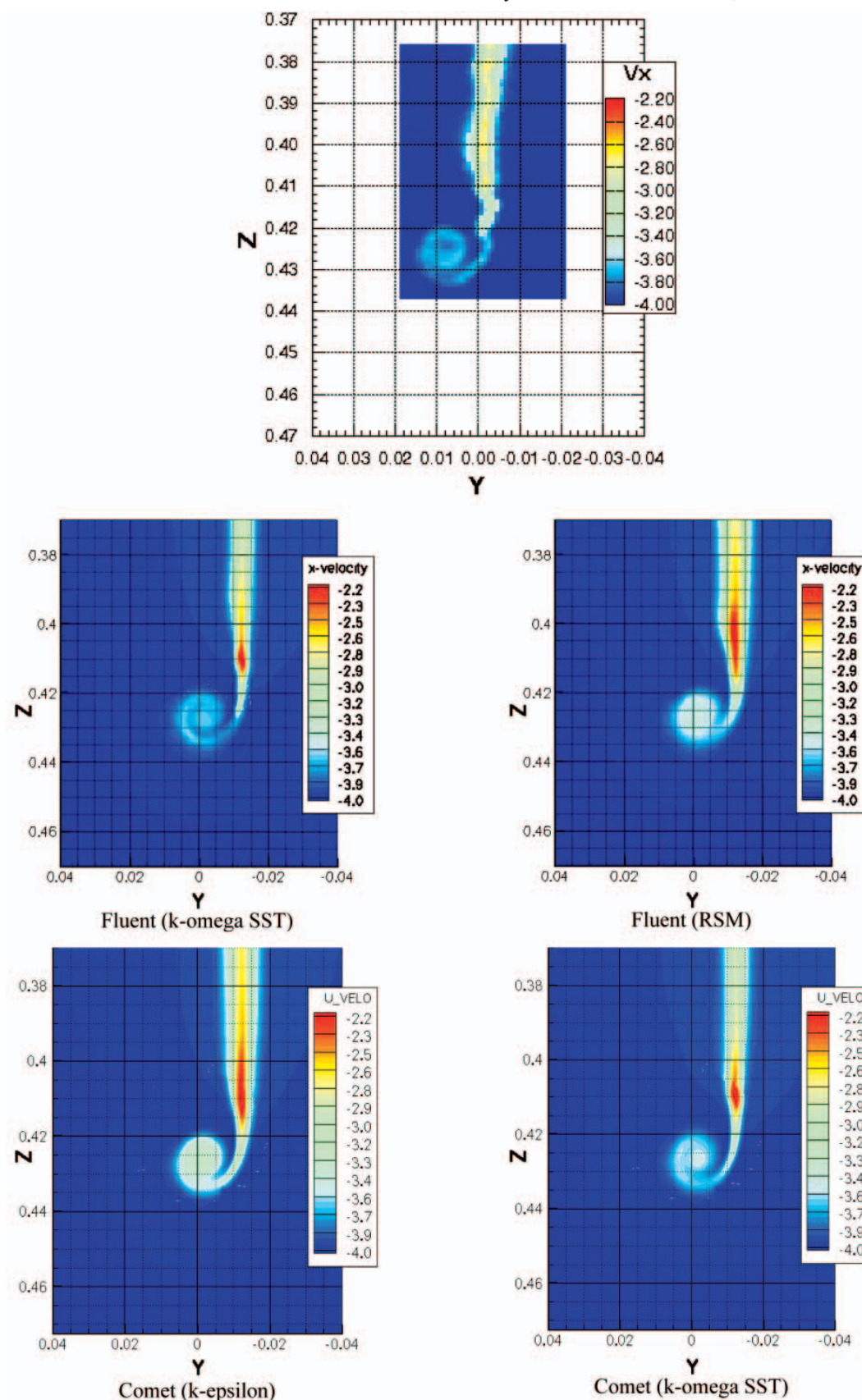
Fig. 6. The comparison of the measured (top) and calculated (below) axial component of the velocity at the control surface 10 mm behind the hydrofoil L at the angle of attack equal +2.5 degrees

these turbulence models which demonstrated the best ability to reproduce the experimental results. All presented results were obtained for the hydrofoil L set at the angle of attack equal to +2.5 degrees, i.e. for the case of the highest hydrodynamic loading at the tip of the hydrofoil. Consequently, the most intensive tip vortex was expected in this condition. Fig. 6 shows the measured and calculated axial velocity component at the cross-section nearest to the hydrofoil trailing edge. This velocity component is the reflection of the viscous wake behind the hydrofoil, generated in the boundary layer on its surface. The analysis of the velocity distributions shown in this figure leads to the following conclusions:

– calculations using all programs and turbulence models give the qualitatively correct picture of the viscous wake behind
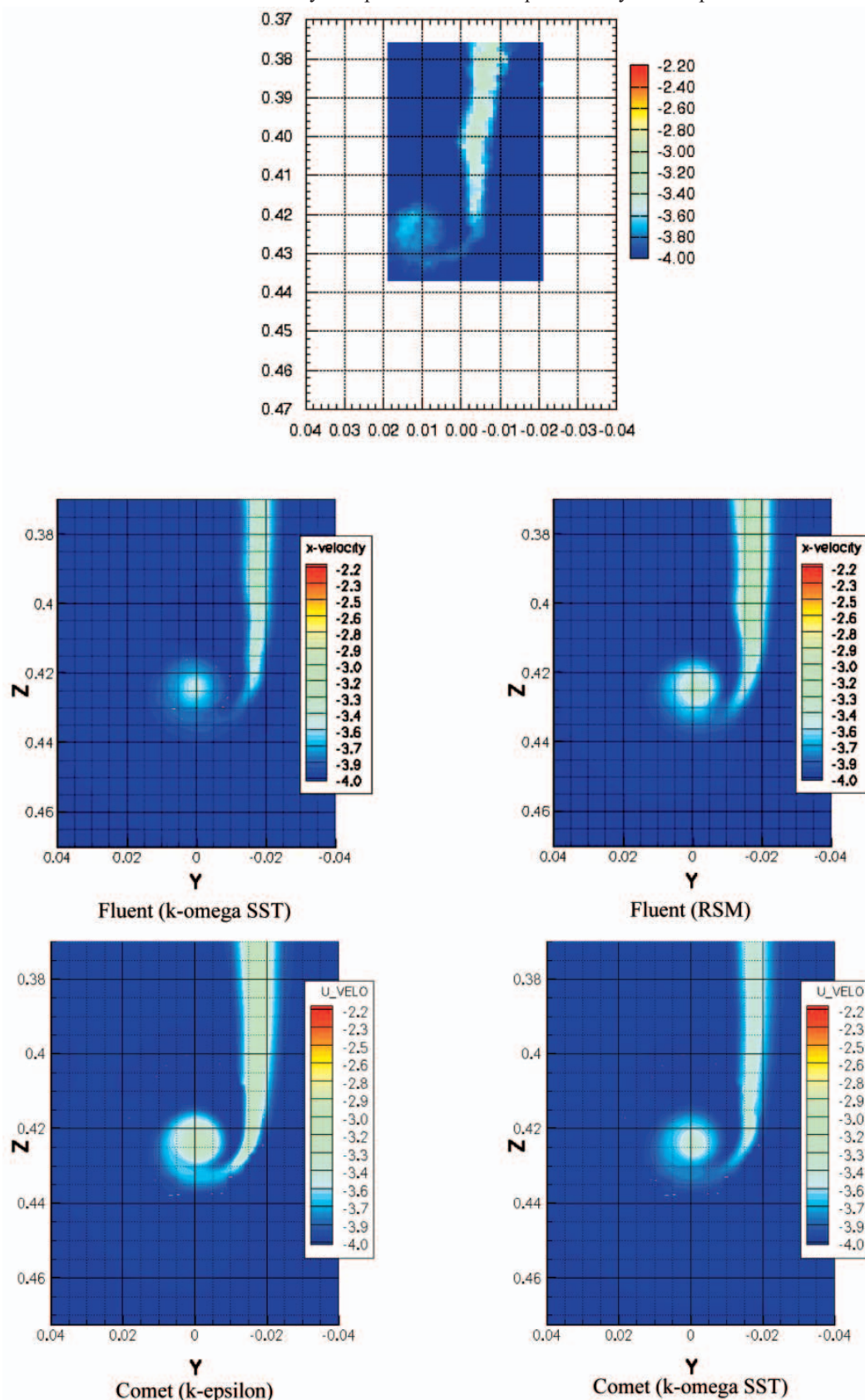
Fig. 7. The comparison of the measured (top) and calculated (below) axial component of the velocity at the control surface 70 mm behind the hydrofoil L at the angle of attack equal to +2.5 degrees

the hydrofoil, which agrees quite well with the results of the measurements,
- the calculated boundaries of the viscous wake are more sharply defined than those determined experimentally,
- the calculated minimum velocity in the viscous wake is markedly smaller than that detected in the course of experiments,

- this over-prediction of the minimum velocity in the wake is much stronger for the RSM and k-epsilon turbulence models than for the k-omega SST turbulence model,
- it is interesting to notice that both Fluent and Comet have produced very similar results using the same turbulence model k-omega SST.
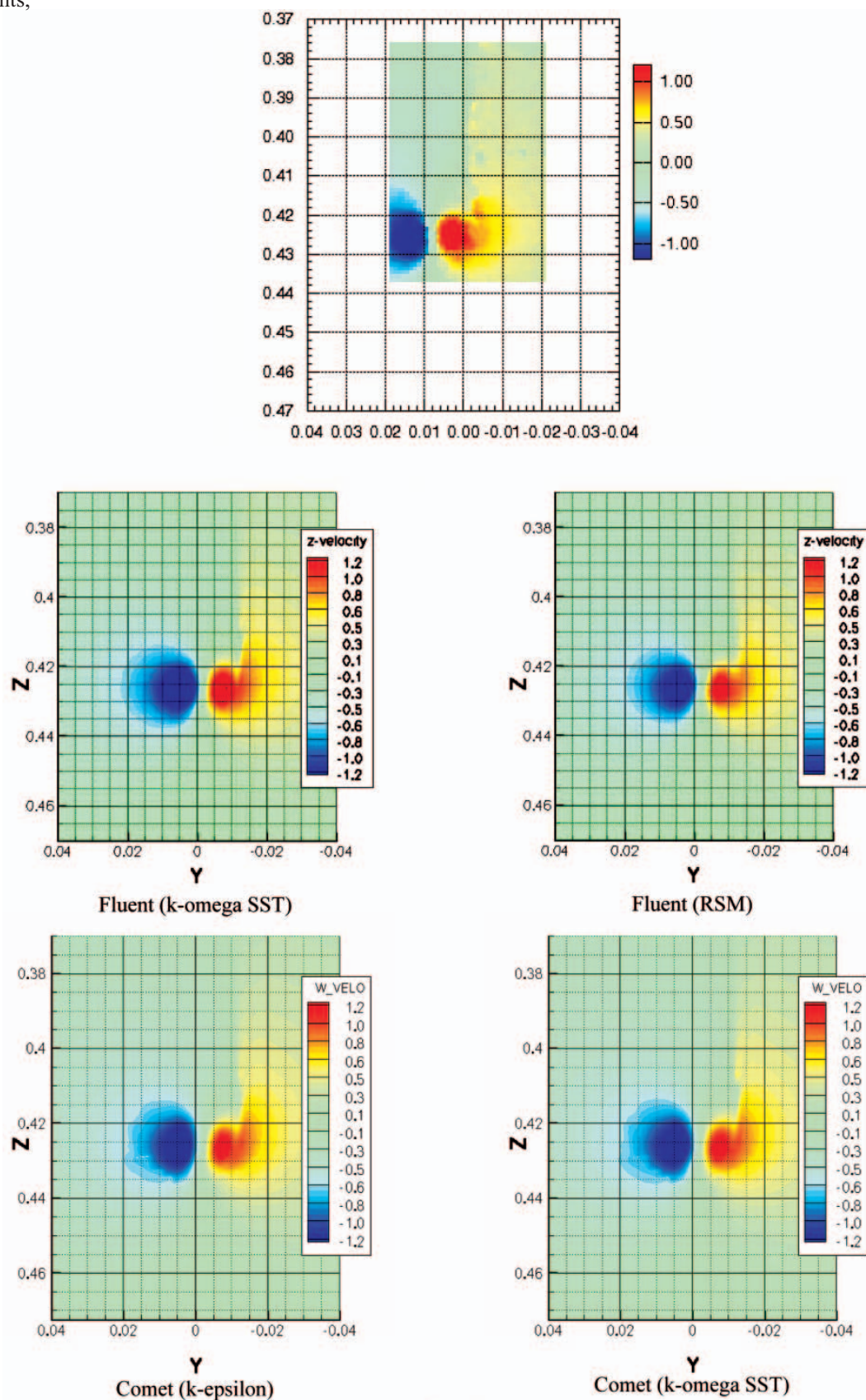
Fig. 8. The comparison of the measured (top) and calculated (below) transverse component of the velocity at the control surface 10 mm behind the hydrofoil L at the angle of attack equal to +2.5 degrees

Fig. 7 shows the analogical comparison of the measured and calculated axial component of the velocity at the cross-section located at 70 mm behind the hydrofoil trailing edge. As could be expected, at this location the viscous wake behind the hydrofoil was already significantly dispersed and damped due to the action of turbulence and fluid viscosity. This effect was correctly qualitatively reproduced in all calculations. However, again the k-omega SST turbulence model gave the best agreement with the results of experimental measurements, both in terms of the spatial distribution of the wake and the minimum velocity. Similarly as for the first cross-section, the k-epsilon and RSM turbulence models again over-predicted the minimum velocity in the wake.

Fluent (k-omega SST)

Fluent (RSM)

Comet (k-epsilon)

Comet (k-omega SST)
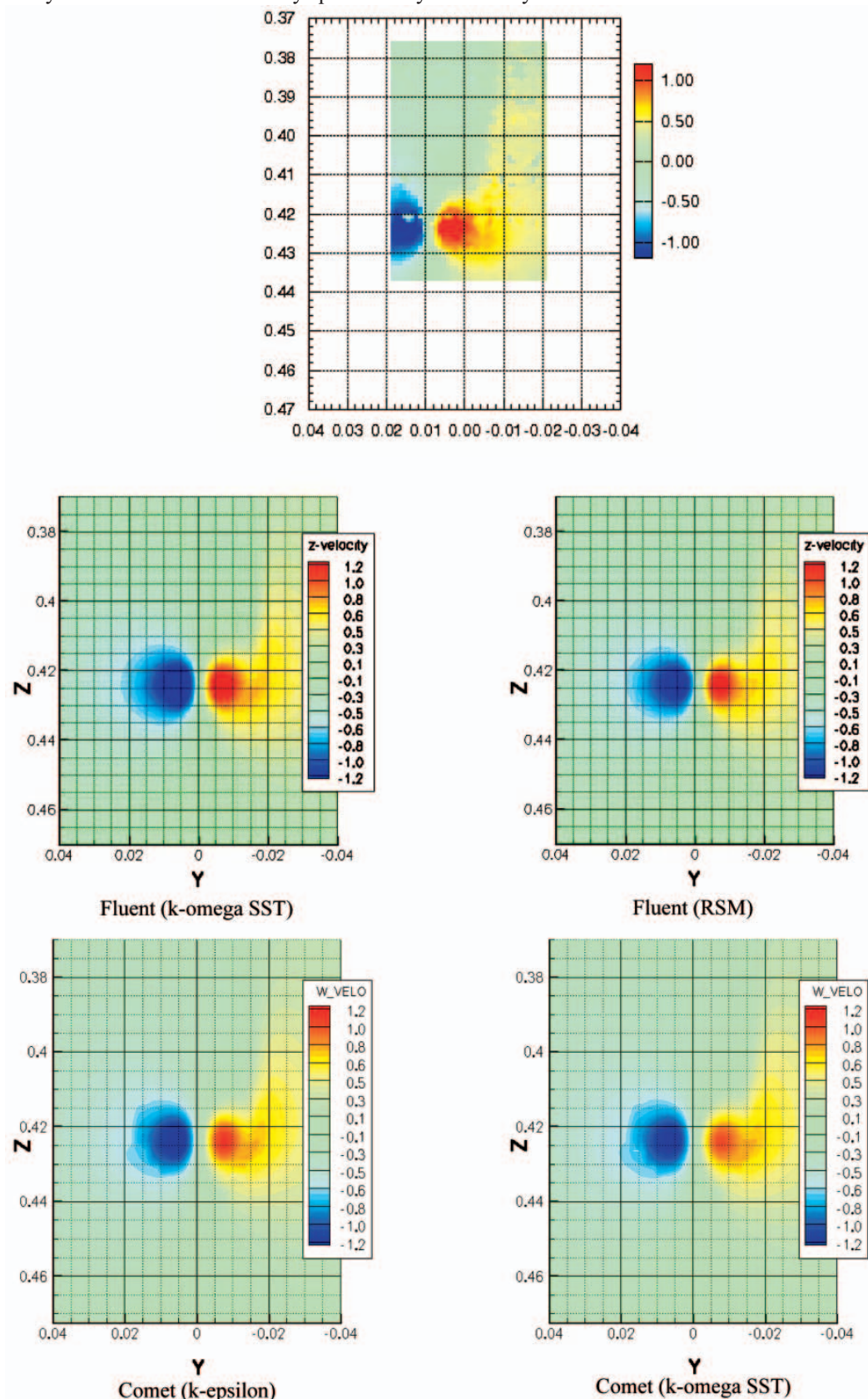
Fig. 9. The comparison of the measured (top) and calculated (below) transverse component of the velocity at the control surface 70 mm behind the hydrofoil L at the angle of attack equal to +2.5 degrees

In Fig. 8 the comparison of the calculated and measured transverse (vertical) component of the velocity in the wake behind the hydrofoil is presented for the cross-section located 10 mm behind the hydrofoil trailing edge. This velocity component may be regarded as the measure of the intensity of the tip vortex. The analysis of the velocity distributions leads to the following conclusions:

– calculations using all programs and turbulence models give the qualitatively correct picture of the intensity of the tip vortex, which agrees quite well with the results of the measurements,
– even the small details of the spatial distribution of the vertical velocity component are very well reproduced in all calculations (cf. the shape of the red field in the pictures),
– again the k-omega SST turbulence model seems to give the results closest to those obtained experimentally.

Fig. 9 presents the distribution of the horizontal component of the velocity at the cross-section 70 mm behind the hydrofoil. Contrary to the picture shown in Figs. 6 and 7, now there is almost no turbulent and viscous dispersion effect of the vortex visible between Figs. 8 and 9.

Simply the vorticity is still being convected towards the centre of the tip vortex. Consequently, the distributions shown in Figs. 8 and 9 are very similar to each other. This phenomenon, detected experimentally, is confirmed by all calculations. In this case no significant differences between the respective turbulence models may be noticed.

CONCLUSIONS

After a thorough analysis of the presented results the following general conclusions may be drawn:

– the state of the art Computational Fluid Dynamics methods are fully capable of predicting the existence, location, spatial extent and intensity of the tip vortices generated by hydrofoils,
– moreover, they are also capable of predicting correctly the intensity and consequences of two mutually counteracting processes of dissipation and concentration of vorticity along the vortex,
– there are visible differences between the performance of different turbulence models and selection of the appropriate model is an important matter – in case of vortex dominated flows the k-omega SST model seems to the most promising,

– there is definitely a room for improvement of the accuracy of numerical prediction of the tip vortex flows through modification of the discrete grid structure in the flow domain, especially in the direct vicinity of the vortex.

The further stages of the research project, concerning the improvement of the performance of the CFD methods in prediction of the vortex dominated flows will be the subject of a separate article.

BIBLIOGRAPHY

1. Dymarski P., Szantyr J., Flaszyński P., Kraskowski M., Biernacki R.: *Modelling of Tip Vortex Behind a Blade Using Different Turbulence Models and Different RANSE Solvers. Comparison with LDA Measurements,* Proc. of the 11th Numerical Towing Tank Symposium, Brest, France, September 8-10 2008
2. Flaszyński P., Szantyr J., Dymarski P., Krasowski M.*: Numerical Prediction of Vortex Generated by a Hydrofoil,* Proc. of the International Symposium on Marine Propulsors, Trondheim, Norway, June 22-24, 2009
3. CTO S.A. Report No. RH-2008/T-133 *Results of measurements of the velocity field in the vortex path behind the hydrofoils* (in Polish)
4. CTO S.A. Report No. RH-2008/T-019 *Calculations for the first variant of the discrete mesh – program Fluent* (in Polish)
5. CTO S.A. Report No. RH-2008/T-020 *Calculations for the first variant of the discrete mesh – programs Comet and Solaga* (in Polish)

CONTACT WITH THE AUTHORS

J. A. Szantyr Prof. e-mail: jas@pg.gda.pl
R. Biernacki Ph. D., e-mail: rbiernac@pg.gda.pl
P. Flaszyński Ph. D. e-mail: pflaszyn@pg.gda.pl

Faculty of Mechanical Engineering
Gdansk University of Technology
Narutowicza 11/12
80-231 Gdańsk

P. Dymarski Ph. D., e-mail: padym@cto.gda.pl
M. Kraskowski M. Sc,
e-mail: Marek.Kraskowski@cto.gda.pl

Ship Design and Research Centre CTO S.A.
Wały Piastowskie 1
80-958 Gdańsk

Drag force on a flat plate in cavitating flows

M.S. Seif, Prof.
A. Asnaghi, Research Assistant
E. Jahanbakhsh, Research Assistant
Sharif University of Technology

ABSTRACT

The present study focuses on the simulation of two dimensional unsteady cavitating flows. For simulation of unsteady behaviors of cavitation which have practical applications, the development of unsteady PISO algorithm based on the non-conservative approach is utilized. For multi-phase simulation, single-fluid Navier–Stokes equations, along with the volume fraction transport equation, are employed. The bubble dynamics model is utilized to simulate phase change between vapor and liquid phases of the water. Unsteady simulation of cavitation around NACA66(MOD) and supercavitation around a flat plate normal to flow direction are performed to clarify accuracy of presented model. Numerical results and comparisons with experimental data are provided. The accuracy is good, and it is possible to apply this method to more complex shapes.

Keywords: numerical simulation; cavitation; psio algorithm; flat plate; unsteady flow

INTRODUCTION

When local static pressure of liquid falls below the corresponding saturated pressure, the phase of fluid changes from liquid into vapor. This phenomenon is named cavitation. The cavitation is departure from evaporation. The evaporation, in definition, is performed by temperature changing but cavitation is performed by pressure changing. Cavitation can be observed in a wide variety of propulsion and power systems like propellers, pumps, nozzles and injectors [1, 2].

Cavitation is categorized by a dimensionless number called cavitation number, where it depends on the saturated pressure, the flow reference pressure, density and velocity, respectively. The cavitation number is defined as follows:

$$\sigma = \frac{P - P_{sat}}{\frac{1}{2}\rho_\infty U_\infty}$$ (1)

Usually cavitation formation of a flow is categorized based on the cavitation number of the flow. Therefore, experimental observations are classified based on the cavitation number of the flow [3]. Undesirable aspects of cavitation are erosion, structural damages, noise and power loss in addition to beneficial features such as drag reduction and the effects of cavitation in water jet washing systems. The drag reduction observed on bodies surrounded fully or partially with cavity strongly encourages one to research on properties of cavitating flows.

In spite of its longstanding practical importance and rich physics, cavitating flow continues to be a topic of significant challenge to the computational community. The simultaneous presence of interfacial dynamics, multiple timescales, and phase change complicates the fluid physics and requires substantial modeling efforts. Numerous modeling strategies have been proposed in the literature, ranging from Rayleigh-Plesset type of bubble formulation, Kubota et al. [4], which separates the liquid and vapor region based on the force balance notion, to homogeneous fluid approach, Senocak and Shyy [5], which treats the cavity as a region consisting of continuous composition of liquid and vapor phases.

In this study the bubble dynamic model which is based on the Rayleigh equation is used for simulating phase change. A finite-volume approach written in body fitted curvilinear coordinates, on collocated grids in 2D and 3D domains is used for the numerical descretization. For the present study, the transport equation-based model, TEM, is implemented into the solver and related modifications, regarding the convection schemes and the PISO algorithm, have been made for time-dependent computations.

The main numerical results of this study are from simulation of sheet cavitation around NACA66(MOD) hydrofoil and supercavitation around a flat plate. Unsteady simulation of cavitating flows around a 2d flat plate oriented normal to flow is performed from range of subcavitation to supercavitation. Apart from their theorical interest (in stability analysis for instant), unsteady supercavitating flows were mainly considered in the past for their applications to hydrofoils under transient or periodic conditions. On the whole, the basis of the modeling of unsteady 2d supercavities is the same as for steady flows.

The main analysis methods are:
1. analytical, non-linear methods: Von Karman [6], Woods [7], Wu [8]
2. analytical, linearized methods: Timmam [9], Geurst [10], Tuln et al. [11]
3. numerical, non-linear methods, which are currently employed and usually use the scheme initially proposed by Plesset et al. [12]. A survey of numerical techniques for unsteady cavity flow modeling was given by Kinnas [13].

Due to the difficulty of conducting tests under unsteady conditions, experimental data in this field are rather rare. Therefore, the published experimental results usually consist of time-averaged properties [14].

The simulated flows around the flat plate consist of unsteady cavitating flows from two-phase vortex shedding to fully supercavitating flows. Based on these simulations, the pressure distribution, cavity region, cavity characters as its length and width are presented. Beside these, the interaction between vapor phase and flow around the flat plate, formation of supercavitation and its effects are analyzed. Finally, the obtained results are compared with available experimental results to demonstrate the accuracy of the current simulation.

GOVERNING EQUATIONS

The equations governing the flow of a compressible fluid are the continuity equation, the momentum equations, the energy equation, and finally the state equation. This set of non-linear, coupled equations is solved for the unknown's parameters ρ, U, T and P. In index notation form, these equations may be written as:

$$\frac{\partial \rho_m}{\partial t} + \frac{\partial(\rho_m u_i)}{\partial x_i} = 0 \qquad (2)$$

$$\frac{\partial(\rho_m u_i)}{\partial t} + \frac{\partial(\rho_m u_i u_j)}{\partial x_j} = \qquad (3)$$

$$= -\frac{\partial(P)}{\partial x_i} + \frac{\partial}{\partial x_j}\left(\mu\left(\frac{\partial u_i}{\partial x_j} + \frac{\partial u_j}{\partial x_i}\right)\right) + \rho_m g$$

$$\frac{\partial(\rho_m T)}{\partial t} + \frac{\partial(\rho_m u_j T)}{\partial x_j} = \qquad (4)$$

$$= \frac{1}{C_P}\left(\frac{\partial}{\partial x_j}\left(K\frac{\partial T}{\partial x_j}\right) + \beta T\left[\frac{\partial P}{\partial t} + u_j\frac{\partial P}{\partial x_j}\right] + \dot{\phi} + \dot{q}\right)$$

Where $\dot{\phi}$ denotes the dissipation term in energy equation and β is the thermal expansion coefficient which is equal to 1/T for an ideal gas. In addition to the above differential equations, an auxiliary equation of state relating density to pressure and temperature [$\rho = f(P,T)$] is needed. In many practical problems related to cavitation phenomena, the change in temperatures is negligible. Therefore the simulation of cavitation in isothermal condition has not any effect on final results, and it is unnecessary to solve the energy equation. Therefore the pressure-density coupling is complex and requires special attention [15].

In this study, instead of a state equation, the TEM of vapor is employed. With this equation, pressure and density

are connected implicitly via a phase change source term. To simulate phase change between vapor and liquid, a term S_α, is added to the right side of vapor volume fraction equation. The vapor volume fraction equation with the phase change source term in its right side is presented in equation (5).

$$\frac{\partial \alpha_v}{\partial t} + \frac{\partial(\alpha_v u_i)}{\partial x_i} = S_\alpha \qquad (5)$$

The source term of the vapor volume fraction equation presents the rate of phase change between vapor and liquid phases. The utilized phase change model is presented in the part of cavitation model.

The Homogenous model

With determination of the volume of fraction, the local properties of fluid can be achieved based on the single state of each phase. This method is named The Homogenous model. In two phase flows, the mixture density and mixture viscosity are defined as follows based on the vapor volume fraction:

$$\rho_m = \alpha_v \rho_v + (1 - \alpha_v)\rho_l \qquad (6)$$
$$\mu_m = \alpha_v \mu_v + (1 - \alpha_v)\mu_l$$

Cavitation model

In TEM approach, numerical models of cavitation differ in cavitation source term, S_α. The cavitation source term defines vapor net mass generation that contains effects of vapor production and destruction. In this study we consider the bubble dynamics method as the phase change model [16, 17]. Therefore S_α may be written as:

$$S_\alpha = \text{sign}(P_{sat} - P)\frac{n_0}{1 + n_0\frac{4}{3}\pi R^3}4\pi R^2\sqrt{\frac{2|P_{sat} - P|}{3\rho_l}} \quad (7)$$

The average nucleus per liquid volume is considered as $n_0 = 10^8$. Other properties such as the minimum radius of bubble can be calculated based on the value of the n_0 [18].

DISCRETIZATION METHOD

A finite volume method is used to discretize the governing equations. The details related to the finite volume discretization methods of the Navier Stokes equations and the conservation of mass equation can be found in different references [19].

Equations descretization

In the descretized form of Navier-Stokes equations, there are three major terms: the unsteadiness, convection and diffusion terms. The discretization of the diffusion flux does not require any special consideration and the method adopted here is the second order estimation. The discretization of the convection flux is, however, problematic and requires special attention. In this study, the First-Order Upwind (FOU) scheme is used to calculate the faces values. However, for increasing the solution stability, high order methods could be utilized such as Jassak method [20]. For the representation of the unsteady term, the time derivative is approximated using the First-Order Euler-implicit formulation [16, 20].

To discretize the volume of fraction transport equation, it is necessary to compute the values on the computational cells interfaces accurately. In high speed flows and for capturing shock, it is necessary to use high order methods such as

HRIC [21, 22]. In low speed flows, the first order Upwind method can be used to calculate the volume fraction values on computational cells faces [15]. With the homogeneous approach and volume fraction values on faces, the density on the cell interface can be calculated.

The velocity fluxes on computational cells faces are calculated by using momentum interpolation. The momentum interpolation avoids pressure oscillations in the solution procedure [21].

Overall Solution Procedure

Selecting a suitable time step for unsteady simulation of cavitating flows is very important. The selected time step should be proper for convection in the vapor transport equation and the continuity equation, as well as Navier-Stokes equations. If the time step is selected inappropriately, final results may be wrong or the solution procedure may diverge. In some researches, the time step is considered in accordance with the non-dimensional time of the flow. The non-dimensional time is obtained by dividing the length scale to reference velocity of the flow [23]. In another approach, the time step is calculated in the beginning of each time step by considering the courant number, CFL [18]. In this study, the CFL parameter is used to calculate the time step.

After calculating suitable time step, it is possible to start the solution procedure. For each time step, first, the vapor fraction transport equation is solved and a new vapor fraction distribution is obtained. Consequently the values of the mixture density and viscosity are updated. Based on these new values, the Navier-Stoks equations and the pressure correction equations are solved until a convergence criterion is reached. Then, the whole procedure is repeated within the next time step. In this study, for solving velocity-pressure coupling, the non-conservative PISO algorithm is used.

For the numerical simulation of cavitating flows, the pressure level usually is defined by a pressure boundary condition at the outlet of the computational domain, and velocity set as an inlet velocity boundary.

NUMERICAL RESULTS

The numerical model was implemented in the CFD-Code developed at the Marine Engineering Lab. of Sharif University of Technology. The accuracy of this software are evaluated through different numerical simulations.

The flow is assumed isothermal and fluid properties are supposed to be constant at a given temperature for the entire flow domain. For all simulations presented, cold water at a constant temperature T = 293.2 K with 10^8 nuclei per m^3 water having a minimal nuclei radius of 30 microns is assumed to match the experimental conditions. The saturated pressure, P_v, is set to a constant value of 2340 Pa.

NACA66(MOD) Hydrofoil

Effects of leading edge cavitation on NACA66(MOD) were experimentally investigated by Shen and Dimotakis [24]. A 2D NACA66(MOD) airfoil with camber ratio of 0.02, mean line of 0.8 and thickness ratio of 0.09 is used in this simulation. The implied boundary conditions and non-orthogonal meshes are shown in Fig. 1.

The published experimental results contain the distribution of static pressure on hydrofoil surface at different angles of attack and Reynolds numbers. In this study, Leading Edge Cavitation simulations were performed at Re = 2 × 10⁶, an

angle of attack of 4 deg, inlet velocity 2.5 m/s and cavitation number of 0.91; under these conditions, the cavitation is confined to the front of the hydrofoil. Calculated Cp values, equation (8), on hydrofoil top surface are shown in Fig. 2 together with experimental data, and good correlation is clear between these results. The vapor volume fraction distribution is shown in Fig. 3, which shows the cavitation zone on the hydrofoil surface.

$$C_p = \frac{P_\infty - P}{\frac{1}{2}\rho_\infty U_\infty^2} \quad (8)$$
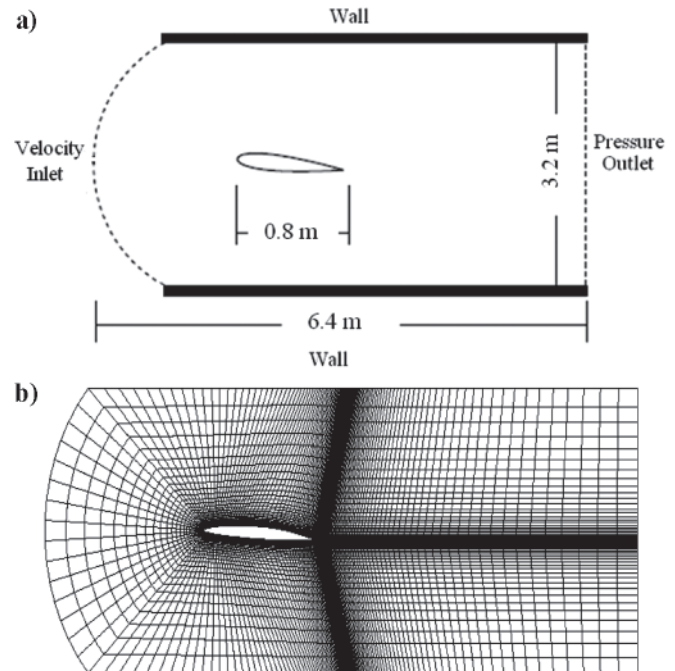
Fig 1. *Implied boundary conditions (**a**) and non-orthogonal meshes (**b**) for simulation of cavitation around NACA66(MOD)*
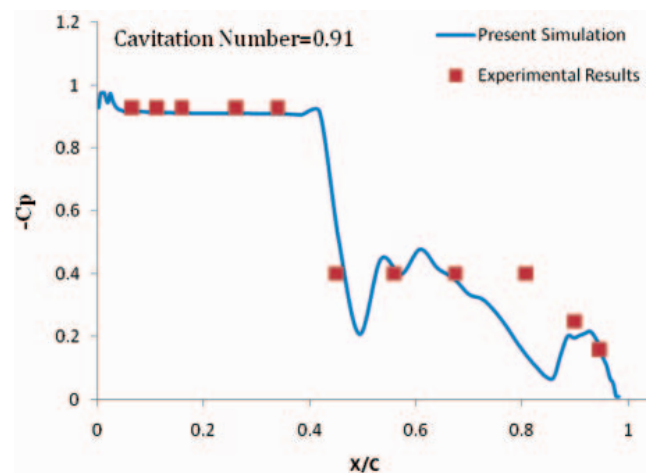
Fig. 2. *Comparison between obtained numerical pressure coefficient distribution and Experimental Results[5] around NACA66(MOD), Inlet velocity = 2.5 m/s. Outlet cavitation number = 0.91*
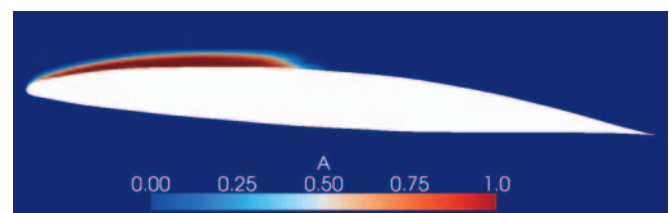
Fig. 3. *Vapor volume fraction distribution around NACA66(MOD), Inlet velocity = 2.5 m/s. Outlet cavitation number = 0.91*
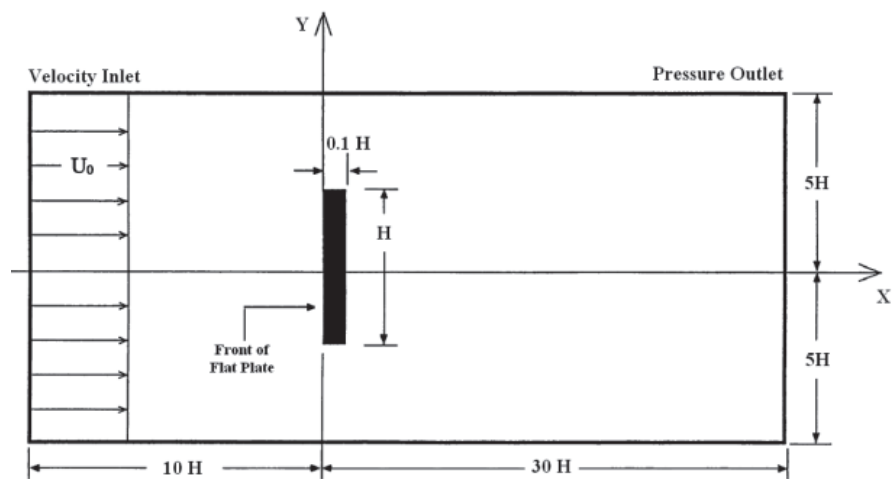
Fig. 4. *Implied computational domain, boundary conditions and coordinate system for simulation of cavitation around the flat plate*
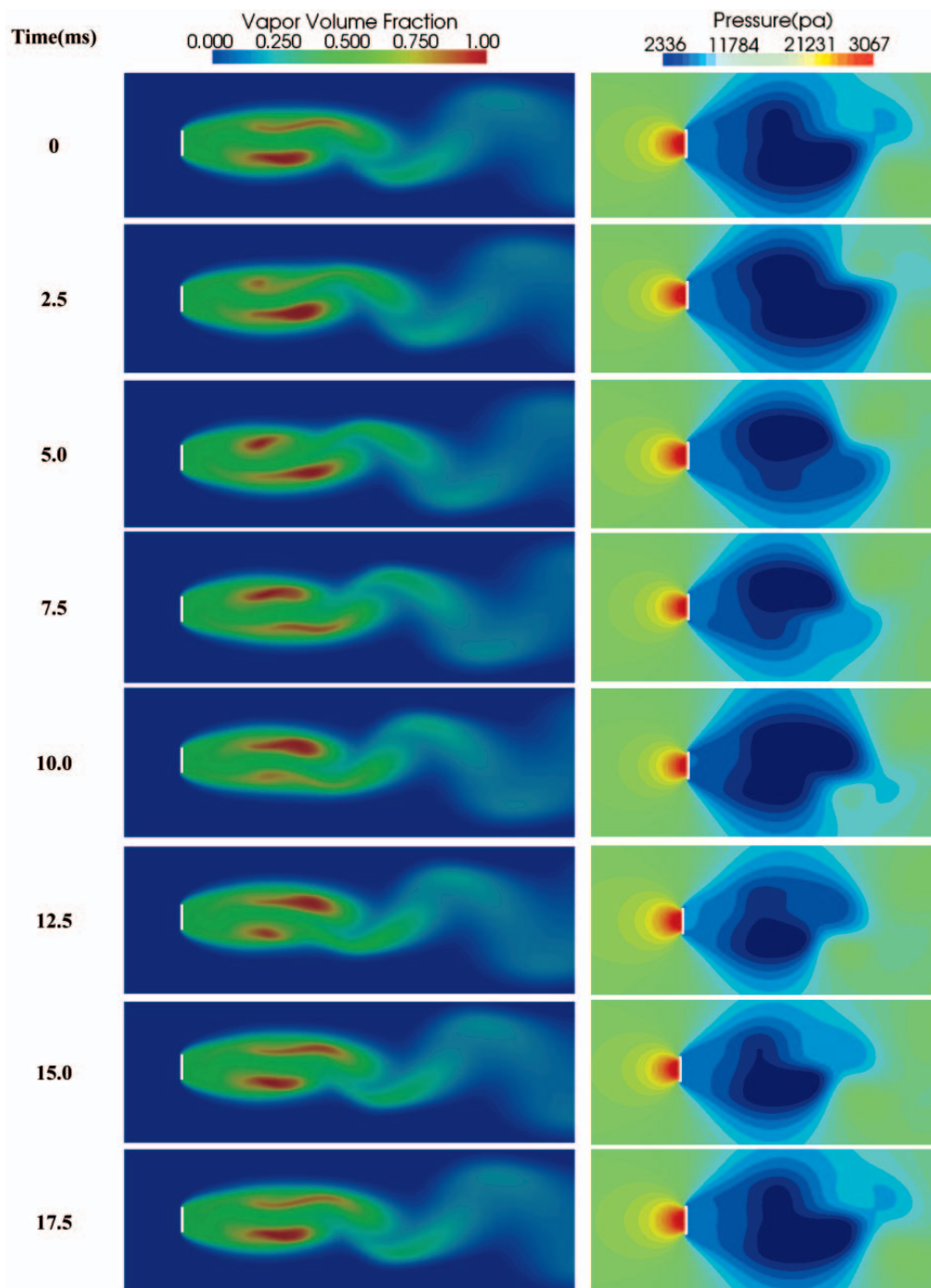
Fig. 5. *Vapor volume fraction and pressure distribution around the flat plate Inlet velocity = 5 m/s. Outlet cavitation number = 1.0*

Flat Plate

Geometry and Boundary Conditions

The used computational domain and geometry are presented in Fig. 4. The plate has height H and thickness 0.1H where H is equal to 0.1 m. The boundaries of upstream and downstream are located at 10H and 30H. The upper and lower boundaries are located at 5H from the center of plate. The constant velocity inlet and constant pressure outlet are considered as inlet and outlet boundaries. The main results are obtained by considering outlet cavitation number equal to 1.0 and 1.25, and velocity inlet equal to 5m/s.

Unsteady behavior of cavitation

For considering unsteady behavior of fully cavitating flows behind the flat plate, the formation of cavitation and its oscillations are presented in Fig. 5. The considered cavitation number is equal to 1.0 at the outlet boundary. As presented in Fig. 5, supercavitation is formed behind the flat plate in these conditions. At the end of this cavity, the two phase vortex shedding occurs, and vapor is separated from cavity by vortexes and moved to the down stream. The cycle of this separation occurs in 17.5 ms. Therefore, the frequency is equal to 57.14 Htz. Along with the vapor contours, pressure contours are presented in Fig. 5, which shows the same oscillating behavior.

Cavity Dimensions

One of the most important characters of supercavitating flows is their cavity dimensions. The cavity dimensions are usually normalized by the height of the flat plate. The vapor iso-surfaces are presented in Fig. 6. In this figure, one snapshot of periodic behaviors of each cavitation number is presented. By using these vapor iso-surfaces, average cavity length and width can be estimated. Besides, non-dimensional cavity length and width are presented in Fig. 7 and Fig. 8. At the

small values of cavitation number, most of the flow domain contains vapor phase. In these situations, the re-entrant jet and vapor volume fraction distributions inside the cavity are much more complicated than sub-cavitation flows. The obtained results for cavity dimensions are compared with experimental results reported by Waid [25]. One of the basic objectives of this paper is to improve simulation of supercavitating flows. For this reason, the obtained results are also compared with other numerical simulations [26]. By this comparison, it is clear that the implied method improves accuracy of supercavitation simulations considerably.
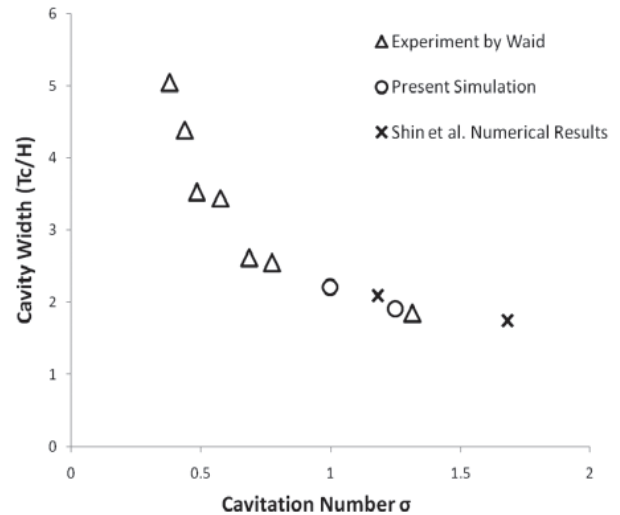
Fig. 7. *Cavity width defined by α = 0.5 for several cavitation number Experimental data by Waid [25], Shin et al. numerical results[26]*

Drag Forces

Drag force variation is another important character of cavitating flows. In the flow around of the flat plate, drag force is mainly pressure drag force. The average pressure distributions around the flat plate is presented in Fig. 9. By integrating these pressure distributions, average drag forces can be obtained.

$$\sigma = 1.0$$
$$L_c/H = 6.2$$
$$T_c/H = 2.2$$

$$\sigma = 1.25$$
$$L_c/H = 2.8$$
$$T_c/H = 1.9$$
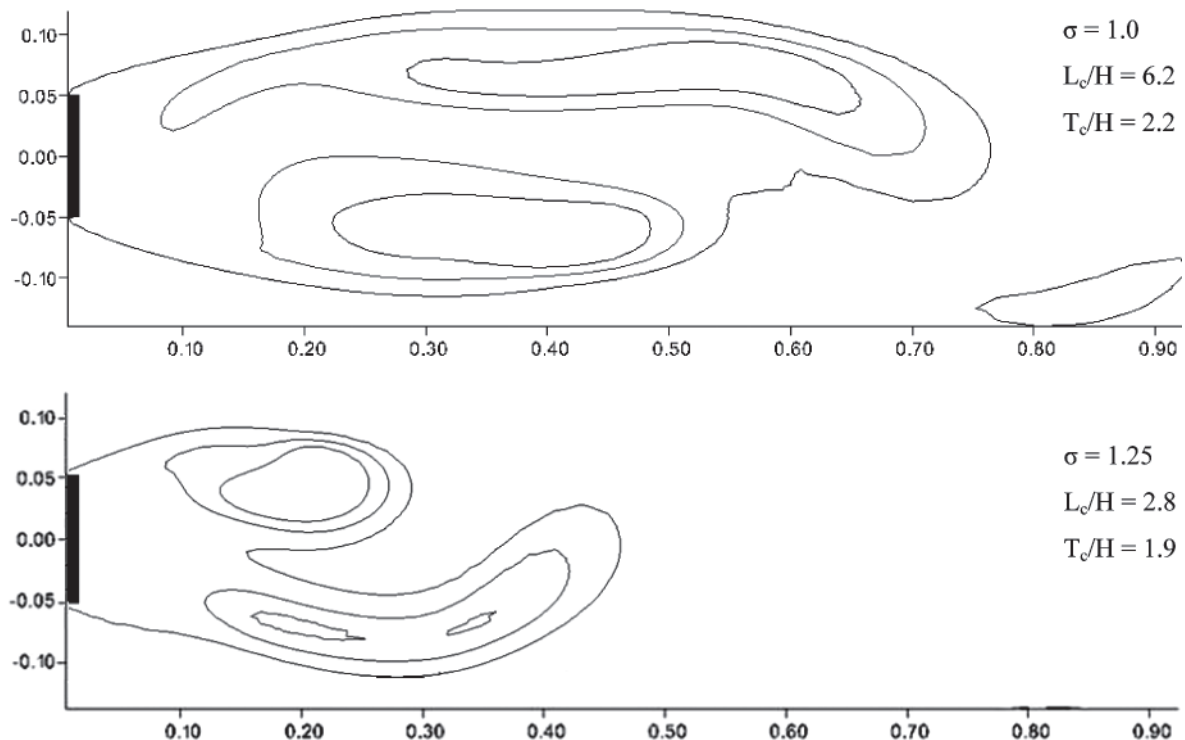
Fig. 6. *Vapor volume fraction Iso-surface and cavity dimensions around the flat plate Inlet velocity = 5 m/s, Outlet cavitation number = 1.0, 1.25*
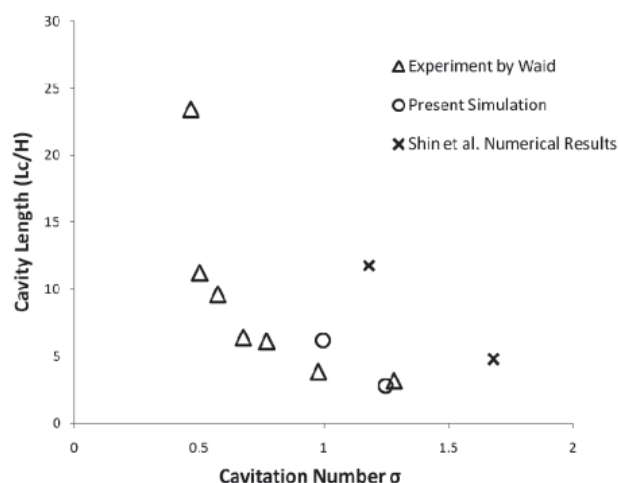
Fig. 8. *Cavity length defined by α = 0.5 for several cavitation number Experimental data by Waid [25], Shin et al. Numerical results[26]*
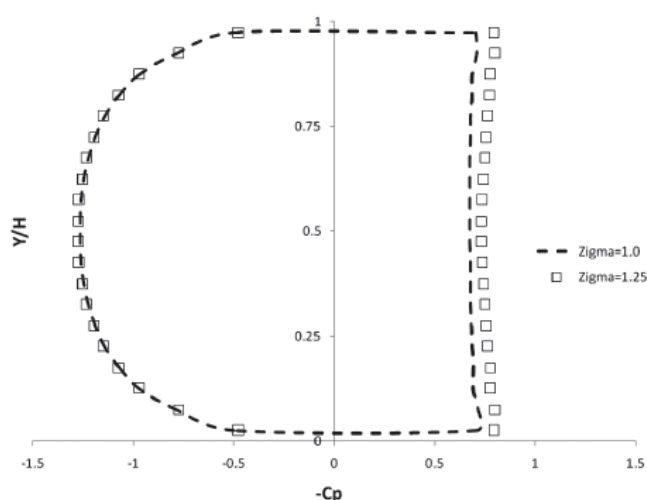
Fig. 9. *Average pressure coefficient distribution of the 2d flat plate for several cavitation number*

In the flow around the flat plate, the drag force consists of the front force implied in the front of plate, and the back force. In the Fig. 10, the unsteady behavior of these two drag forces, and total drag force are presented for one cycle. From this figure, it is obvious that variations of these forces are similar. The average forces for the front and back of the plate, and also the total drag force can be obtained from this figure. By using the average of the total drag force, part (c) of Fig. 10, and the reference velocity and density values, the average drag coefficient can be calculated. In the Fig. 11, variations of average drag coefficient against cavitation number are presented. In this figure, the free stream prediction [12], Shin et al. numerical results [26] and experimental results by Waid [25] are presented together with present numerical results.

Beside the undesirable aspects of cavitating flows such as noise and erosion, the developed cavity can reduce drag forces, especially in supercavitating flows. This beneficial aspect of cavitating flows can help to increase the velocity of vehicles in constant power. When speed of vehicle isn't enough to create supercavitation naturally, Ventilation can be used to create or to enhance a supercavity called ventilated cavitation. In the Fig. 11, it is presented that by development of cavitation and reduction of cavitation numbers of the flow, drag force reduces. The summery of obtained numerical results for simulation of cavitation around the flat plate are presented in Tab. 1.
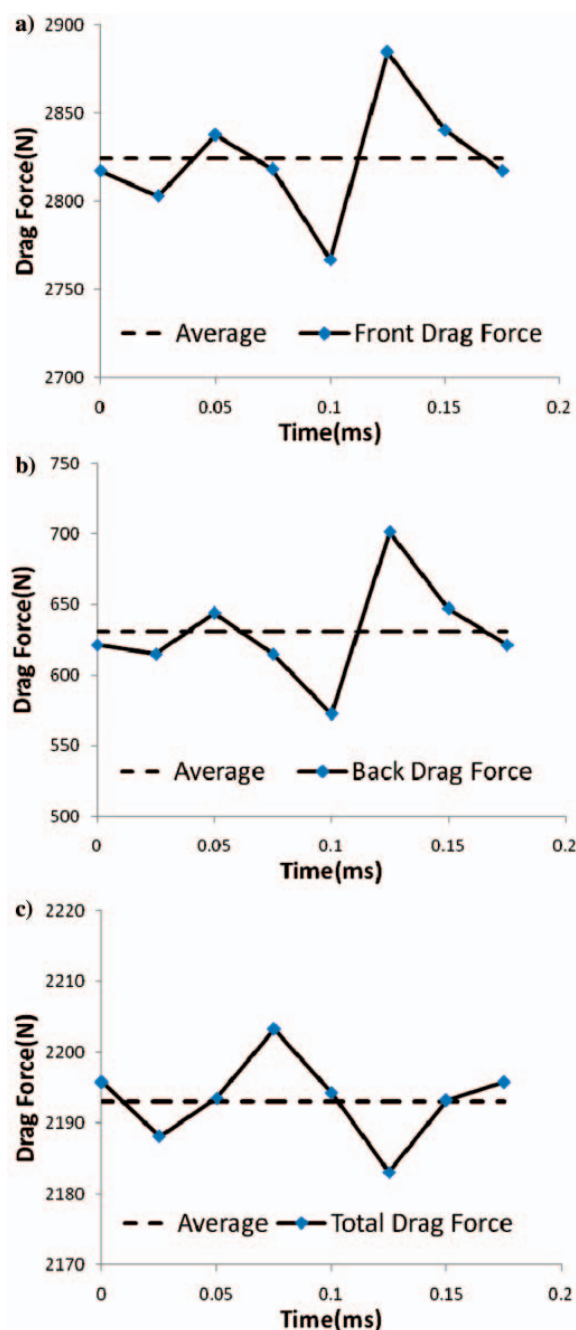
Fig. 10. *Unsteady behavior of the front (a), back (b) and total drag force (c) of the 2d flat plate Inlet velocity = 5 m/s, Outlet cavitation number = 1.0*
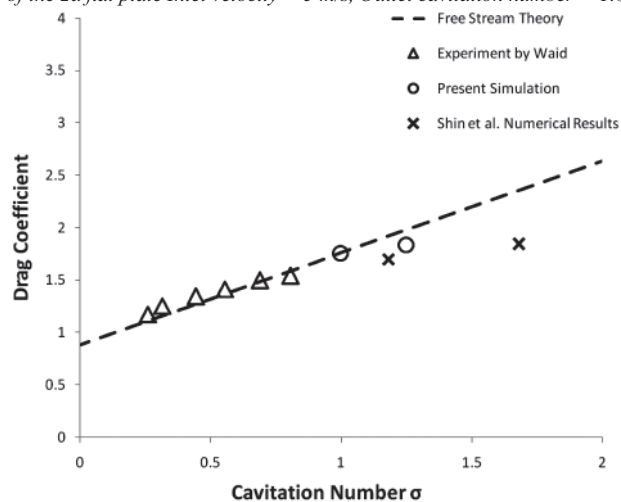
Fig. 11. *Average drag coefficient of the 2d flat plate for several cavitation number Experimental data by Waid [25], Shin et al. Numerical results[26], Free Stream Theory[12]*

Tab. 1. The summery of obtained results for simulation of cavitation around the flat plate

σ	Re_∞	L_c/H	T_c/H	Ave. Drag Force (N)	Ave. Drag Coefficient
1.0	5×10^5	6.2	2.2	2193	1.75
1.25	5×10^5	2.8	1.9	2888	1.83

Tab. 2. The comparison between cavitating and non-cavitating simulation results

	Cavitation Simulation Results		Non-Cavitation Simulation Results	
σ	Ave. Drag Force (N)	Ave. Drag Coefficient	Ave. Drag Force (N)	Ave. Drag Coefficient
1.0	2193	1.75	3903	3.12

It seems necessary to estimate gain accuracy via simulation of cavitation in a flow. For this reason, the simulated cavitating flows are compared with results of non-cavitating simulations. This comparison shows simulation of cavitation can provide more accurate results for drag force, periodic behavior, and pressure distributions. The comparison between caviatiting numerical results and non-cavitating numerical results are presented in Tab. 2.

CONCLUSIONS

− Unsteady simulations have been performed for 2D cavitating flows. For phase change modeling, the Bubble dynamics cavitation model is utilized, which is presented as the source terms in the volume of fraction equation and the continuity equation. The non-conservative PISO method is used to solve coupling between the continuity and N.S. equations. Unsteady behavior of cavitation around a flat plate oriented normal to flow direction, and sheet cavitation around a NACA66(MOD) hydrofoil are performed to demonstrate the accuracy of the selected algorithm.

− Based on the implied phase change model, the supercavitating flow behind the flat plate has been simulated in a good agreement with the experimental results. The size of the vapor region and the separation of the cavitation are clearly predicted by the developed CFD-code. These predictions provide information that will be helpful for understanding behaviors of unsteady cavity flows such as cavitation occurrence and development. The effects of vapor generation on drag reduction are investigated and presented. It is presented that by growth of cavity and reduction of cavitation number, the drag force reduces.

− The results of the unsteady simulation show the development of a re-entrant jet and two-phase vortex shedding. The predicted cavity dimensions, drag coefficients and pressure distributions show a very good agreement with the experiments.

NOMENCLATURE

C   – hydrofoil chord
CFL – courant number
C_p – pressure coefficient
g_i – gravity
H   – plate height
K   – termal expansion coefficient

L_c – cavity average length
n_0 – average nucleus per liquid volume
P   – pressure
P_{sat} – saturation pressure
$\dot{q}$ – energy source term
R   – gas constant (eq. ())
R   – nucleus radius
Re   – reynolds number
S_α – vapor phase change term
t, t_∞ – time, mean flow time scale
T   – temperature
T_c – cavity maximum thickness
u_i – cartesian velocity components
U   – velocity
x_i – cartesian coordinates

α – volume fraction
β – termal expansion coefficient
σ – cavitation parameter
$\dot{\phi}$ – energy dissipation term
μ – viscosity
ρ – density

subscripts, superscripts
∞ – free stream
m   – mixture
l   – liquid phase
v   – vapor phase
sat   – saturation condition
i, j   – coordinate indices

BIBLIOGRAPHY

1. Wiesche S.: *Numerical simulation of cavitation effects behind obstacles and in an automotive fuel jet pump*, Heat Mass Transfer, 2005.
2. Frobenius M. and Schilling R.: *Three-Dimensional unsteady cavitating effects on a single hydrofoil and in a radial pump-measurement and numerical simulation*, Cav03-GS-9-005, Proceedings of the 5th international symposium on cavitation, Osaka, 2003.
3. Singhal A.K., Vaidya N. and Leonard A.D.: *Multidimensional simulation of cavitating flows using a PDF model for phase change*, ASME Fluids Engineering Division Summer Meeting, ASME Paper FEDSM97-3272, 1997.
4. Kubota A., Kato H., Yamaguchi H.: *A New Modeling of Cavitating Flows: A Numerical Study of Unsteady Cavitation on a Hydrofoil Section*. J. Fluid Mech. 1992
5. Senocak I., Shyy W.: *Evaluation of cavitation models for Navier-Stokes computations*, Proceeding of FEDSM 02, ASME fluid engineering division summer meeting, Montreal, Canada, 2002

6. Von Karman T.: *Accelerated flow of an incompressible fluid with wake formation*, Ann. Mathem. Pura Applic. IV(29), 1949

7. Woods L.C.: *Unsteady plane flow past curved obstacle with infinite wakes*. Proc. Roy. Soc. A 229, 1955

8. Wu T.Y.T.: *Unsteady supercavitating flows*. Proc. 2nd Int. Symp. on Naval Hydrodynamics, 1958

9. Timmam R.: *A general linearized theory for cavitating hydrofoils in non steady flow*. Proc. 2nd Int. Symp. on Naval Hydrodynamics, 1958

10. Geurst J.A.: *Some investigations of a linearized theory for unsteady cavity flows*. Arch. Rat. Mech. Anal. 5(4), 1960.

11. Tulin M.P., Hsu C.C.: *New applications of cavity flow theory*. Proc. 13th Int. Symp. on Naval Hydrodynamics, Tokyo, 1980

12. Knapp R.T., Daily J.W., Hammitt F.G.: *Cavitation*. McGraw-Hill Book Co, New York, 1970

13. Kinnas S.A.: *The prediction of unsteady sheet cavitation*. Proc. 3rd Int. Symp. on Cavitaton, Vol. 1, Grenoble(France), 1998

14. Franc J.P., Michel J.M.: *Fundamental of cavitation*, Kluwer Academic Publishers, 2004.

15. Moukalled F. and Darwish, M.: *A Unified Formulation of the Segregated Class of Algorithms for Fluid Flow at All Speeds*, Numer. Heat Tr. B-Fund, 37, 2000

16. Delannoy Y., Kueny J.L.: *Two-phase flow approach in unsteady cavitation modelling*. Cavitation and Multiphase Flow Forum, FED ASME 98, 1990

17. Sauer J.: *Instationär kavitierende Strömungen - Ein neues Modell, basierend auf Front Capturing (VoF) und Blasendynamik*. Universität Karlsruhe, 2000

18. Senocak I., and Shyy W.: *Numerical Simulation of Turbulent Flows with Sheet Cavitation*, CAV2001, Proc. 4th International Symposium on Cavitation, CAV2001A7.002, California Institute of Technology, Pasadena, CA, 2001

19. Jahanbakhsh E., Panahi R. & M.S. Seif: *Numerical Simulation of Three-Dimensional Interfacial Flows*, International Journal of Numerical Methods for Heat & Fluid Flow, Issue 4, 2007

20. C.M. Rhie and W.L. Chow: *Numerical study of the turbulent flow past an airfoil with trailing edge sepration*, AIAA J, 1525, 1983

21. Issa, R.I.: *Solution of the Implicitly Discretized Fluid Flow Equations by Operator-Splitting*, J. Comput. Phys., 62, 1985

22. Kunz R.F., Boger D.A., Stinebring D.R., Chyczewski T.S., Lindau J.W., Gibeling H.J., Venkateswarn S., Govindan T.R.: *A pre Preconditioned Navier–Stokes method for two-phase flows with application to cavitation prediction*. Computers & Fluids, 2000

23. Shen Y. J. and Dimotakis P. E.: *The Influence of Surface Cavitation on Hydrodynamic Forces*, Proc. 22nd ATTC, St. Johns, 1989

24. Waid RL: *Water tunnel investigation of two-dimensional cavities*. In: Knapp RT, Daily JW, Hammitt FG (eds) Cavitation. McGraw-Hill Book Co, New York, 1957

25. Shin B.R., Iwata Y., Ikohagi T.: *Numerical simulation of unsteady cavitating flows using a homogenous equilibrium model*, J. Comput. Mechanics. 2003

CONTACT WITH THE AUTHORS
M.S. Seif, Prof.
A. Asnaghi, Research Assistant,
E. Jahanbakhsh, Research Assistant,
Sharif University of Technology
11155-9567, Azadi Avenue,
Tehran, IRAN
email: seif@sharif.edu

On the possible increasing of efficiency of ship power plant with the system combined of marine Diesel engine, gas turbine and steam turbine in case of main engine cooperation with the gas turbine fed in series and the steam turbine

Marek Dzida, Assoc. Prof.
Jerzy Girtler, Prof.
Gdansk University of Technology
Sebastian Dzida, M. Sc.
Petrobaltic S.A.

ABSTRACT

The article presents a concept of a combined large power ship propulsion system consisting of the leading Diesel main engine, associated with a power gas turbine and the steam turbine system which utilise the energy contained in the exhaust gas leaving the Diesel engine. In the examined variant of the combined system the power turbine is fed in series with the exhaust gas. A calculation algorithm is given along with the results of calculations of particular subsystems of: the turbocharging system, the power gas turbine, and the steam turbine cycle. Assumptions and limits adopted in the calculations are presented. Selected system parameters were confronted with the results of experimental investigations available in the literature. The power optimisation of the entire combined ship power plant was only performed taking into account the thermodynamic point of view, leaving aside technical and economic aspects. Numerical calculations were performed for the 52 MW low-speed Diesel engine produced by Wärtsilä.

Keywords: Ship power plants; combined systems; Diesel engine; gas turbine; steam turbine

INTRODUCTION

The low-speed main engine used for driving a ship has the highest efficiency of all heat engines. What is more, it burns the cheapest residual fuel. However, there are some problems with keeping the emission of harmful substances by this engine to the atmosphere at a permissible level.

The article analyses a variant in which the turbocharger and the power turbine are connected in series. An option was also taken into account in which the exhaust gas was utilised in the waste heat boiler working for the steam turbine.

The analysed combined power plant consists of a Diesel engine 9RTA-96C, identical to that discussed in [2, 3], the power turbine, fed in series, and the steam system with a steam turbine. Additional power of the propulsion system, obtained both from the power turbine and the steam turbine, is transmitted to the ship propeller shaft via a mechanical gear. Behind the turbocharger, a power gas turbine is installed in series, from which the exhaust gas flows through the waste heat boiler producing the steam to drive the steam turbine. Steam consumption for ship's own needs was taken into account in the calculations.

For the assumed efficiency of the turbocharger and the power turbine, the power of the gas turbine was calculated, while the steam turbine cycle was optimised with respect to the maximum power of the adopted two-pressure waste-heat boiler. The optimisation of the steam turbine system took into account limits resulting from practical solutions used in power transmission systems.

CONCEPT OF A COMBINED SYSTEM – SERIES FEEDING OF POWER TURBINE

The combined cycle includes an additional power turbine and a waste heat boiler which produces the steam for ship's own needs and for an additional steam turbine. The use of the power gas turbine is possible due to high efficiency of the turbochargers, which makes it possible to increase the pressure of the gas behind the turbocharger turbine. This pressure is higher than the pressure of the exhaust gas in front of the waste heat boiler, which results from pressure losses connected with the flow of the exhaust gases through the boiler. The pressure difference between these two pressures provides opportunities for the use of an additional gas turbine, bearing the name of the power turbine, in the system.

This solution leads to the increase of power of the entire power transmission system, as the volume of fuel delivered to the Diesel engine does not change, while both the power turbine and the steam turbine deliver additional power.

It results from operating low-load tests of conventional power transmission systems with Diesel engines with turbocharging that the amount of the exhaust gas in the
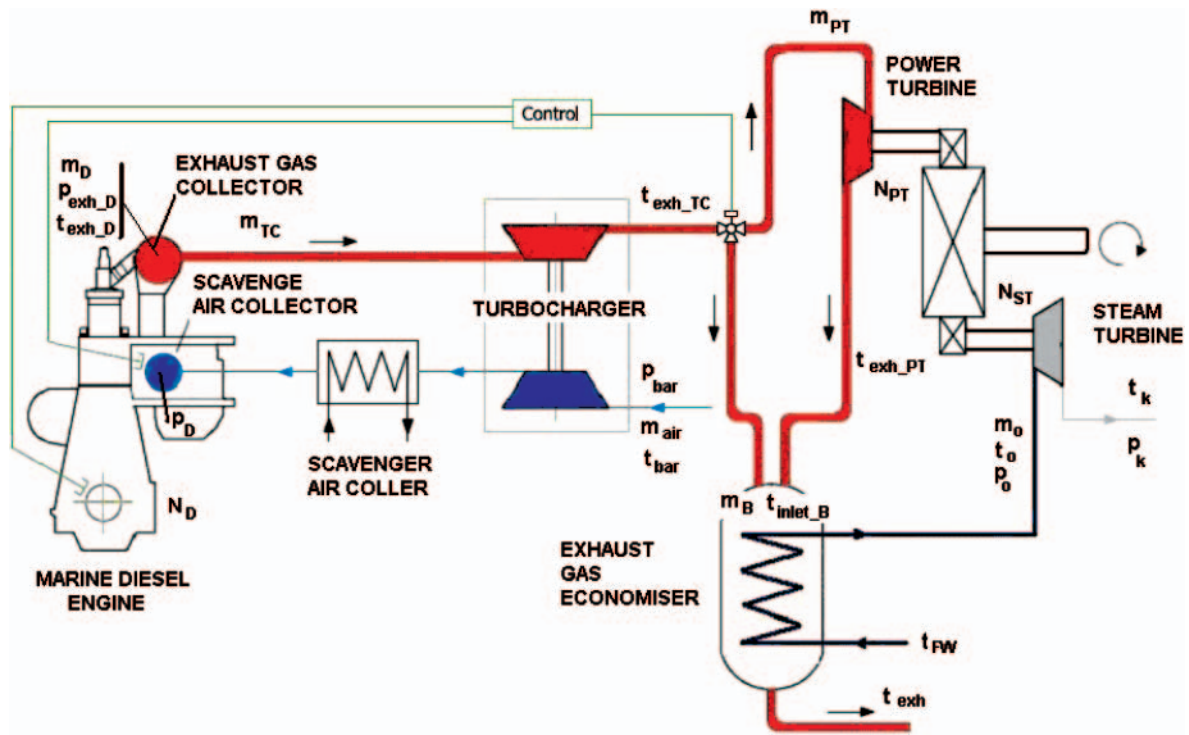
Fig. 1. Combined ship power transmission system

turbocharger is not sufficient to secure stable engine operation. In that case additional air blowers, situated at engine inlet, are started. That is why the proposed combined power transmission system should have power turbine bypass pipes (Fig. 1) which direct the exhaust gas from the turbocharger to the waste heat boiler during low-load intervals. This system will be controlled automatically by a valve for which the control signal will be the pressure of the turbocharging air, the engine torque, or the angular speed of the propeller shaft. This control system also seems to provide opportunities for the operation of the ship power transmission system without the power turbine. A possibility to switch off the power turbine results in the increase of the turbocharger's power output, which further leads to the increase of both the turbocharging pressure and the volume of the turbocharging air, all this increasing the ability to manoeuvre the engine, in particular fast reaching the maximum power at important moments of power transmission system operation points. Also in cases of large power of the main (piston) engine, increasing the power of the power turbine may lead to the decrease of the power of the turbocharger, thus increasing the power of the entire power transmission system.

OPERATING PARAMETERS OF THE MAIN ENGINE TURBOCHARGER

The engine 9RTA-96C has constant-pressure turbocharging [5]. Three PCL-type turbochargers were produced by ABB. From the exhaust gas collector the exhaust gas, having the temperature t_{exh_D} and the pressure p_{exh_D} flows directly to the turbochargers. In the catalogue the producer [5] does not present all parameters concerning turbocharging. In further calculations the temperature t_{exh_D} and the pressure p_{exh_D} of the exhaust gas in the exhaust collector were assumed based on the analysis reported in [2].

It was assumed in turbocharging calculations for the combined system that the power needed for driving turbocharger turbines is sufficiently large if the pressure behind the turbocharger turbine is higher than the inlet pressure of the exhaust gas in the waste heat boiler.

The pressure of the exhaust gas behind the turbocharger is calculated from its power balance:

$$\pi_T = \left[\cfrac{1}{1 - \cfrac{1}{\eta_{TC}} \cdot \cfrac{m_{air}}{m_{TC}} \cdot \cfrac{c_a}{c_g} \cdot \cfrac{t_{bar}}{t_{inlet\_TC}} \cdot \left(\pi_C^{\frac{\kappa_s - 1}{\kappa_s}} \right)} \right]^{\frac{\kappa_g}{\kappa_g - 1}}$$

$$p_{exh\_TC} = \frac{p_{exh\_D}}{\pi_T} \qquad (1)$$

where:

$\pi_C = p_{exh\_C}/p_{bar}$ is the compression ratio in the turbocharger compressor

$\pi_T = p_{exh\_TC}/p_{exh\_D}$ is the expansion ratio in the turbocharger turbine.

The efficiency of the turbocharger was defined as:

$$\eta_{TC} = \eta_C \cdot \eta_T \cdot \eta_m \qquad (2)$$

The compressor efficiencies η_C and η_T in the above formula were determined in the following way: the compressor efficiency was calculated from the line of cooperation of the engine RTA-96C with the ABB compressor. Changes of turbocharger turbine efficiency were calculated from MAN B&W experimental tests [4]. It was assumed that the efficiency of the ABB turbine changes in the similar way. This relation made the basis for determining the efficiency of the ABB turbocharger turbine cooperating with the engine 9RTA-96C as a function of its load. The results are shown in Fig. 2.

The temperature of the exhaust gas leaving the turbocharger turbine was calculated from the transformed formula which defines the turbine efficiency as:

$$t_{exh\_TC} = (t_{exh\_D} + 273.15) \cdot \left[1 - \eta_T \left(1 - \frac{1}{\pi_{TC}^{\frac{\kappa_g - 1}{\kappa_g}}} \right) \right] - 273.15 \qquad (3)$$
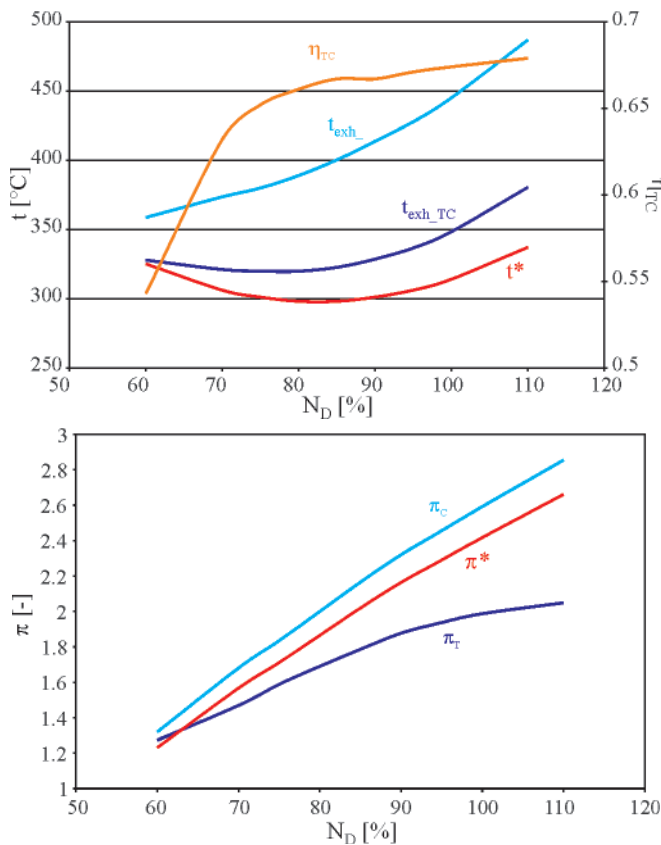
Fig. 2. *Characteristics of turbocharger parameters as function of main engine load: **t*** - turbocharger outlet temperature in a standard engine (producer's data), **π*** - expansion rate in the turbocharger turbine (producer's data)*

It results from the performed calculations that when the load is larger than 65%, the operation of the power turbine in the system is possible, Fig. 2. For the presently used turbochargers the turbocharger turbine power is reached at low compression. The excess pressure of the exhaust gas can be expanded in the additional power turbine.

POWER TURBINE CALCULATIONS

In the adopted concept of the combined power transmission system, Fig. 1, the power turbine is situated behind the turbocharger. The exhaust gas from the turbocharger flows to the power turbine. The entire mass flow rate of the exhaust gas leaving the main engine expands in the power turbine, thus delivering extra power to the ship power transmission system.

The pressure behind the power turbine depends on the losses taking place during the flow through the waste heat boiler and outlet silencers. Following common practice, it was assumed in further calculations that the pressure behind the power turbine is by 3% higher than the barometric pressure, i.e.

$$p_{exh\_PT} = 1.03 \, p_{bar} \qquad (4)$$

The expansion ratio in the power turbine can be calculated as:

$$\pi_{PT} = \frac{p_{inlet\_PT}}{p_{exh\_PT}} \qquad (5)$$

The power of the power turbine was calculated from the following formula

$$N_{PT} = \eta_{PT} \cdot m_{PT} \cdot c_g \cdot t_{inlet\_PT} \cdot \left(1 - \frac{1}{(\pi_{PT})^{\frac{\kappa_g - 1}{\kappa_g}}} \right) \qquad (6)$$

It was assumed in the calculations that the power turbine efficiency η_{PT}, depends on the expansion ratio, according to the data presented by MAN B&W for the turbocharger turbine [1]. This assumption can be considered correct, as the producers make use of gas turbines installed in turbochargers as power turbines.

The temperature of the exhaust gas leaving the power turbine was calculated from the following relation:

$$t_{exh\_PC} = (t_{inlet\_PT} + 273.15) \cdot \left[1 - \eta_{PT} \left(1 - \frac{1}{\pi_{PT}^{\frac{\kappa_g - 1}{\kappa_g}}} \right) \right] - 273.15 \qquad (7)$$

The power turbine parameters were calculated using a computer programme (the source code is included as Appendix) taking into account the above assumptions. Fig. 3 presents the calculated values of the selected power turbine parameters as a function of the internal combustion engine load.

The use of the power turbine in the system resulted in power increase of the entire system from 3 to 9 %, compared to the standard engine power. The power of the power turbine increases with the increase of power of the internal combustion engine. It results from the performed calculations that when the load is smaller than 65 % of the internal combustion engine power, the power turbine cannot be used as its power nears zero. In this case the power turbine is to be disconnected from the system. This conclusion is in accordance with the results of turbocharging process calculations.
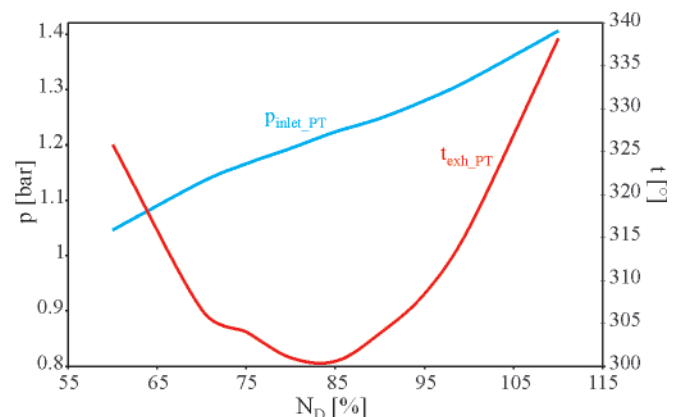
Fig. 3. *Selected power turbine parameters vs. main engine load*

STEAM CYCLE OPTIMISATION CALCULATIONS

In the analysed combined power transmission system, Fig. 1, the exhaust gas leaving the power turbine is directed to the waste heat boiler, where it produces steam used to meet ship's own needs and supply the steam turbine. The steam turbine transmits the power, via a gear, to the propeller shaft. The system of the steam turbine cycle was adopted following the description given in [2]. In the steam system a two-pressure waste heat boiler was used. The calculations were preformed using the computer programme [2] to search the maximum power of the steam turbine. The steam cycle was optimised for two main engine loads, i.e. for the power corresponding to 100% and 90% of the thermal load of the piston engine.

Table 1 collects the results of calculations for two internal combustion engine load regimes which corresponded to the maximum available power of the steam turbine. It results from the analysis of the steam cycle calculations performed for the examined combined power transmission system that the maximum available power of the steam turbine equals 7.25

or 7.96 % of the internal combustion engine load, depending on the load.

In practical application, the steam turbine system needs some limits to be placed on its parameters as a result of the adopted designing, constructional and operating assumptions. For the adopted limits [2] the steam power transmission system was optimised for the second time to find a solution for which the power of the steam turbine reaches its maximum. Tab. 1 presents the parameters of this system, obtained taking into account the adopted limits. Due to the limits in the steam turbine cycle we cannot utilise the entire power resulting form the calculations performed for the cycle without limits. The presented analysis of the steam cycle reveals that the additional use of the steam turbine in the combined system increases the power output of the system by about 6.5 ÷ 7.8 % and decreases the fuel consumption.

THERMODYNAMIC ANALYSIS OF THE COMBINED POWER TRANSMISSION SYSTEM

The application of the combined system in a classical ship power transmission system with a low-speed Diesel engine leads to the increase of power and to the decrease of the specific fuel consumption. Tab. 2 collects the results of calculations of particular components of the combined system. It results from the performed analysis that the sole use of a power turbine increases the power output of the system by 5.5 ÷ 7 %, depending on the Diesel engine load. At the same time the steam system alone (without the power turbine) increases the power output of the plant by 6.5 ÷ 7.5 %. In the complete combined system composed of the piston engine as a leading engine, the power turbine, and the steam turbine, the power output of the system increases by 12 ÷ 15 %. This power output increase is not generated by extra fuel delivered to the system but is connected with deep utilisation of the exhaust gas leaving the piston engine. This system also makes it possible to reduce the specific fuel consumption by 11 ÷ 13 % compared to the traditional power plant with an internal combustion engine.

COMPARING VARIANTS OF SHIP POWER TRANSMISSION SYSTEMS

Tabs 3, 4 and 5 show selected parameters of the calculated combined systems, which were taken from the above presented variants of the combined ship power transmission system composed of the main engine, and the power and steam turbine systems.

In the steam turbine cycle of the combined system, the cycle parameters differ little between each other in the analysed variants. The live steam temperature differs by 3°C in one case, while the live steam pressure also does not differ much. The pressure in the first stage of the boiler and in the degasifier, as well as the temperature of the exhaust gas leaving the power transmission system are the same for all variants, Tab. 3. The largest power output of the steam turbine cycle is reached in the combined system variant with the steam turbine and power turbine fed in series with the exhaust gas, Tab. 4. Differences in steam turbine power output for particular variants for 90% of the main Diesel engine load are approximately equal to 4%.

Tab. 1. Optimum steam cycle parameters in a combined cycle consisting of Diesel engine - power turbine (series feeding) - steam turbine

No	N_D [%]	t_o [°C]	p_o [bar]	p_I [bar]	t_I [°C]	p_g [bar]	t_{exh} [°C]	t_{FW} [°C]	x	m_o [t/h]	m_I [t/h]	m_u [t/h]	N_{ST} [kW]	N_{ST}/N_D
							without limits							
1	100	301	25.0	7.0	165	0.50	154	82	0.8753	15.02	11.17	1.93	4097	0.0796
2	90	286	23.0	7.0	165	0.50	153	82	0.8742	12.52	9.66	1.79	3361	0.0725
							with limits							
1	100	301	23.0	7.0	165	2.00	162	121	0.8786	15.79	10.78	3.85	3880	0.0754
2	90	286	23.0	7.0	165	2.00	164	121	0.8742	12.52	10.01	3.22	3193	0.0689

Tab. 2. Power output, efficiency and specific fuel consumption of the combined ship power transmission system with the two-stroke engine 9RTA 96C, power turbine (fed in series) and steam turbine

N_D [%]	N_D [kW]	N_{PT} [kW]	N_{PT}/N_D [%]	N_{ST} [kW]	N_{ST}/N_D [%]	$N_{PT}+N_{ST}$ [kW]	N_{combi}/N_D [%]	N_{combi} [kW]
100	51480	**3643**	**7.08**	**3880**	**7.54**	**7523**	**14.61**	**59003**
90	46332	**2572**	**5.55**	**3193**	**6.89**	**5765**	**12.44**	**52097**
N_D [%]	N_D [kW]	b_{ed} [g/kWh]	b_{ePT} [g/kWh]	$\Delta b_{ePT}/b_{eD}$ [%]	b_{eST} [g/kWh]	$\Delta b_{eST}/b_{eD}$ [%]	b_{ecombi} [g/kWh]	$\Delta b_{ecombi}/b_{eD}$ [%]
100	51480	**174**	**162.5**	**-6.61**	**161.8**	**-7.01**	**151.8**	**-12.75**
90	46332	**169.8**	**160.9**	**-5.26**	**158.9**	**-6.45**	**151.0**	**-11.07**
N_D [%]	N_D [kW]	η_D [%]	η_{PT} [%]	$\Delta\eta_{PT}/\eta_D$ [%]	η_{ST} [%]	$\Delta\eta_{ST}/\eta_D$ [%]	η_{combi} [%]	$\Delta\eta_{combi}/\eta_D$ [%]
100	51480	**48.43**	**51.89**	**7.08**	**52.11**	**7.54**	**55.54**	**14.61**
90	46332	**49.66**	**52.41**	**5.55**	**53.07**	**6.89**	**55.84**	**12.44**

Tab. 3. *Comparing steam cycle parameters for load equal to 90% of main engine power*

Combined system	t_o [°C]	p_o [bar]	p_I [bar]	p_g [bar]	t_{exh} [°C]	t_{FW} [°C]	x	m_o [t/h]	m_I [t/h]	m_u [t/h]
Steam turbine	289	19	7	2	165	121	0.88	15.02	7.15	2.86
Power turbine - fed in parallel	286	19	7	2	164	121	0.88	13.59	7.87	2.86
Power turbine - fed in series	286	23	7	2	164	121	0.87	12.52	10.02	3.22

Tab. 4. *Comparing power outputs for different variants of the combined system – with power output of the standard main engine as the reference*

Main engine power output		Main engine – steam turbine [2]		Main engine – power turbine – steam turbine			
				Feeding in parallel [3]		Feeding in series	
[%]		[kW]	[%]	[kW]	[%]	[kW]	[%]
Steam turbine	100	3823	7.43	3794	7.37	3880	7.54
	90	3182	6.87	3075	6.64	3193	6.89
Power turbine	100			3203	6.22	3643	7.07
	90			2211	4.77	2572	5.55

For combined system variants with the power turbine, the largest power is obtained in the variant with the power turbine fed in series, Tab. 4. In this cases the power output is higher by about 16.3 % compared to the power turbine from the variant of parallel turbine feeding with the exhaust gas for 90% of main engine load.

In the analysed variants the power output of the steam turbine is larger than that of the power turbine by 6.1 - 28.8 %, depending on the system variant and main engine load, Tab. 4.

Depending on the variant and main engine load, the application of the combined ship power transmission system makes it possible to increase the power output of the power plant by 6.9 – 14.6 % as compared to the conventional power plant, without delivering extra fuel, Tab. 5. The additional power output of the system is obtained by utilisation of the energy in the exhaust gas leaving the piston engine. This way the combined system reduces the specific fuel consumption by 6.4 – 12.8 % compared to the conventional power plant.

Depending on the adopted solution, the application of the combined power plant makes it possible to reach the assumed power output of the power transmission system at smaller main engine loads, thus reducing the 24-hour fuel consumption of the ship power plant. Tab. 6 presents, for the assumed power output of the ship power plant, the main engine power output and the reduction of the 24-hour fuel consumption, in relation to the conventional power plant, as a function of the adopted variant of the combined power plant.

Tab. 5. *Comparing different combined system variants*

		Main engine load	Main engine	Combined power transmission system		
				Steam turbine [2]	Power turbine fed	
					In parallel [3]	In series
System power output	[kW]	100 %	51480	55303	58477	59003
		90 %	46332	49514	51618	52097
$\Delta N_{combi}/N_D$	[%]	100 %		7.43	13.59	14.61
		90 %		6.87	11.41	12.44
be_{combi}/be_D	[g/kWh]	100 %	174.0	162.0	153.2	151.8
		90 %	169.8	158.9	152.4	151.0
$\Delta be_{combi}/be_D$	[%]	100 %		-6.91	-11.97	-12.75
		90 %		-6.43	-10.24	-11.07
Efficiency η_{combi}	[%]	100 %	48.43	52.05	55.05	55.54
		90 %	49.66	53.06	55.33	55.84
$\Delta\eta_{combi}/\eta_D$	[%]	100 %		7.43	13.59	14.61
		90 %		6.87	11.41	12.44

Tab. 6. *Reduction of 24-hour fuel consumption of the 49500 kW ship power plant for particular combined system variants*

		Conventional power plant	Combined system		
		D	D & ST [2]	D & PT & ST - feeding:	
				In parallel [3]	In series
Main engine load	[kW]	49500	46319	44701	44345
	[%]	96	90	86.8	86.1
24-hour fuel consumption	[t/24 h]	205	189	181	179
Fuel consumption reduction	[t/24 h]	-	16	24	25.8
	[%]	-	7.8	11.7	12.6

FINAL CONCLUSIONS FROM THE ANALYSIS OF COMBINED SHIP POWER TRANSMISSION SYSTEM VARIANTS

- It results from the analysis of the optimised combined ship power transmission system that the highest efficiency is obtained when particular power transmission system components are used:
  - diesel engine with maximum efficiency
  - turbocharger. Most highly efficient turbocharger is to be used, to provide opportunities for reducing the exhaust gas pressure at its outlet, and, consequently, increasing the power of the power turbine
  - power turbine. High efficiency power turbine is required to increase its power output
  - steam turbine cycle. The waste heat boiler is expected to reveal low exhaust gas flow losses (they decrease the expansion end pressure in the power turbine) and small temperature concentration in boiler evaporators (pitch point). Observed is the high impact of sulphur content in the fuel on the permissible temperature of the exhaust gas and the low temperature limit for the supply water. The least possible number of heat exchangers (none, as an ideal case) is to be used in the steam turbine cycle. The optimum parameters of this cycle also depend on the piston engine load.

- The power transmission system of the combined ship power plant of a big transoceanic container ship, consisting of the main Diesel engine, the power turbine and the steam turbine, makes it possible to:
  - increase the power plant power output by 6.9 ÷ 14.6 % compared to the conventional power plant, without delivering extra fuel
  - increase the power efficiency of the power plant from 53 % to about 56 % (which, so far, was impossible to reach by the internal combustion engine alone) depending on the applied variant of the combined power plant. Reducing the content of sulphur in the fuel provides opportunities for reaching higher efficiencies resulting from larger power of the steam turbine – lower temperature of the exhaust gas leaving the waste heat boiler
  - reduce the specific fuel consumption by 6.4 ÷ 13 %, without delivering extra fuel, as a consequence of the increased power output compared to that of the conventional power plant
  - use the internal combustion engine having lower power output, due to the extra power obtained in the combined system, or to reach 100% of power output of the power plant when the Diesel engine load is at an approximate level of 90%.

- In the article, only thermodynamic analysis of the power plant is presented, without additional technical and economic analyses, which could fully justify the application of this power plant system for driving a large container ship.

NOMENCLATURE

b_e	-	specific fuel oil consumption
c_g, c_a	-	specific heat of exhaust gas and air
i	-	specific enthalpy
m	-	mass flow rate
N	-	power
p	-	pressure
T, t	-	temperature
Wu	-	caloric value of fuel oil
χ	-	steam dryness ratio
η	-	efficiency
κ_g, κ_a	-	isentropic exponent of exhaust gas and air

Indices

bar	-	barometric conditions
B	-	boiler
combi	-	combined system
D	-	marine diesel engine, supercharging
f	-	fuel
inlet	-	inlet duct
k	-	parameters in a condenser
o	-	live steam, calculation point
air	-	air
ss	-	ship living purposes
π	-	compression ratio in a compressor, expansion ratio in a turbine
C	-	compressor
g	-	exhaust gas
T	-	turbine
TC	-	turbocharger
PT	-	power turbine
ST	-	steam turbine
exh	-	outlet duct
FW	-	water supplying a waste-heat boiler

BIBLIOGRAPHY

1. *A new turbocharger generation*. ABB Turbo Systems Ltd. Publication No. CH-Z 2035 98E.
2. Dzida M.: *On the possible increasing of efficiency of ship power plant with the system combined of a marine diesel engine, gas turbine and steam turbine, at the main engine-steam turbine mode of cooperation.* PMR No 1(59), Vol. 16, 2009
3. Dzida M., Mucharski J.: *Possible ways of increasing the efficiency of the ship power plant with the piston internal combustion engine - gas turbine - steam turbine system in case of main engine cooperation with the gas turbine fed in parallel and the steam turbine.* PMR No 2(60), Vol. 16, 2009
4. Schrott K. H.: *The New Generation of MAN B&W Turbochargers.* MAN B&W Publication S.A. 236 5581E. 1995
5. *Sulzer RTA 96C. Engine Selection and Project Manual.* June 2001. Wärtsilä.

CONTACT WITH THE AUTHORS

Marek Dzida, Assoc. Prof.
Faculty of Ocean Engineering
and Ship Technology
Gdansk University of Technology
Narutowicza 11/12
80-233 Gdansk, POLAND
e-mail: dzida@pg.gda.pl

Assessing diagnostic applicability of heat release characteristics determined based on ship engine indicator diagrams

Stanisław Polanowski, Prof.
Polish Naval University

ABSTRACT

In order to determine indicator diagrams-based heat release characteristics, a single- zone model of net heat release was used for perfect gas. It was proved that when a constant value for isentropic exponent is assumed, the error in determining the characteristics can be limited to 1% at the nominal load. The effect of errors in determining the position of piston TDC, as well as that of gas passages and indicator valves on the calculated characteristics was evaluated. It was shown that for low-speed engines the effect of gas passages in negligible, while for medium-speed engines the characteristics reveal some deformations (waves), which are repeatable for an individual cylinder in the examined engine construction. The results of the performed investigations and analyses suggest possibility and advisability of the use of heat release characteristics in diagnosing ship engines, in particular low-speed machines.

Keywords: ship piston engines; indicator diagrams; heat release characteristics; diagnostic application

INTRODUCTION

Since the production of the combustion pressure analyser NK-5 by Autronica, and the analyser Cyldet 1800 by ABB in the seventies of the last century, the range of use of the information contained in the indicator diagrams has not changed.

For the time being, the main functions executed by pressure analysers include: calculating average indicated pressure, determining maximum combustion pressure, recording TDC pressure, and the presentation of the determined values in the tabularised form and histograms, as well as the presentation and comparison of indicator diagrams on a monitor screen. Some analysers have also included an option of determining the rate of combustion pressure building up.

Diagnostic inference based on tables of parameters, histograms and comparison of indicator diagrams is rather unreliable and highly inaccurate. Hence, some monitoring and diagnostic systems have included an additional option of pressure measurement and analysis in the fuel injection system.

Perception of the diagnostic information contained in the indicator diagram can be extended by making use of heat release characteristics determined based on the indicator diagrams.

SELECTING THE HEAT RELEASE MODEL

It is Paul Henry Schweitzer [5] who is believed to be the author of the first heat release model for the Diesel engine [1, 4]. Remarkable development of advanced calculation models, observed since the late fifties of the last century, is connected with the appearance of possibilities for computer aided data processing and computer simulations.

At present, model investigations of combustion processes make use of complicated, multidimensional models of heat release processes. For instance, most advanced models include simulation programmes KIVA worked out in the Los Alamos National Laboratory. These model are characterised by a large number of immeasurable quantities and parameters, and their use requires high computational potential.

The simplest and most frequently used model which calculates heat release in a Diesel engine based on indicator diagrams is believed to be the single-zone model developed by Krieger and Borman [1, 4]. It is assumed in this model that at each time instant the working medium (charge), having the form of uniform mixture of air and combustions products, is in the state of thermodynamic equilibrium.

The first law of thermodynamics in the differential form for an open system can be written as:

$$dQ_{sp} - dQ_{ch} - dQ_r = dQ_n = dU + dW \qquad (1)$$

where:

dQ_{sp} — heat released as a result of fuel combustion
dQ_{ch} — heat of cooling
dQ_r — heat lost as a result of transfer of substances through system boundaries
dQ_n — net heat release
dU — internal energy of the charge
dW — work done by the system.

The heat Q_r is the result of fuel flow to the cylinder and gas scavenge through piston rings and valves.

The quantities Q_{ch} and Q_r cannot be determined in operating conditions due to the lack of required measurable data. Therefore for diagnostic purposes it is advisable to use net heat release characteristics Q_n.

The formula for heat dQ_n for perfect gas can be written as:

$$dQ_n = (\kappa - 1)^{-1} (V\, dp + \kappa\, p\, dV) \qquad (2)$$

where:
κ – adiabatic exponent
V – gas volume
p – gas pressure.

After dividing equation (3) by the displacement volume, the formula for the net heat release rate as a function of the crankshaft rotation angle takes the form:

$$q' = \frac{dq}{d\alpha} = (\kappa - 1)^{-1}\left(v\frac{dp}{d\alpha} + \kappa p \frac{dv}{d\alpha}\right) \qquad (3)$$

where:
v – dimensionless gas volume [3],
α – crankshaft rotation angle.

Here, the basic unit for the quantity q' is [J/m^3·° OWK].

The net heat release, q, in relation to the stroke volume and as a function of the crankshaft rotation angle, is expressed by the integral:

$$q = \int_0^\alpha q'\, d\alpha \qquad (4)$$

where the beginning of integration is assumed at BDC piston position.

ASSESSING THE EFFECT OF CHANGES OF THE EXPONENT κ ON THE ACCURACY OF THE DETERMINED CHARACTERISTICS

For both the air and the exhaust gas, the κ values almost linearly depend on the gas temperature (Fig. 1).
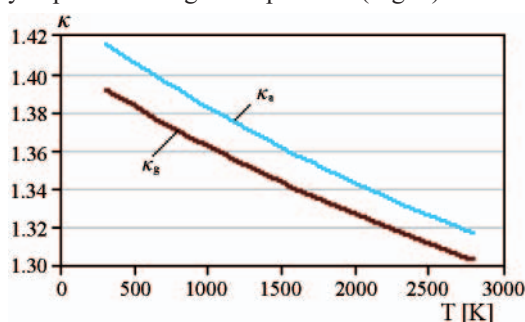

*Fig. 1. Adiabatic exponent **κ** vs. temperature **T**. The characteristic was made based on the approximation of tabularised data [7]: κ_a – dry air, κ_g – exhaust gas*

The effect of changes of the adiabatic exponent κ on q' can be taken into account using, for instance, the method of successive approximations. For the first approximation we assume a constant (average) value of κ. In the next calculation step the fuel consumption and the volume of the produced exhaust gas are assessed based on the heat release determined in the precious calculation step. Although it looks simple, this algorithm would make the calculation process take much longer without delivering any additional diagnostic information. The level or the possible error made when we stop at the first approximation of the characteristics is to be estimated.

The temperatures at characteristic points of the working cycle for ship engines are within the ranges of : 800-1100 K for the end of compression, 1700-2000 K for the end of combustion, and 900-1200 K for the end of expansion [6], which in total covers the temperature range of 800-2000 K. If we assume in the calculations that the value of κ is the average calculated for the middle temperature within the above range, then the errors which we make when determining the maximum value of q' do not exceed ± 3.5 %, and for q they do not exceed ± 2 %, which was checked on a number of types of ship engines. The scale of this error can be even more reduced (below 1 %) when we take into account the range of temperatures of the working medium which is characteristic for the examined type of engine and given load.

DEFORMATIONS OF CHARACTERISTICS INTRODUCED BY GAS PASSAGES AND INDICATOR VALVES

In order to recognise the nature of the effects of the gas passages and indicator valves on the heat release characteristics, a series of tests were performed on the research rig of the medium-speed engine Sulzer 6AL20/24. The arrangement and dimensions of the gas passages and the distribution of pressure sensors are schematically presented in Fig. 2, preserving relevant proportions.
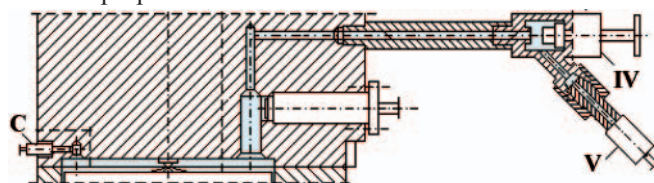
*Fig. 2. Scheme of indicator passages in the Sulzer engine 6AL20/24, with the distribution of pressure sensors: **IV** – indicator valve, **C** – Optrand pressure sensor in the cylinder **V** – Kistler pressure sensor on the indicator valve*

For technical reasons, the measurements were performed using pressure sensors of two different types and made by two different producers. The measuring paths were calibrated before the measurements and checked after the measurements for 100% and 50% of the nominal load of the engine. The sensors were installed on a special connector fixed to the indicator valve in such a way that during the calibration and final check their front plates were opposite to each other, at a distance of 5 mm. Differences in indications in the assumed range of measurement did not exceed ± 0.5 % of the maximum value of the measured pressure for the nominal load.

Before calculating the heat release characteristics, the indicator diagrams p_C and p_V (Fig. 4) were smoothed using the method of multiple approximation and a third-order power polynomial [2]. Without this procedure the heat release rate curves would not be readable. The smoothing removed (smoothed) the high-frequency measuring noise, Dp_{C1} and Dp_{V1}, introduced by the sensors, and the disturbances Dp_{C2}, Dp_{V2} generated by gas oscillation in the passages (Fig. 3).

The above smoothing is necessary to obtain sufficient smoothness of the heat release characteristics. However, it does not remove the deformation of the pressure time-history p_V on the indicator valve (Fig. 4), caused by gas compression and expansion in the passages, heat transfer, and adding up of the remaining errors introduced by the sensors.

The deformation of the p_V curve, as compared to the pressure p_C in the cylinder, was a source of relevant deformations in the heat release characteristics q'_V and q_V, compared to the characteristics of q'_C and q_C (Fig. 4).
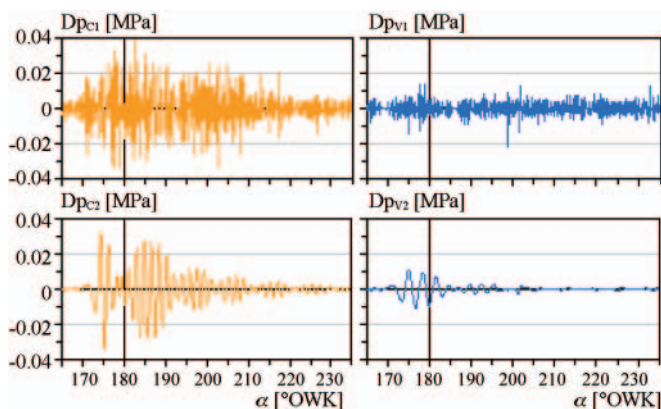
Fig. 3. Disturbances removed (smoothed) from the indicator diagrams after their smoothing using the method of multiple moving approximation and the third-order power polynomial: Dp_{C1}, Dp_{C2} – for p_C (Fig. 4) in the cylinder, Dp_{V1}, Dp_{V2} – for p_V (Fig. 4) on the indicator valve
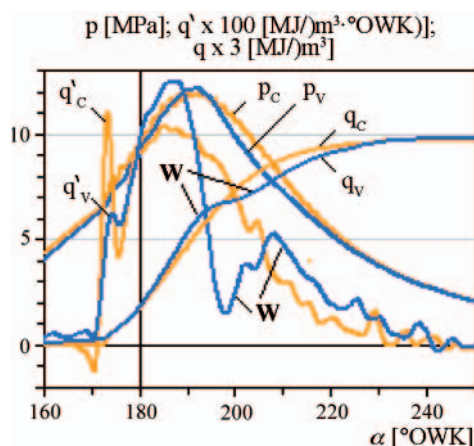
Fig. 4. The effect of gas passages and indicator valves (Fig. 2) on the time-history of pressure p_V, and the heat release characteristics q'_V and q_V for nominal load: p_C, q'_C, q_C – for cylinder, p_V, q'_V, q_V – for indicator valve, W – deformation (waves) observed on q'_V and q_V curves

Along with smaller peak values, characteristic deformations (waves) W can be observed on the q'_V and q_V curves. They can also be noticed on the characteristics of medium-speed engines of other types (Fig. 7). On the other hand, this type of deformation does not exist, in practice, on the characteristics recorded on low-speed engines (Fig. 6).

THE EFFECT OF TDC POSITION ESTIMATION ERROR ON THE SHAPES OF CHARACTERISTICS

It is noteworthy that in the case of the examined engine (Fig. 2) the deformation of the pressure time-history recorded on the indicator valve is accompanied by a pressure signal delay, amounting to 2.7° OWK, which was removed by shifting the diagrams to their TDC points. In the examined case for the measurement on the indicator valve at nominal load, the TDC position estimation error, which was equal to $\pm 1°$ OWK, was a source of errors in determining maximum q' and q values which approximately amounted to $\pm 7\%$ (Fig. 5).

For engines of different types, the effect of TDC position estimation error on the maximum values of q' and q is comparable with its effect on the errors in determining the average indicated pressure. The applied method of TDC position estimation on indicator diagrams secures high accuracy, especially in case of low-speed engines [3].
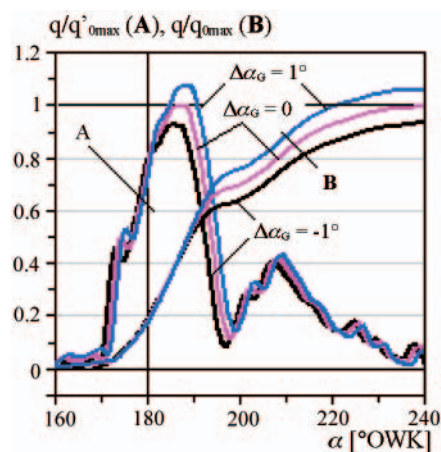
Fig. 5. The effect of the TDC position estimation error $\Delta\alpha_G$ on the shapes of heat release characteristics q'_V and q_V (Fig. 4): q'_{0max} and q_{0max} are the maximum values for the reference characteristics ($\Delta\alpha_G = 0$)

ASSESSING THE POTENTIAL FOR DIAGNOSTIC APPLICATION OF HEAT RELEASE CHARACTERISTICS

For a newly built and properly adjusted engine, strong convergence of q' and q characteristics is observed for particular cylinders (Fig. 6).
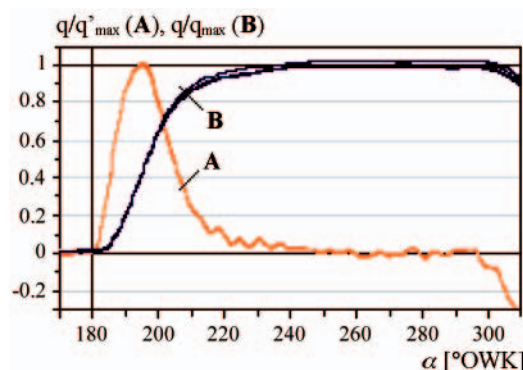
Fig. 6. Comparing heat release characteristics q' and q for all 5 cylinders in a newly built low-speed engine 5RTA52 (sea trials): $\overline{q}'_{max}$, $\overline{q}_{max}$ (referential values) – maximum q' and q values recorded in particular cylinders and averaged for the entire engine

Noteworthy is the coincidence of the waves in particular A curves (Fig. 6), irrelevant of the location of the measuring point (cylinder). This tendency is also characteristic for other types of low-speed engines and for medium-speed engines.

For an engine after large number of operating hours or an inefficient one, the q' and q characteristics differ between each other depending on the technical condition of fuel system components (Fig. 7).

These characteristics (Fig. 7) were determined after the running repair and the adjustment of the injection system. Remarkable differences in the characteristics are caused by advanced wear of injection system components due to a large number of operating hours without engine renovation.

Based on the heat release characteristics we can make a judgement about the course of the fuel injection and combustion process, and evaluate the accuracy of its adjustment, efficiency and wear of particular injection systems. Additional information can be obtained by analysing trends of selected parameters of the characteristics.

It is advisable to create a catalogue of symptoms (patterns) of typical inefficiencies for engines of certain types. This can be done via observation of engines in operation or simple simulation tests.
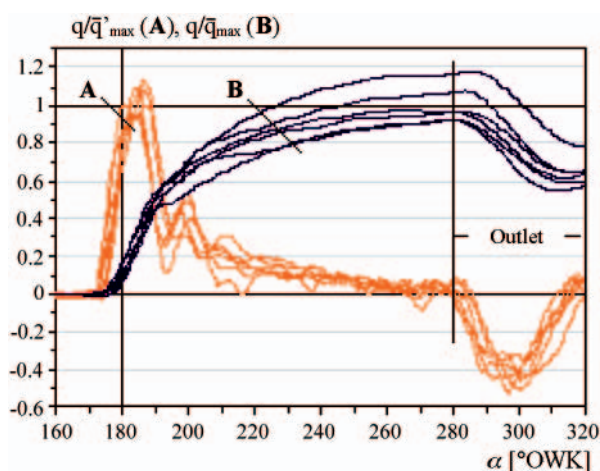
Fig. 7. *Comparing heat release characteristics q' and q determined for one block of cylinders in the 12-cylinder two-stroke medium-speed engine 40DM (n = 750 rev/min, nominal load) after large number of operating hours:* $\overline{q}'_{max}$, $\overline{q}_{max}$ *(referential values) – maximum q' and q values averaged for the entire engine, **Outlet** – exhaust space*

The permeability of exhaust ducts, in particular in two-stroke engines which burn heavy fuel, can be diagnosed using characteristics parts corresponding to the exhaust space (Fig. 7). Some inadequacy of the adopted heat release model for this space is of no importance here.

CONCLUSIONS

- The net heat release characteristics can be determined based on ship engine indicator diagrams, with the accuracy sufficient for diagnostic purposes.
- For low-speed engines, deformations of the characteristics introduced by passages and indicator valves are negligible. For medium-speed engines the deformations of pressure time-histories are large but repeatable, which provides opportunities for their use for diagnostic purposes.
- Based on the heat release characteristics one can conclude about the range and uniformity of load distribution over particular cylinders, condition of the control, correctness of work and technical condition of the injection system, as well as on the level of exhaust gas resistance.
- It is advisable to create a catalogue of inefficiency symptoms, which will help ship engineers to detect and recognise inefficiencies based on the heat release characteristics.

NOMENCLATURE
(repeated symbols which need defining)

TDC	–	top dead centre (of a piston)
BDC	–	bottom dead centre (of a piston)
p_C	–	pressure (indicator diagram) measured in the cylinder
p_V	–	pressure (indicator diagram) measured on the indicator valve
q'	–	net heat release rate related to the stroke volume, [J/m³·° OWK]
q	–	net heat release related to the stroke volume, [J/m³·° OWK]
q'_C, q_C	–	q', q determined for the indication in the cylinder
q'_V, q_V	–	q', q determined for the indication on the indicator valve
°OWK	–	degree of crankshaft rotation angle (crank angle).

BIBLIOGRAPHY

1. Heywood J. B.: *Internal Combustion Engine Fundamentals*. McGraw-Hill Book Company, 1988.
2. Polanowski S.: *Application of movable approximation and wavelet decomposition to smoothing-out procedure of ship engine indicator diagrams*. Polish Maritime Research, No. 2/2007
3. Polanowski S.: *Determination of location of Top Dead Centre and compression ratio Valle on the basis of ship engine indicator diagram.* Polish Maritime Research, No. 2/2008
4. Rychter T., Teodorczyk A.: *Mathematical modelling of piston engine working cycle (in Polish)*. PWN, Warsaw 1990.
5. Schweitzer P.: *The Tangent Method of Analysis of Indicator Cards of Internal Combustion Engines*. Biulletin No. 35, Pensylvania State University, September 1926.
6. Wanszejd W. A.: *Sudowyje dwigatieli wnutrienniewo sgoranija*. Sudostrojenie, Leningrad 1977.
7. Wiśniewski S.: *Fundamentals of internal combustion engine thermodynamics (in Polish)*. WNT, Warsaw 1962.

_____

CONTACT WITH THE AUTHOR

Prof. Stanisław Polanowski
Mechanic-Electric Faculty,
Polish Naval University
Śmidowicza 69
81-103 Gdynia, POLAND
e-mail: SPolanowski@o2.pl

The diagnosis of onboard generators (alternators)

Andrzej Gębura, Ph. D.
Tomasz Radoń, M. Sc.
Air Force Institute of Technology

Abstract

In the paper selected problems related to diagnostics of onboard generators and alternators fitted with control systems are discussed. Problems refer to commutator generators and synchronous single- and three-phase alternators. Special attention is paid to commutation effects. Results of incorrectness and possibility to detect them are discussed. There are also discussed effects associated with changes in a character of pulsation, which occur during shortings or insulation clearances in rotor or stator wiring. Possibility of diagnosis of generator's or alternator's parts by means of analysis of pulsation component parameters is indicated. In the case of alternators a number of diagnostic methods based on observation of changes in shape of voltage or frequency modulation, is discussed. This allows to detect many mechanical or electrical faults of generators, alternators or their control systems.

Keywords: technical diagnostics; frequency modulation

CHARACTERISTICS OF VOLTAGE PULSATION OF DIRECT CURRENT (DC) GENERATOR

In a classical educational approach the DC commutator generator is presented in the schematic form, as given in Fig. 1, and run of its electromotive force - in Fig. 2. The DC commutator generator is consisted of:
– the motionless stator which can be schematically presented in the form of pair of permanent magnets (Fig. 1, where: „N" – north pole, „S" – south pole), producing constant magnetic field of B intensity and the sense from „N" to „S"
– the rotor rotated with ω_2 velocity by an external mechanical force. On the rotor winding turns are winded in which the electromotive force e, (EMF), is induced. The force can be described as follows:

$$e = \left| k \cdot B \cdot \sin(\omega_2 t) \right| \tag{1}$$

where:
k – design coefficient of a given generator
B – magnetic field intensity
ω_2 – instantaneous angular velocity of generator rotor

– the commutator, i.e. the ring fastened on the rotor and made of a conductive material. The ring is cut into segments which are electrically insulated from each other and form the so called commutator sectors (bars). To each of the sector the end of winding turn is connected; the commutator serves this way as a mechanical electric current rectifier

– the electric brushes: „+" and „-", which slide around commutator bars. To the brushes are connected wires conducting electric current to consumers.

In order to increase magnitude of the inductivity B, rotor's winding turns are placed on a core made of silicon steel sheets, that amplifies magnitude of EMF (e) about 10 thousand times. To correctly fasten the winding turns on the core they are placed in grooves. As cross-sections of the grooves have a toothlike form they are further called the „ rotor teeth".

Comparison of the theoretical run described by Eq. 1 (Fig. 2) with the real run of generator pulsation component (Fig. 3) does not show any similarity between them.
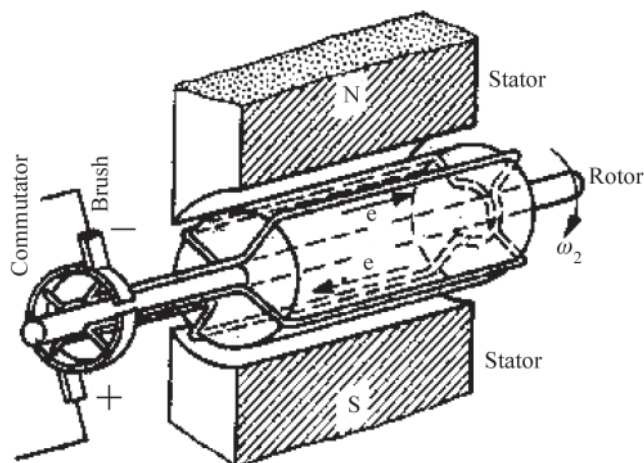
Fig. 1. *Rotor with two winding turns and commutator of four segments*
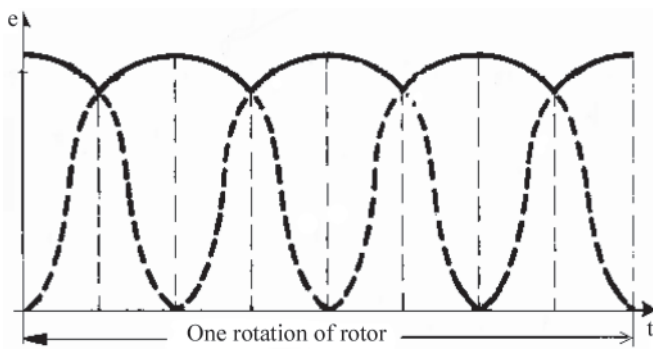
Fig. 2. Run of electromotive force between brushes in DC generator

Groove pulsations of generator's output voltage are produced as a result of change of reluctance due to whirling the grooved rotor. The groove pulsation frequency $f_{\dot{Z}}$ can be expressed as [1÷4]:

$$f_{\dot{Z}} = \dot{Z} \cdot n/60 \qquad (2)$$

where:
$\dot{Z}$ – number of rotor grooves
n – rotational speed.

In the literature [1÷3] voltage pole pulsations are often associated with the so-called rotational pulsations because of their mutual similarity. The phenenomenon of voltage pole and rotational pulsations is manifested in the run of output voltage of DC commutator generator, that can be observed in the form of changes of the run of the envelope shown in Fig. 3. Frequency of the modulation is directly proportional to the product of number of stator poles and angular velocity of rotor, whereas depth of its amplitude is proportional to changes of magnetic reluctance between rotor and stator. The pole pulsation frequency f_b can be presented by means of the formula:

$$f_b = 2p \cdot n/60 \qquad (3)$$

where:
p – number of pairs of stator magnetic poles.

Signal of pole modulations carries information on anisotropy of sheets of generator magnetic circuit. In the subject-matter literature the pole modulation is usually associated with
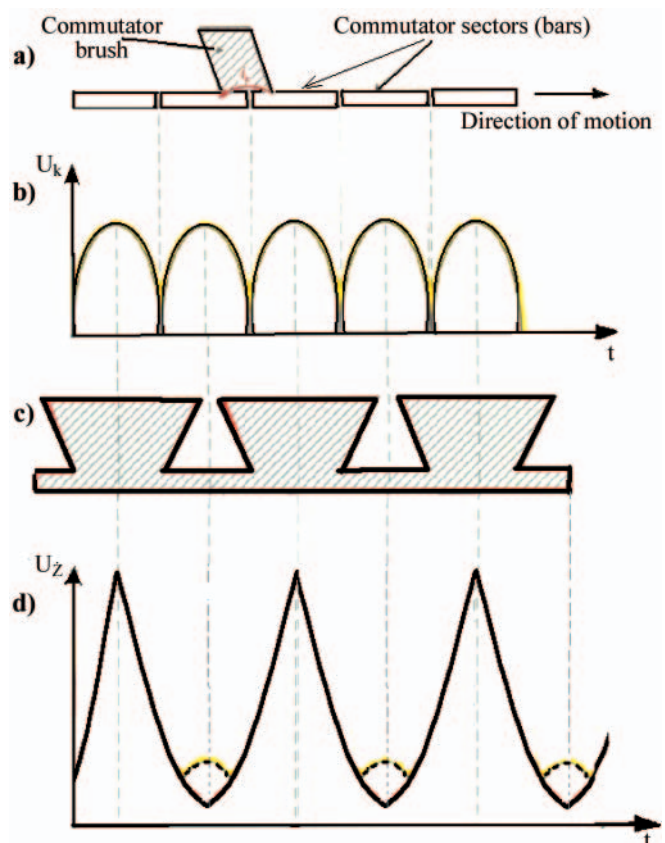
Fig. 4. Shape of pulsation curve for DC generator: a) developed view of mechanical elements of commutator unit, b) run of commutator pulsations - $U_K = f(t)$, developed view of rotor grooves, c) run of groove pulsations (continuous line) - $U_{\dot{Z}} = f(t)$ with added commutator pulsations (broken line), d) run of groove pulsation

rotational modulation which is characteristic of that such modulation frequency is equal to the first or second harmonic frequency (in certain cases - to the first subharmonic) of rotational speed of generator rotor. The signal carries diagnostic information on the errors:
– of workmanship of the generator, especially on inaccuracy of geometrical dimensions manifested as an asymmetry of air-gap between stator and rotor
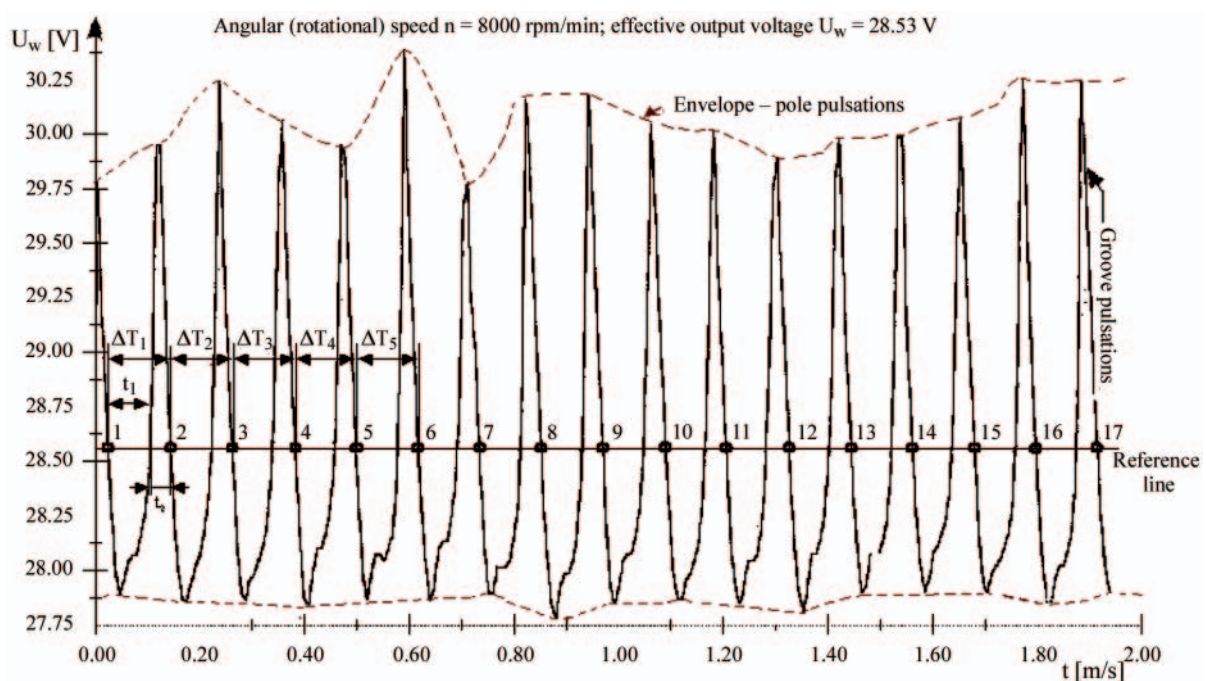
Fig. 3. Changes of pulsation component of an aircraft DC generator under minimum load

– of assembling the generator, such as parallelism error, i.e. shift of rotor shaft axis with respect to that of drive shaft, sometimes called also eccentricity error, as well as angular error of shift of rotor shaft axis against drive shaft axis.

Voltage commutator pulsations are associated with interaction of brushes and commutator. During armature rotation the brushes short-circuit alternately different number of winding turns, that introduces a change in number of turns in parallel branches and generates periodical pulsations of voltage at the brushes. The ferquency f_k of the pulsations depends on number of commutator sectors and can be expressed by means of the formula [1, 2]:

$$f_k = K \cdot n/60 \qquad (4)$$

where:
K – number of commutator sectors.

GROOVE PULSATIONS

The phenomenon of various groove pulsations is well described in the literature dealing with alternate-current (AC) induction generators [1, 2]. They do not possess any winded rotor and their useful signal is obtained from the stator winding. Their rotor is made of a ferromagnetic material (usually of a packet of silicon steel sheets) it has milled grooves (teeth) due to which modulation of magnetic field intensity of stator magnets is generated. In the generators groove pulsations are the crucial phenomena producing the useful signal. As there is no rotor winding - in contrast to the classical DC commutator generator - therefore only changeable component of pulsation is generated (commutator pulsations are not present because of lack of commutator and rotor winding).

As results from the literature information [1, 2], to induction generators, in order to achieve an output voltage signal close to sinusoidal one, skew form of teeth is usually applied (Fig. 5b).

Rotors having „dovetail" grooves (Fig. 5c) are rarely used in induction generators as then an unsymmetrical form of output voltage appears [1]. However such shape of grooves is commonly used in classical DC commutator generators. The shape makes firm fastening the winding onto rotor, possible. Time intervals between crossings of groove pulsations through the rotational speed reference level set for generator rotor, $\omega_2 = $ const., are dependent only on error in angle of milling the teeth. As the errors cyclically appear after every full rotation of the rotor they can be easily filtrated out. However the fact of stiff mutual angular position of grooves remains undeniable. Hence for $\omega_2 = $ var the time intervals between successive „zero"- level crossings (after filtrating any possible errors in milling the rotor grooves) will constitute a measure of instantaneous changes in angular velocity of rotor. The described features of groove pulsations have been used as a source of diagnostic information on technical state of generator drive system, on the basis of which the FDM-A diagnostic method (described in [5]) has been elaborated.

The measuring of amplitude of groove pulsations makes it possible to localize breaks in rotor winding. As results from the data collected by these authors [7] after a winding failure a decrease of the relative value (related to the effective value of the generator output voltage U_w) of the groove pulsation $\delta_{\dot{Z}}$, is observed. The value can be expessed as follows:

$$\delta_{\dot{Z}} = \Sigma (U_{max\,m} - U_{min\,m}) \cdot 100\%/\dot{Z} \cdot U_w \qquad (5)$$

where:
m – natural number being that of successive interval of groove pulsation
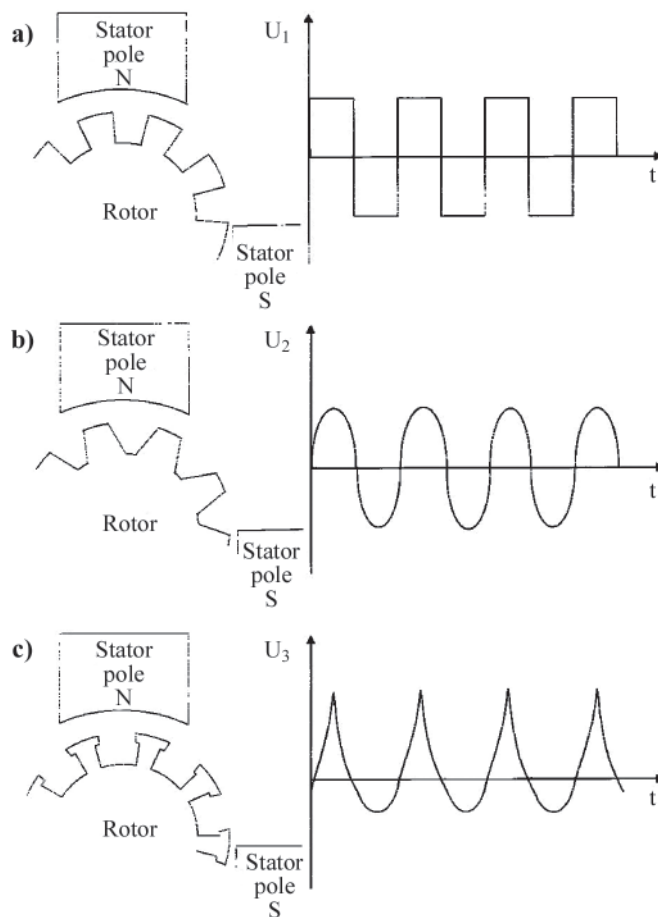
Fig. 5. *Typical runs of output voltage of induction generators with rotor teeth of the form: a) trapezoidal, b) rectangular, c) „dovetail" – like*

$U_{max\,m}$ – maximum instantaneous value of pulsation component within a given interval m
$U_{min\,m}$ – minimum instantaneous value of pulsation component within a given interval m
$\dot{Z}$ – number of rotor grooves.

Simultaneously, after a failure of DC generator winding, the effective output voltage value changes, ΔU_w(practically imperceptible, especially at lower values of ω_2 shown in Tab. 1 based on the data of [7], occur. The relative value of the changes, δU_w, due to failure of a single winding turn, does not exceed 0.01 %. In practice to detect a generator failure, i.e. occurrence of a break of its winding, by aircraft personnel under operation is entirely impossible. However this is fully possible, as results from experience gained by the team supervised by these authors, by making use of special measurement instruments.

A failure of generator winding, e.g. its break, results in the decrease of the values of groove pulsation, given as the index $\Delta\delta_{\dot{z}}$ in Tab. 1, from 0.8 % to 1.6 %, that can be practically measured by using measurement instruments of 0.1% class.

POLE PULSATIONS

The phenomenon of pole pulsations can be clearly observed on the run curve of DC generator output voltage [5] in the form of amplitude modulation, shown in Fig. 3. The modulation frequency is directly proportional to the product of number of stator poles and angular velocity of rotor, and the amplitude depth - proportional to magnetic reluctance changes between rotor and stator. The signal carries information on anisotropy of sheets of magnetic circuit of generator. The modulation

Tab. 1. Parameters of groove pulsations before and after failure of generator winding

$\omega_2 \rightarrow$	[rpm]	4000	4500	5000	5500	6000	6500	7000	7500	8000	8500	9000	9500	State of winding
U_{ws}	[V]	28.6	28.5	28.5	28.5	28.6	28.7	28.7	28.6	28.6	28.6	28.6	28.9	Capable
$\delta_{\dot{z}}$	[%]	6.3	5.8	5.6	5.8	5.5	5.6	5.7	5.8	5.4	5.4	5.9	5.5	
U_{wz}	[V]	28.6	28.5	28.5	28.9	28.6	28.6	28.5	28.9	28.6	28.6	28.5	28.5	Failed
$\delta_{\dot{z}}$	[%]	5.0	3.6	4.7	4.0	4.4	4.6	4.1	4.2	4.5	4.3	4.8	4.7	
ΔU_w	[V]	0	0	0	-0.4	0	0.1	0.2	-0.3	0	0	0.1	0.4	Indices used to compare parameters before and after failure
δU_w	[%]	0.00	0.00	0.00	-0.01	0.00	0.00	0.01	-0.01	0.00	0.00	0.00	0.01	
$\Delta\delta_{\dot{z}}$	[%]	1.3	2.2	0.9	1.8	1.1	1	1.6	1.6	0.9	1.1	1.1	0.8	

can introduce small errors in measuring ΔT_i. It can be easily filtrated out because of its repeatability characteristic for a given generator. The relative value of pole pulsation, δ_b, can be expressed as follows:

$$\delta_b = \{(U_{max\,o} - U_{min\,o})100\%/(U_{max\,o} + U_{min\,o})\}_{MAX} \quad (6)$$

where:

o – natural number standing for successive number of pole pulsation interval
$U_{max\,o}$ – maximum instantaneous value of voltage pulsation component in the o-th period
$U_{min\,o}$ – minimum instantaneous value of voltage pulsation component in the o-th period.

The pole pulsations carry a few kinds of diagnostic information:
a) phase parameter informs on possible errors in geometrical distribution of stator pole shoes,
b) pulsation amplitude (run of the envelope shown in Fig. 3) generally shows a non-uniformity of magnetic field distribution under stator magnetic poles and, in some cases, a shorting or break of rotor or stator winding:
   - if pole pulsation amplitude reaches, during the whole period, values uniformly increased and close to those of rotor groove pulsations, it means that one turn of winding is overloaded due to an increased leakance of its insulation or a partial fault to frame or between rotor winding turns in a given groove
   - if pole pulsation amplitude reaches non-uniform values during the whole period, e.g. during one rotation of rotor, the peak value of the envelope undergoes a decrease; it means that one turn of winding is overloaded due to an increased leakance of its insulation or a partial fault to frame or between winding turns of one pole of stator
   - if pole pulsation amplitude value uniformly decreases during the whole period of rotor's rotation, as shown in Tab. 2, it may constitute information on a break of rotor winding.

With a view of a diagnostic complexity of such signal and of its small amplitude with respect to the carrier component (groove pulsation), location of failed winding turns by measuring pole pulsations seems rather inaccurate.

However the pole pulsation signal becomes greatly increased in case of a failure, e.g. shorting of an arbitrary winding, consquently its amplitude increases many times with respect to that of groove pulsations. The shorting phenomenon is below described in detail as commutator pulsation amplitude greatly increases during shorting the winding turn.

COMMUTATOR PULSATIONS

The phenomenon of commutator pulsations has been not used in the FDM-A method [5, 6] as it has been regarded as a disturbing signal. The investigations performed under supervision of these authors [5, 8] have showed that amplitude value of the pulsations is directly proportional to current-load level. In Fig. 4 are presented mutual relations between commutator pulsations and groove ones, as well as location of rotor grooves and commutator bars. From the investigations performed with the use of an aircraft DC generator it results that at the generator's current load lower than 10% of its rated value the commutator pulsation amplitude (Fig. 4b) is rather

Tab. 2. Parameters of pole pulsations before and after failure of generator winding

$\omega_2 \rightarrow$	[rpm/min]	4000	4500	5000	5500	6000	6500	7000	7500	8000	8500	9000	9500	State of winding
U_{w1}	V	28.6	28.5	28.5	28.5	28.6	28.7	28.7	28.6	28.6	28.6	28.6	28.9	Capable
δ_{b1}	%	4.2	4.2	3.9	4.4	4.1	4.1	4.0	4.4	4.1	4.1	4.3	4.3	
U_{w2}	V	28.6	28.5	28.5	28.9	28.6	28.6	28.5	28.9	28.6	28.6	28.5	28.5	Broken
δ_{b2}	%	3.6	3.2	3.6	3.3	3.4	3.6	3.4	3.5	3.4	3.3	3.7	3.5	
$\Delta\delta_b$	%	0.6	1	0.3	1.1	0.7	0.5	0.6	0.9	0.7	0.8	0.6	0.8	Compari-son

unperceptible against groove pulsation background (Fig. 4d). At the current load of the order of 10% the pulsations are barely visible on the output voltage run. Angular displacements of particular halves of sinusoids of commutator pulsations (Fig. 4d) change with respect to groove pulsations and undergo individual angular displacements due to mechanical vibrations of brushes in brush-holder and during current loading the generator. Therefore the commutator pulsations cannot be used to diagnosing magnitude of failures of drive system's kinematic pairs.

Under rated load, the peak value of commutator pulsations reaches the level of about 50% of groove pulsations. It means that they may serve as a source of diagnostic information on e.g. commutator-brush unit failures.

Trials of a controlled shorting in rotor have provided interesting data. In the case of shorting in the middle of one of the rotor winding turns it was revealed that the pole pulsation visible in Fig. 6 as the slow-varying component, became dominating, and the commutator pulsation visible in Fig. 6 as the fast-varying component, appeared to be that of the second order.
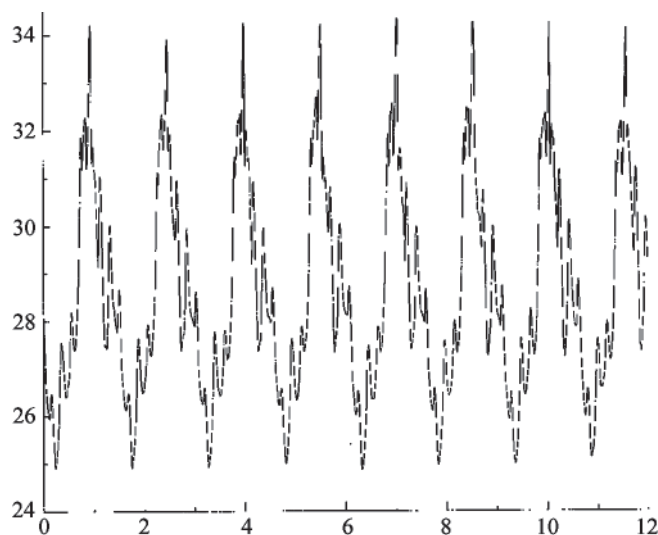

Fig. 6. Diagram of DC generator output voltage in the case of rotor winding's shorting (the shorting localized in the middle of one of winding turns)

However if the pole pulsation component was stable with respect to its frequency and amplitude, the commutator pulsation component reached its greatest value in the instant of passing under successive pole of generator stator. The unambigous change of the relation between amplitudes of pulsation components makes it possible to detect shortings in rotors of commutator generators.

CONCLUSIONS

− In this paper different kinds of output voltage pulsations of DC generator were described. Although they simultaneously occur in practice their amplitude-phase relations are very different. The subject-matter literature fully describes each of them separately.

− These authors, basing on their personal experience, have made an attempt to highlight practical relations between the pulsations. The pulsation component carries several diagnostic signals both concerning technical state of drive system and DC generator itself, i.e. the very source of the information, which has been not mentioned at all in the literature.

− The diagnostic symptoms contained in the pulsations, precisely recognized by these authors, have been implemented by them to practice a few years ago. The other, ambiguous and not fully identified ones will be ready for application only after performing many arduous investigations aimed at finding accurate relations between successive parameters of kinematic faults and parameters of output voltage component.

BIBLIOGRAPHY

1. Wróbel T.: *Theoretical study and experimental problems of voltage pulsations of DC tachometric generators* (in Polish). Dodatek do Biuletynu WAT (Supplement to Bulletin of Military Technical Academy) no. 3(259), Warszawa 1974

2. Wróbel T.: *Study of the problem of output voltage pulsations of DC tachometric generators* (in Polish). Dodatek do Biuletynu WAT (Supplement to Bulletin of Military Technical Academy) no. 6(298), Warszawa 1977

3. Liwschitz-Garik M.: *Direct-current machines* D. Van Nostand Company, New York 1962.

4. Plamitzer M.: *Electric machines* (in Polish). Wydawnictwo Naukowo-Techniczne (Scientific Technical Publishers), Warszawa 1962.

5. Biarda D., Falkowski P., Gębura A., Kowalczyk A.: Patent Specification No. PL 175674B1: *A method for technical diagnosing elements which connect an engine, especially aircraft diesel engine, with direct current generator* (in Polish). Submitted on 08.07.1996, Issued on 29.01.1999.

6. Biarda D., Falkowski P., Gębura A., Kowalczyk A.: Patent Specification No. PL 175645B1: *A method for technical diagnosing elements which connect an engine, especially aircraft diesel engine, with direct current generator* (in Polish). Submitted on 08.07.1996, Issued on 29.01.1999.

7. Gębura A., Prażmowski W., Kowalczyk A., Falkowski P., Głowacki T., Budzyński P., Pisarska K.: *On determination of relations between power quality parameters of onboard generators and wear state of their drive units* (in Polish). Unpublished research report No. BT ITWL 11818/I, Warszawa 1997

8. Gębura A., Prażmowski W., Kowalczyk A., Falkowski P., Głowacki T., Budzyński P., Gajewski T., Pisarska K.: *On determination of relations between power quality parameters of onboard generators and wear state of their drive units*, Part I (in Polish). Unpublished research report No. BT ITWL 12023/I, Warszawa 1997

CONTACT WITH THE AUTHORS
Andrzej Gębura, Ph. D.
Tomasz Radoń, M. Sc.
Air Force Institute of Technology,
Księcia Bolesława 6,
01-494 Warsaw, POLAND
P.O. box 96
e-mail: andrzej.gebura@itwl.pl

Discussion on microbial contamination of naval fuels

Wojciech Dzięgielewski, Ph. D.
Jarosław Sarnecki, Ph. D.
Air Force institute of Technology

ABSTRACT

Article Deals with problem of naval fuels' microbial contamination. This problem in Poland is not well known and described, but operational problems encountered very often prove that this is a very serious problem. Examples of laboratory tests performed on real samples are presented as well as possible effects of microbial contamination are discussed. Authors also suggest continuous monitoring of naval fuels as main preventive tool. Article covers following topics:
• general information about microorganisms present in naval fuels
• conditions necessary for microbial growth, with special attention to conditions encountered on vessels
• operational problems resulting from microbial contamination
• methods of microorganisms detection and examples of preventive actions.

Keywords: naval fuels; microbes on fuels; microbial growth; microorganisms; fungi; ulphate-reducing bacteria

INTRODUCTION

It has been known for over 100 years that some microorganisms can feed with hydrocarbons but only for about 40 years people have started to realise the adverse effect of microbes on fuels' cleanness as well as their corrosiveness to materials used in distribution systems (storage and operational tanks, pipelines etc.) and in fuel systems of vessels.

The core factor for microbial growth in fuels, not only the naval ones, is presence of water. Every case of fuel contaminated with water brings real and big risk of microbial growth. In fuel tanks ideal conditions for microbial growth exist on fuel-water surface. Fig. 1 presents, as a scheme, storage tank with layers that exist during fuel storage.
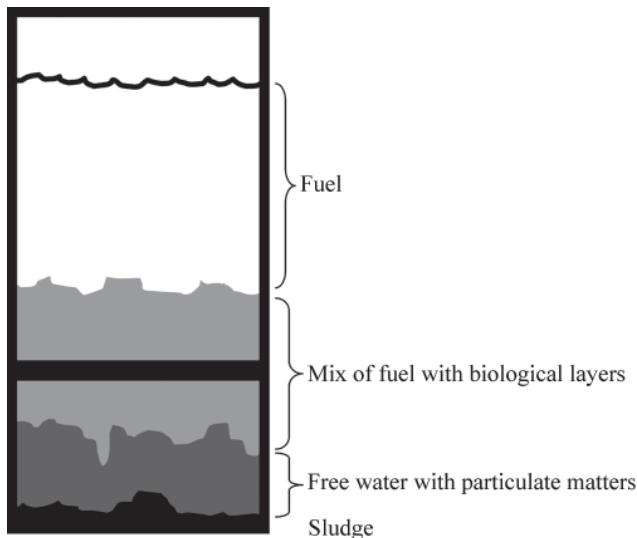
Fig. 1. Scheme of layers present in storage tank

Microbial growth is stimulated also by other factors, i.e. fuel composition (as naval fuels most vulnerable are heavy fuels, fuel distillates (diesel fuels) and light fuels), storage conditions (temperature between 15 and 40 °C) and amount of free water in storage tank.

Microbial contamination of naval fuels has posed some operational problems for many years. Such problems can be avoided by discarding of water, but practically it is impossible to discard all of the water. Water as separate phase in fuel tanks can origin from condensation of water dissolved in fuel as well as from water deliberately added to fuel tanks for ballast and to eliminate vapour space.

MICROORGANISMS ENCOUNTERED IN FUELS

Microorganisms having the biggest effect on fuels' performace can be differentiated into two main categories:
• fungi
• sulphate-reducing bacteria.

There are also yeast, but they are nor as important as fungi and bacteria.

Fungi can create coherent mats at the fuel - water interface. Fungi enter the fuel from soil as airborne spores.

Bacteria usually enter fuel tanks with water. They grow in water under the fuel layer, without oxygen presence [1].

Gloriah Hettige in her work [2] has isolated thirty one types of fungi and five types of bacteria. Neyhof and May have also described other types of fungi and bacteria [3].

The main types of fungi were the following:
• Cladosporium resinae
• Penicillium corylophilum

- Paecilomyces variotti
- Aspergillus
- Mucorales
- other, unidentified.

The bacteria were the following:
- Pseudomonas
- Desulfovibrio.

Among yeast there were the following types:
- Candida
- Rhodotorula.

MICROBIOLOGY OF FUELS

The first reports regarding microorganisms were in the early 1930's. The reports described problems connected with fuels and oils infected by bacteria [4, 5].

Most of work concerned aviation fuels, though probably there also were problems with naval fuels, but they were used in less sophisticated (compared to jet ones) engines.

Liggett [6] has performed comprehensive work on microbial contamination of marine, rail and road diesel fuels.

Hydrocarbons C_{10} - C_{18} are much readily assimilated by microorganisms than the C_5 - C_9 ones. Test results showed that microbial growth had taken place also in naval fuels, but effect of their activity was no as severe as for aviation fuels.

This was why some contamination and corrosion in naval fuel recognised as of no importance so it was not justified to take appropriate countermeasures similar to ones for aviation (water discarding, microbial monitoring).

As a result the problems regarding microbial growth at vessels became bigger.

Such unfavourable occurrences were linked mainly with chemical changes in fuel resulting from refinery processes [7] as well as from wider use of additives, which sometimes promote microbial growth.

Hill [8] has found severe microbial growth both in heavy fuel oils and lighter diesel oils.

The biggest problems were because of fungi *"Cladosporium resinae"* which were superseded by a lot of other types of fungi, bacteria and yeast.

Distillate fuels contain ample of oxygen sustaining aerobes growth, but in case of dormant tanks, content of oxygen decreases and anaerobes such as sulphate-reducing bacteria *Desulfovibrio* can grow. Such bacteria never exist alone, but also together with other organisms, creating big complexes living in water and feeding on fuel. Fuel with its additives is not the only nutrition source. It is permanently used and replenished, opposite to water and microorganisms contained there.

Conditions in naval fuel tanks, especially presence of large amounts of water, effect on variety of types of microorganisms as well as on their growth rate. It can be assumed that microbial growth in vessel's fuel systems is bigger and faster than in aviation ones.

The ratio of water to fuel in water-displaced tanks can be high. There is wide range of nutrients in such mixture, in addition to those already contained in water. The nature and quantity of such nutrients depend on type of water used to fill the tanks. It can be saline deep-seawater as well as estuarine one. Extent of colonisation can be affected by sewage content and trace metal contamination in the water.

The ratio of water to fuel in standard fuel tanks is low and there is less particulate organic matter when compared to water-displaced tanks. Amount of nutrients will be determined by the previous history of the fuel and such factors as condition of tank linings and seals.

RESULTS OF MICROBIAL ACTIVITY

Inconsiderable amount of water, even strongly infected, does not influence on significant fuel deterioration. Such water can result in severe corrosion. It is well known that more the water much bigger threat to cleanness of fuel in terms of microbiology. Activity of microorganisms can lead to:
- presence of slimes and clogging pipes, valves and filters
- coalescers malfunction due to fungi growth on filter cloth sleeve
- malfunction of volume measurement systems
- accelerated corrosion due to aggressive substances (acids, sulphides) and electro-chemical corrosion cells creating, corrosion inhibitors depletion and degradation, protective coatings degradation and preventing formation of stable oxide layers.

Symptoms of severe contamination of naval fuels are the following:
- filter clogging
- coalescers malfunction
- injector fouling
- fuel system components corrosion.

MICROORGANISMS DETECTION

Crucial matter is to obtain water bottom sample. For such sample it is possible to perform both qualitative and quantitative testing using a routine culture methods. But sometimes it is impossible to obtain such excellent sample, so in order to evaluate level of fuel contamination we can use different methods. Some of them are summarised below:

Microscopic method

It is used mostly to detect motile bacteria, fungal hyphae, protozoa, algae and unusual debris. It also allows identification of small particles such as non-motile bacteria and spores in the presence of large amounts of mineral particulate matter. Disadvantage of this method is the high cost of devices and necessity of highly qualified personnel, but major advantage is short time of analysis.

Centrifuge method

It bases on centrifuging sludge sample previously homogenised. The length of specific layers in test tube is read from calibration graph. Its disadvantage is, as in previous metod, high cost of equipment.

Chemical methods

- pH of water phase measurements
- acidity measurements
- metallic elements content
- sulphides presence
- burning at 500°C.

Membrane filters method

It is based on passing fuel being examined through defined membrane filter and evaluation of substances collected on filter's surface.

Dip-slide method

The nature of this method is to dip a small plastic paddle coated with nutrient into a sample. Next step is to return the paddle into its container and to incubate. One type of nutrient detects ant evaluates bacteria while the another detects yeast and fungi, and allows for quantitative assessment of contamination. Disadvantage of this method is long incubation time, up to 3 days, but major advantage is simplicity so it can be used my not qualified personnel. Examples of results obtained with this method are presented on Fig. 2.

Fig. 2. Plastic paddle coated with nutrient (prod. Merck)
used in dip-slide method

ATP method

This is a new method evaluated recently. It uses presence of ATP in microorganisms contained in fuels. Its main advantage, when compared with other methods, is short time of measurements that allows for reliable results within approx. 10 min. Example of test device used in this method is presented on Fig. 3.

Fig. 3. Hy-Lite device (prod. Merck) used in ATP metod for microbial
contamination assessment.

EXAMPLES OF NAVAL FUELS MICROBIAL CONTAMINATION

Examples of naval fuel samples, where microbial contamination has been confirmed, are presented on Fig. 4. The samples were taken from operating vessels. Easily visible is fuel colour change and microbial layer on fuel-water interface.

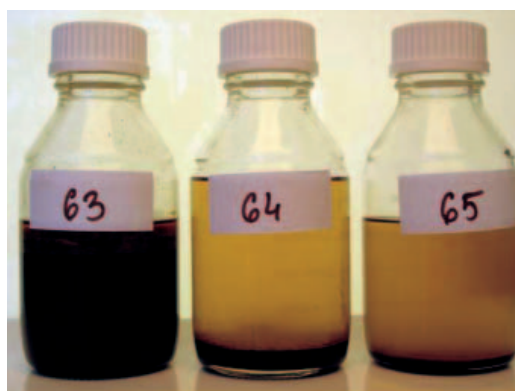Slides with cultures of fungi, bacteria and yeasts are presented on Fig. 5.

Fig. 4. Naval fuels samples with confirmed microbial contamination
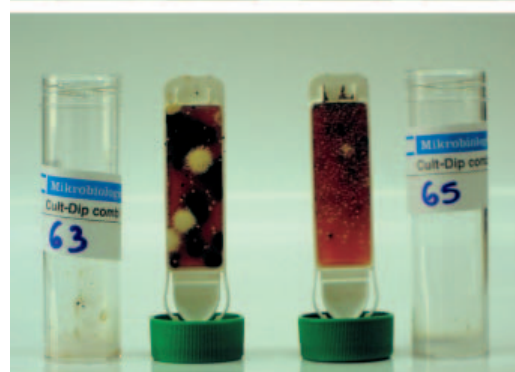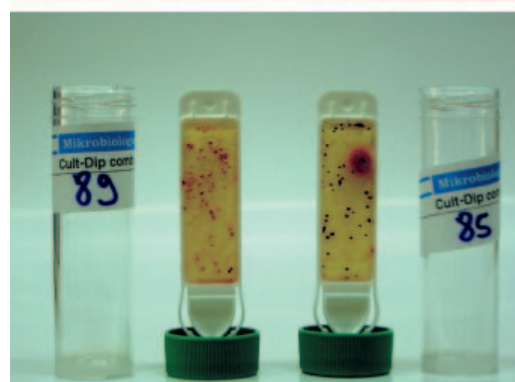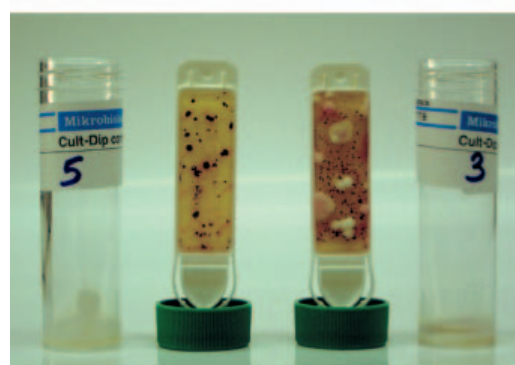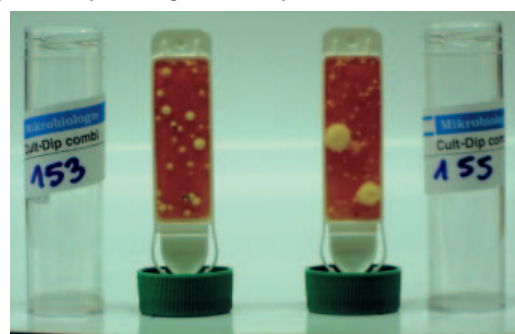
Fig. 5. Slides after tests of microbial contamination

COUNTER MEASURES AND PREVENTIVE ACTIONS

Fuel composition

Fuel should be formulated that it is no longer good nutrient for microbial growth. Straight hydrocarbon chains are more vulnerable than branched ones. Some additives promotes microbial growth and some prevents that. So far, there is no comprehensive study concerning fuel composition effect on microbial growth, and refineries are using established production processes, therefore changes in fuel composition are not currently feasible.

Good housekeeping

This mean includes:
- minimising water content
- rust and scale discarding
- high temperatures avoidance
- avoidance of fuel contact with contaminated surfaces
- active fight against microbial growth at the beginning of the process of growing.

Mechanical decontamination

This preventive action includes:
- filtration
- centrifugation.

Biocide treatment

Biocides are the chemicals used to destroying microbes. There are wide range of chemicals used as biocides. Some of them are the following:
- Biobor JF
- Kathon 886
- Grotan OX
- Bodoxin
- Omadine TBAO
- Bioban FP etc.
- Grota Mar.

Biocides should have the following properties:
- be combustible, without ash
- have no adverse effect on fuel properties or engine performance
- be soluble or very miscible in fuel, but preferably in water
- be not corrosive
- be able to total killing of all microbes at minimum dose.

CONCLUSIONS

- Microbial contamination of naval fuels pose problems and threat to proper use of vessels.

- Effect of microorganisms can be minimised by adhering to rules of good housekeeping, as well as by the use of relevant chemicals (biocides and biostats). Use of the chemicals should be based on relevant laboratory testing to check its influence on fuel system's components.

BIBLIOGRAPHY

1. Parbery D. G.: *Transactions*, British Mycological Society, Vol. 53, part 1, 1969
2. Gloriah Emily Gres Hettige: *Identification, documentation and control of biological contamination in middle distillate fuels*, Victoria University of Wellington, Jan. 1987.
3. Neihof R. A., May M. E.: *Microbial and particulate contamination in fuel tanks of naval ships* - International Biodeterioration Bulletin ISSN 0020-6164 19(2) Summer 1983.
4. Tausson W. O., Aleshina, W. A.: *Uber die bakterielle sulatreduktion bei Anwesenheit der Kohlenwasserstoffe*(in Russian), Microbiology 1
5. Tausson T. A.: *Oxidation of paraffin by yeast and yeast-like organisms*. Microbiology 8
6. Ligett S.: *The extent and significance of micro-organisms in hydrocarbon fuel oil storage systems*. M. Sc. Thesis, University of Wales, Cardiff, 1976.
7. Unzelman G. H. *Diesel fuel demand - a challenge to quality*, Institute of Petroleum Technical paper IP 84-001
8. Hill E. C. and Associates Fuels Marine Engineers Review, Dec. 1985.
9. Klemme D. E. and Neihof R. A.: *Control of marine sulfate-reducing bacteria in water-displaced shipboard fuel storage tanks*. Naval Research Laboratory Report No 2069.

_____

CONTACT WITH THE AUTHORS

Wojciech Dzięgielewski, Ph. D.
Jarosław Sarnecki, Ph. D.
Air Force institute of Technology
Księcia Bolesława 6
01-494 Warsaw, POLAND
e-mail: jaroslaw.sarnecki@itwl.pl

Self-organizing wireless monitoring system for cargo containers

Ryszard J. Katulski, Assoc. Prof.
Jarosław Sadowski, M. Sc.
Jacek Stefański, Ph. D.
Sławomir J. Ambroziak, M. Sc.
Bożena Miszewska
Gdansk University of Technology

ABSTRACT

This paper presents a description of new global monitoring system for containers with its layer-modular structure, as a solution for enhance security and efficiency of container transport with particular emphasis on the practical implementation of that system for maritime container terminals. Especially the Smart Container Module (SCM) architecture and its operation as a part of the Self-Organizing Container Monitoring Network is presented.

Keywords: wireless monitoring; container transport; container module realization; global system concept; ad-hoc networks

INTRODUCTION

Since 26 March 1956 when the first goods transport was made by using freight containers on board of the *Ideal X* – the world's first container ship - this kind of transportation gained very rapidly on popularity. Meanwhile, the concept of the container has been clearly defined, its dimensions have been standardized and on the whole world have been created numerous container terminals: land and sea, specialized in handling this type of cargo. Currently container transport includes more than 90% of the global trade and takes place along trade lanes, both marine and terrestrial.

However, despite all the advantages of this mode of transport, it carries a lot of risk, as a result of the exploitation of containers. First of all, containers are closed during the transportation, so the load on their interior remains beyond any control. For this reason, in peer-reviewed literature on the safety of transport, container is known as *the Trojan Horse of twenty-first century*. In this state of affairs it is particularly important issue of controlling and monitoring of cargo container, both during transportation and storage. Several years ago, the Group of Self-Organizing Ad-Hoc Wireless Sensor Networks was founded at the Department of Radiocommunication Systems and Networks in the Gdansk University of Technology. This Group developed the original concept of a global wireless system for monitoring of container cargo, with particular emphasis on the practical implementation of that system for maritime container terminals [1, 2, 3].

A GLOBAL GRASP OF THE SYSTEM

The proposed new monitoring system solution for containers has a layer-modular structure (Fig. 1). The basic layer of the system is the *Smart Container Module (SCM)*, designed for installation on containers and eventually should be an integral part of each container. Another, higher layer of the system is the Ship/Port Subsystem with the self-organizing container monitoring network, based on the *802.11* standard, working on the container ship or in the container terminal and the sea ports. Due to the fact that the typical container ship can carry up to dozen thousand containers, there is a necessity for the location a special database on the ship. In case of container terminals and sea ports there is the Port Administration Data Base, equipped with wireless access points located at entrances to ports and wireless radio networks covering container depot. All containers data are regularly sent to the ship/port network controller. Information can also be sent on request. All of the Port Subsystems located inside the country are connected to each other and provide all data to the Land Subsystem - The State Administration Data Base. The Land Subsystem is the third layer of the monitoring system.

Transmission of information between each part of the system is in accordance with certain rules, using an appropriate transmission medium. In the case of a container ship, the period of reporting depends on its position, i.e. on distance to the mainland, the home port and/or destination port. Frequency of sending the relevant data increases with the approach to the mainland.
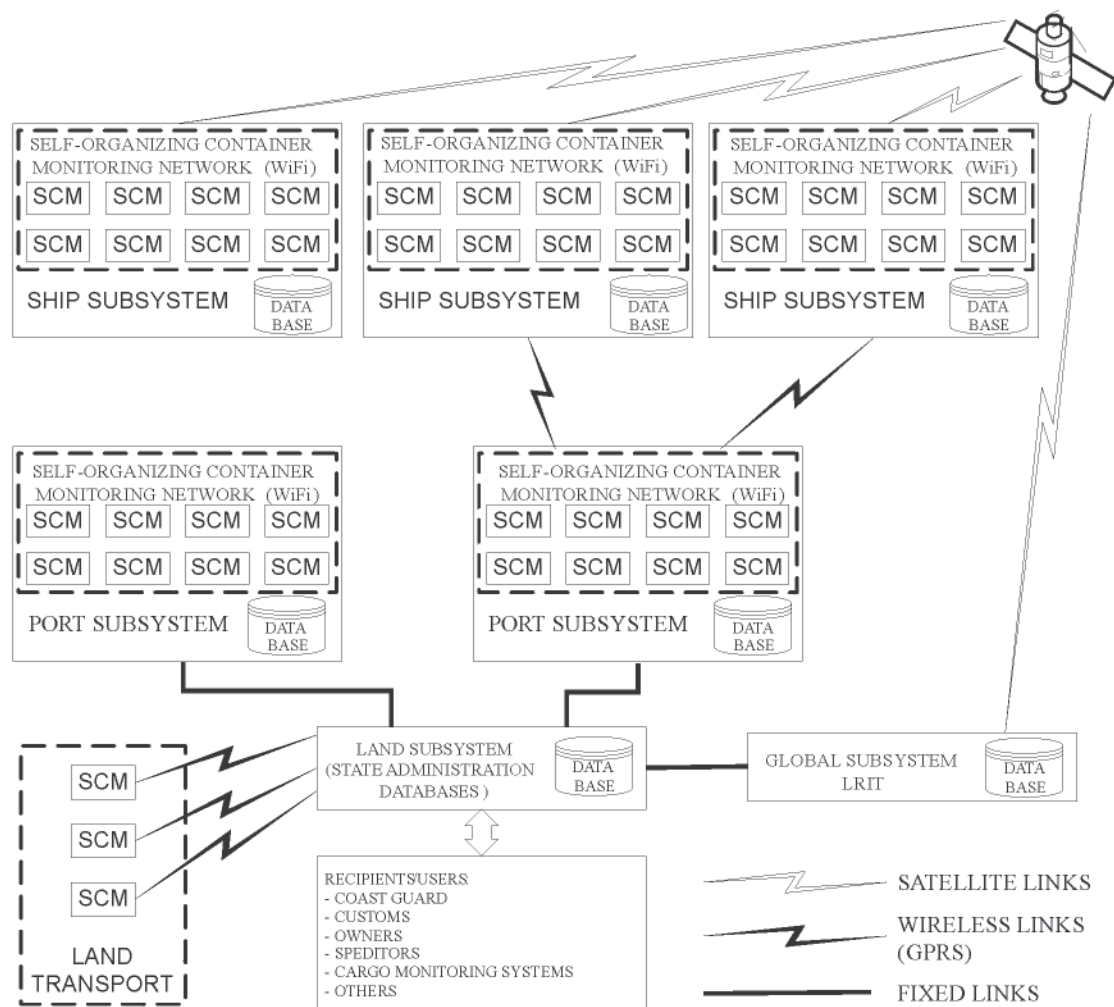
Fig. 1. *Architecture of the global wireless monitoring system for containers*

The Global Subsystem is the highest layer of the monitoring system, which can use the database of a new *LRIT* (*Long Range Identification and Tracking*) system for long-range ship monitoring. Data are transferred to the global database via satellite system (e.g. *INMARSAT*), when the vessel is on the open sea. Approaching the mainland and entering the harbour, information are communicated to the Port Subsystem that supports appropriate area. Transmission of this information is carried on using the *GPRS* system. It is also necessary to realize co-operation and data exchange between local and global databases, and also co-operation between databases inside the country. It can be realized by means of fixed lines, e.g. optical fiber.

In case of land transportation all data about monitoring cargo are sending via GPRS to State Administration Database. The SCM modules are mounted on containers carried on container lorries and there is no need to organize SCM modules in ad-hoc network.

The recipients (users) form a separate layer of the system. We can distinguish two classes of users: the services responsible for cargo security and the carriers. The first group is formed by the relevant services, such as Coast Guard, Customs and Police. The owners and the shipping companies belong to second group of users, which access to the system is carried out by authorized employees.

THE SMART CONTAINER MODULE

The Smart Container Module is one of the most important elements of the monitoring system [1]. Fig. 2 depicts its functional diagram. The versatility of the SCM stems from the possibility of parameters measuring and monitoring of state within the container. To this end, the module is equipped with various sensors placed inside the container [4]. This sensor network enables detection of movement, temperature changes, pressure, humidity, presence of gases or radioactive substances, etc. An important aspect is also the location of the container, so each SCM is equipped with the *GPS* receiver. The GPRS module and the *WiFi* module are components of SCM. This parts of container module enable communication with port database (GPRS) or the local wireless network working on the container ship (WiFi).

Transportation documents concerns shipment (such as contents of the container, a shipper, a point of shipment, a point of destination and other information) are stored in SCM's memory. This data are sent to the appropriate database, whenever necessary. In case of lack of connection with the radio resources of the system, it is necessary to store data about status of container in the module's internal memory and send them shortly after the SCM gets in a range of network.

The container module has to be characterized by very low power consumption to enable unattended work for a long time (from several months to even few years). Equally important is compact construction of the SCM and to minimize its dimensions. The module's casing has to be matched to construction of the container, to damage prevent during transshipment. It also has to be resistant to the weather conditions and a protection against removal or modification of its interior, with automatic alert generating in these cases is needed.
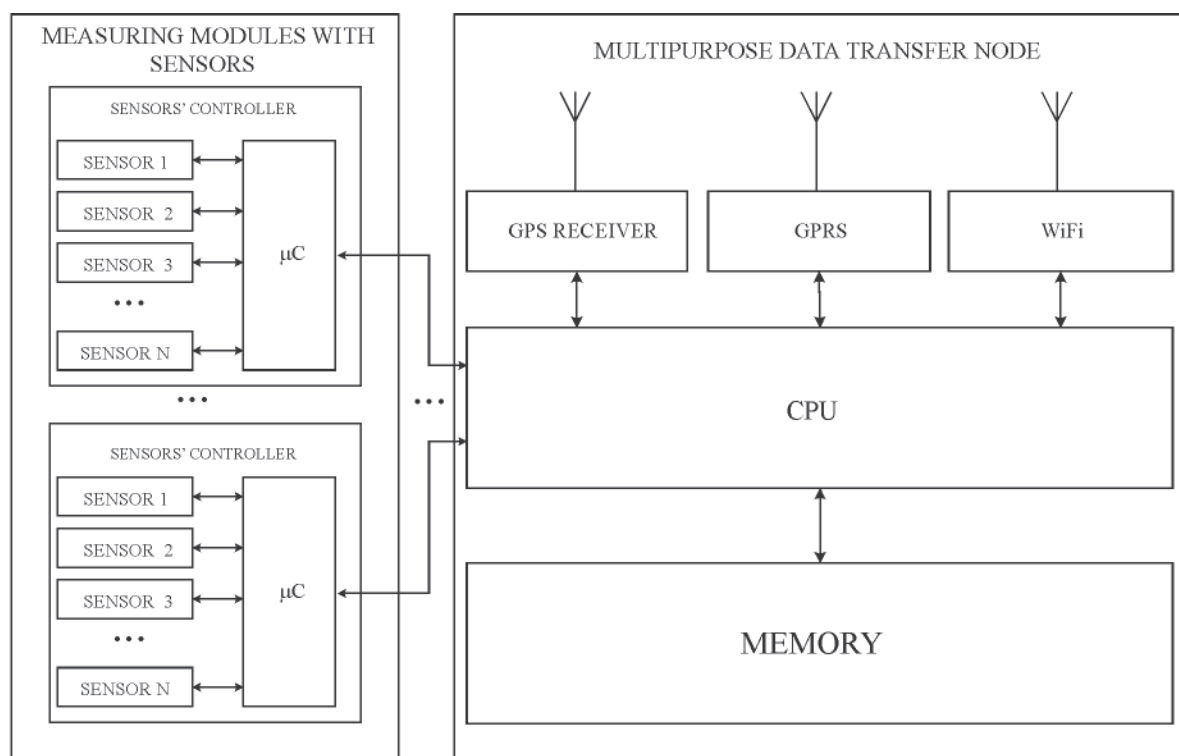
Fig. 2. *Functional diagram of the Smart Container Module*

During the research on the SCM, it was decided to use two types of industrial computers: the *Axiomtek SBC84710* and the *Advantech ARK1380*. Three prototypes of the SCM have been produced basing on these computers. The Smart Container Module prototype using the ARK1380 is shown in Fig. 3. The module is enclosed in a sealed casing and there are various connectors available, as following:

* *COM1, COM2* - used to connect Sensors' Controllers in various configurations
* *USB1, USB2, USB3, USB4* - two of them are used to connect external GPRS and GPS modules, next two are designed for future purposes
* *LAN* - used to connect the SCM with the ship/port local network, in case of usage the SCM as a gateway
* *DC IN* - used to connect the supply voltage range from 9V to 35V, but because of the usage of this voltage by Sensors' Controllers, it is recommended not to exceed a value of 15V
* *PCMCIA* - used to connect the WiFi module
* *VGA* - used to connect the monitor
* *PS2* - used to connect the keyboard
* *AUDIO* - not used, designed for future purposes
* *LVDS* - not used, designed for future purposes.

Additionally, there are LEDs placed on the SCM's casing, which indicate supply voltage connection and work of the hard disk. There is also the on/off button placed on the casing.

The internal construction of the Smart Container Module is presented on an example of the SCM prototype based on SBC84710. The top view of internal construction of the SCM, with marked available interfaces, connectors, power supply voltage and connected the WiFi module is shown in Fig. 4. The bottom view of the internal SCM construction, with marked the RAM chip and the Compact Flash Card, which stores the operating system and all of the SCM's data is shown in Fig. 5.

The container module is powered by two batteries thus it enables unattended work for a long time, which depends on batteries capacity. The first of batteries has a smaller capacity and it is enclosed in the SCM's casing. The second of batteries could have as large capacity as necessary. It is placed inside the container and connected to SCM. The SCM is equipped with a voltage control circuit, whereby it is possible to distinguish SCM turning off for lack of power against other cases.

The Sensors' Controller have been designed in a manner making construction of the measuring module independent from a type of using computer model and to enable free deployment

Fig. 3. *A prototype of the Smart Container Module*
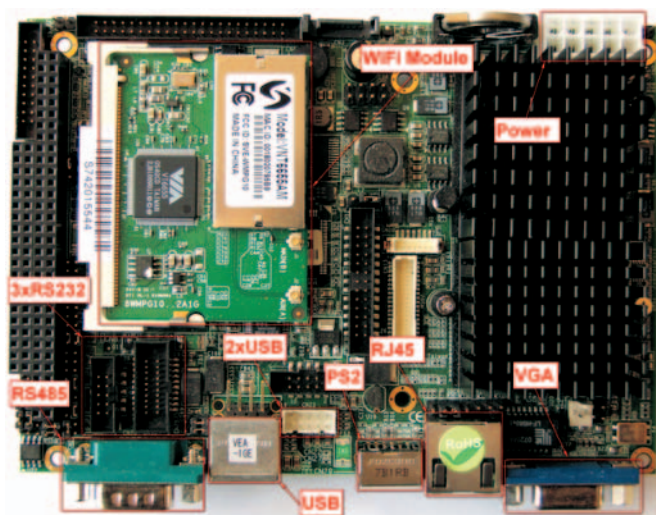
Fig. 4. Top view of the internal SCM construction
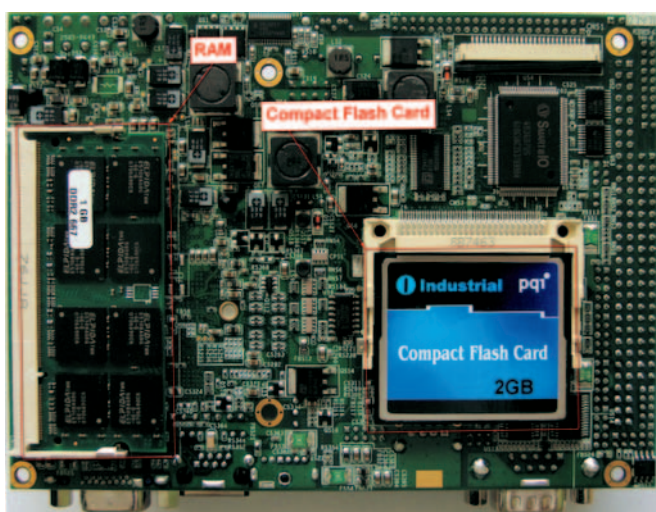
Fig. 5. Bottom view of the internal SCM construction

of reconfiguring sensors inside the container. The exemplary Sensors' Controller board is shown in Fig. 6. Composition of this circuit includes three parts: the microcontroller, the RS485 converter with auxiliary circuits and the set of sensors dedicated to the specific cargo container. Sensors, which can be connected the Sensors' Controller with:
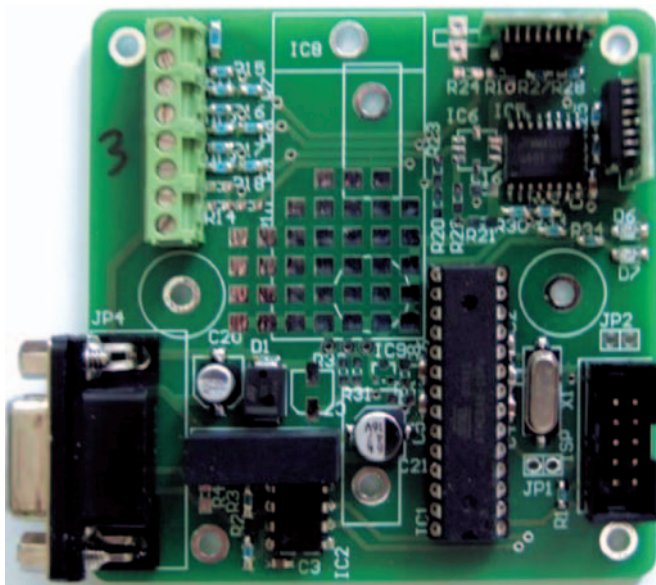
- *sabotage* - this sensor allows to detect a sabotage, e.g. SCM's casing tamper or cutting off any of Sensors' Controllers
- *door switch* - this sensor indicates whether the door of the container is open or not
- *motion* - this sensor allows to detect movement inside the container
- *smoke* - this sensor allows to detect smoke inside the container
- *temperature* - this sensor measures ambient temperature inside the cargo container
- *humidity* - this sensor measures relative humidity inside the cargo container
- *acceleration* - this sensor measures acceleration on three axes (range to 10g or to 50g)
- any other sensor with electrical output.

Usage of Sensors' Controllers allows connect many sensors to the SCM simultaneously. Additionally it allows to unrestricted changes types of sensors and their deployment inside the container.

SELF-ORGANIZING NETWORK OF SCM MODULES

Because of the vertical way of containers storage on container ships, there is a problem of access to the on-board wireless network for Smart Container Modules mounted on the containers at the lowest level. Additionally, GPS satellites are beyond the sight of view of the GPS receiver, installed in the adversely located SCM modules, thus it is impossible to read the geographical position. In order to solve this problem SCM modules have been programmed in a manner that allows them to self-organize in ad-hoc network. During the research a new algorithm for data transmission control over a multi-hop ad-hoc network (assuming slow-moving nodes) has been developed [3].

By dint of this solution it is possible to transfer data about cargo to the Ship Subsystem's database, even from the Smart Container Module installed on the lowest container. The data about the cargo are transferred to adjacent modules by the WiFi radio link. If module has a connection to the on-board wireless network, it will forward data to the database. If this module is beyond the reach of the on-board wireless network, it will forward the data to the next SCM, etc. Additionally, the self-organizing ad-hoc network enables SCM modules beyond the

Fig. 6. The sensors' controller board

Fig. 7. The SCM self-organizing ad-hoc network tests

reach of GPS system to read and save the geographical position on the basis of data from modules at the top of containers' stack. The ability to self-organize modules in the ad-hoc network can also be useful in harbours or container terminals, where direct access to the Port Subsystem's wireless network or receiving signals from GPS satellites can be impossible. Fig. 7 depicts the laboratory for testing the Self-Organizing Container Monitoring Network composed of three Smart Container Modules.

The results of these tests have proved the ability of testing network to self-organize in real time, especially to choose SCM module to communicate with the database.

USER INTERFACE

In the course of the research, the user interface including a database storing all data about the system has been created. Depending on the granted access privileges, user may get the following information: state of the system, defined types of containers, registered containers (with the assigned sensor network), ongoing and completed shipments and communication history. In addition, there is the ability to users manage (adding/removing user, changing password) only for users with administrator privileges.

Each transport can be remotely monitored. Cargo information (parameters from the sensor network, current position and route of transport) are available in three forms: a table, graphs and a map. Fig. 8 depicts a map of portion of the transport route. This function uses the Google Maps available for free by Google.

Data can also be presented in a transparent form of graphs, which are created on the basis of data from various sensors. Sample record of the temperature inside the cargo is presented in Fig. 9.

Using the interface is intuitive and user-friendly, which greatly facilitates access to the system at any point on earth with access to the Internet.
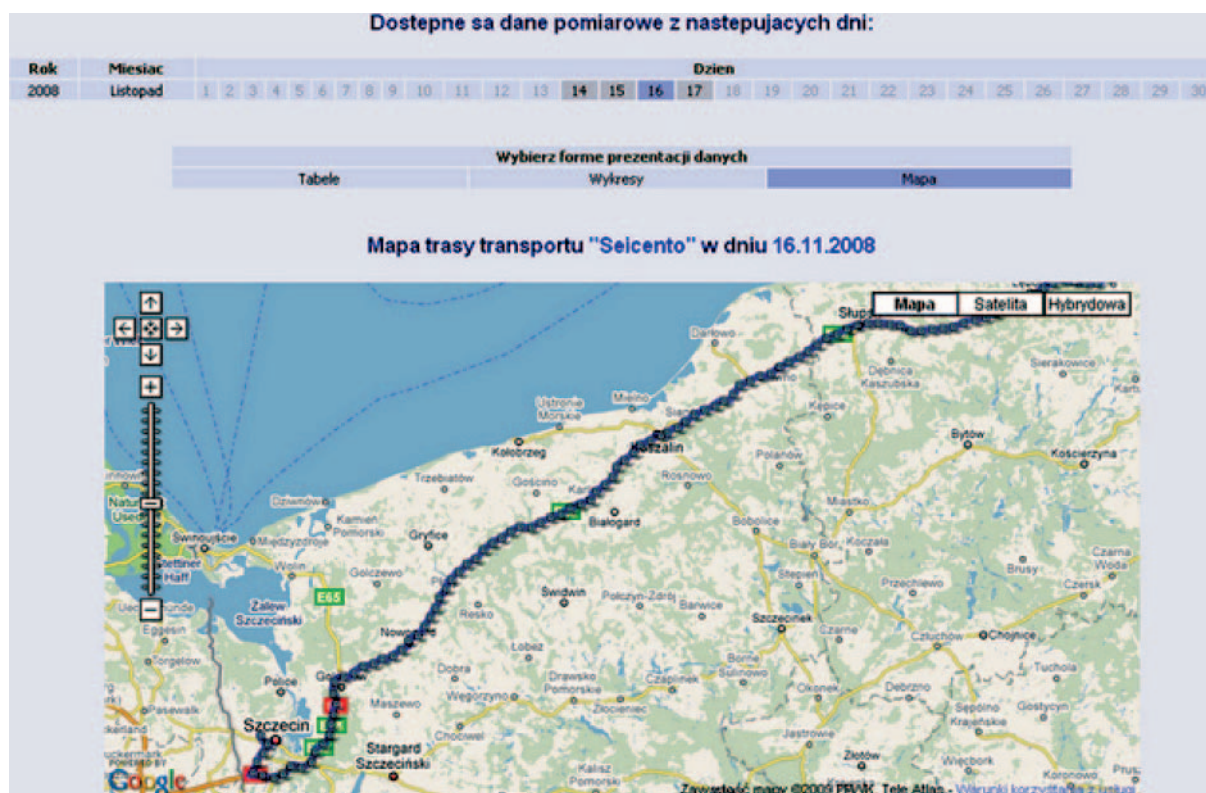
Fig. 8. *Sample view of the user interface with a map of the transport route*

Fig. 9. *Sample view of the user interface in the control of temperature scope*

CONCLUSIONS

– This is a fully operational global system for wireless monitoring of cargo containers that enhances the safety and effectiveness of this mode of transport. The Smart Container Module (SCM) is a basic element in a global grasp of the system. The module is equipped with various sensors placed inside the container that enable detection of many parameters. Each SCM is equipped with the GPS receiver, the GPRS module and the WiFi module. Due to the vertical way of containers storage, there are problems with individual SCM to communicate with the local wireless on-board network or in the container terminal. The self-organizing network of smart container modules is a proposed solution of those problems.

– Described concept of global system for monitoring of cargo containers, especially self-organizing monitoring network consisting SCM modules is a part of a wider security subject matter, which currently has a high priority, both in Poland and the world. In addition, increasing the efficiency of container transport is possible by dint of the safe and efficient user interface.

Acknowledgments

BIBLIOGRAPHY

1. Katulski R., Niski R., Stefański J., Żurek J.: *Concept of the container monitoring system in Polish harbours*, 2006 IEEE Conference on Technologies for Homeland Security, Enhancing Transportation Security and Efficiency, Boston, USA, June 7 2006

2. Katulski R.J., Ambroziak S.J., Miszewska B., Sadowski J., Stefański J.: *Global wireless monitoring system for cargo containers*, Przegląd Telekomunikacyjny i Wiadomości Telekomunikacyjne, No 06/2009

3. Katulski R., Ambroziak S., Białowąs A., Mazurkiewicz B., Miszewska B., Niski R., Pawłowski W., Sadowski J., Stefański J., Rauchut-Sobczak B., Żurek J.: *Description of the system for cargo containers monitoring in a container terminal*, Gdańsk University of Technology, Faculty of Electronics, Telecommunications and Informatics, Department of Radiocommunication Systems and Networks, Scientific Report 5/2009, 254 pages, 84 figures, 78 tables, 29 references, 2009

4. Karl H., Willig A.: *Protocols and Architecture for Wireless Sensor Networks*, Wiley & Sons, 2006

CONTACT WITH THE AUTHORS

Ryszard J. Katulski, Assoc. Prof.
Jarosław Sadowski, M. Sc.
Jacek Stefański, Ph. D.
Sławomir J. Ambroziak, M. Sc.
Bożena Miszewska,
Faculty of Electronics, Telecommunications
and Informatics
Gdansk University of Technology
Narutowicza 11/12
80-231 Gdańsk
e-mail: sj_ambroziak@eti.pg.gda.pl

An integrated framework for various operation plans in container terminals

S. H. Won,
K. H. Kim,
Pusan National University, South Korea

ABSTRACT

This study provides a framework for integrating various planning activities in container terminals. First, we introduce various planning activities in container terminals and identify decision-making problems for each planning activity. Input parameters, decision variables, objectives, constraints, time buckets, and the planning horizon for each decision activity are identified. Next, we introduce the concept of a resource profile and planning procedure simultaneously by considering availabilities of various resources and resource requirements in a planning activity.

INTRODUCTION

Port container terminals are located at places where containers are transshipped from a transportation mode to another. Their main functions are to provide transfer facilities for containers between vessels and land transportation modes, such as trucks and trains. They are characterized by highly complex systems that involve numerous pieces of equipments, operations, and handling steps. Operations in container terminals can be classified into a vessel operation process during which containers are discharged from and loaded onto a vessel and receiving and delivery operation processes during which containers are transferred from and to external trucks. During these operations, assigning resources to these operations and scheduling these operations become major planning issues in container terminals.

Many researchers reviewed planning problems in an operation of container terminals (Ramani, 1996; Bontempi *et al.*, 1997; Meersmans and Dekker, 2001; Vis and de Koster, 2003; Steenken *et al.*, 2004; Murty *et al.*, 2005; Crainic and Kim, 2007). Ramani (1996) divided the basic task in the management of container terminals into a berth allocation, yard planning, stowage planning, and logistics planning in container operations. A berth allocation issue is to plan which berth is to be assigned to a given ship for loading and unloading its containers. A yard planning involves the allocation of storage spaces to import, export, and transshipment containers. A stowage planning assigns stowage locations to outbound containers in bays of a ship. A logistic planning deals with scheduling and coordinating the operation of port equipments, such as quay cranes, prime movers, and yard cranes for

moving containers among different sources and destinations (for example, gates, vessels, rail stations, storage yards, and container freight stations).

Bontempi *et al.* (1997) assigned a different time horizon to each planning problem in container operations. They used the solution obtained in long-term problems (container storage policies) as an input for mid-term problems (resource allocation problems) and the solution obtained in mid-term problems (resource allocation policies) as an input for short-term problems (load and unload scheduling problems). Meersmans and Dekker (2001) and Vis and de Koster (2003) distinguished decisions on container handling operations into strategic, tactical, and operational levels according to the time horizon involved. A time horizon in decisions for the strategic, tactical, and operational level covers one to several years, a day to months, and a day, respectively.

Steenken *et al.* (2004) reviewed terminal logistics and optimization methods. They described the important processes in container terminals that can be optimized by means of operations research methods: ship planning processes (consisting of berth allocation, stowage planning, and crane split), storage and stacking logistics, transport optimization, and simulation systems. Murty *et al.* (2005) introduced nine decisions to be made in daily operations: allocation of berths to arriving vessels, allocation of quay cranes to docked vessels, appointment of arrival times to external trucks, routing of trucks, dispatch policy for trucks at terminal gatehouses and docks, storage space assignment, yard crane deployment, internal truck allocation to quay crane, and optimal internal truck hiring plans. Günther and Kim (2006) divided planning and control levels in container terminals into three categories:

terminal design, operative planning, and real-time control. A terminal design level contains multi-modal interfaces, terminal layout, equipment selection, berthing capacity, and IT-system and control software. An operative planning level contains storage and stacking policies, crane assignment and split, berth allocation, and stowage planning. A real-time control level contains landside transport, quayside transport, slot assignment, and crane scheduling operation sequencing. Crainic and Kim (2007) introduced models for the operational planning control in container terminals. Their models include scheduling of berths, scheduling of quay cranes, stowage planning and sequencing, storage activities in a yard, and allocation and dispatching of yard cranes and transporters.

This study provides a framework for integrating various planning activities in container terminals. First, we introduce planning problems in container terminals and identify a decision activity for each planning problem. Input parameters, decision variables, time buckets, and the planning horizon for each decision activity are identified. Next, we introduce the concept of a resource profile and planning procedure simultaneously by considering resource capacities and resource requirements.

Section 2 provides a framework for the operation planning process in container terminals. Section 3 discusses resource profiles for certain decision activities related to various operational plans. Three subsections illustrate examples of the capacity planning in berth planning, scheduling of quay cranes, and yard planning, respectively. Finally, Section 4 presents a conclusion.

FRAMEWORK FOR A PLANNING PROCEDURE

Container terminals perform various handling operations by utilizing such resources as quays or berths, quay cranes (QCs), storage yards (SYs), yard cranes (YCs), traveling areas (TAs), and transporters (TRs). A traveling area represents a traffic zone or a set of transfers for trucks. Two most important performance measures in a container terminal are turnaround time of a vessel and road trucks in a terminal. Turnaround time of a vessel and road truck highly depends on the capacity of applied resources and methods to allocate the capacity of resources in handling tasks. This section describes how the capacity of resources can be explicitly considered during each of planning processes and information on the capacity can be shared among different planning processes in container terminals.

Resource capacities are represented as follows: the capacity of berths can be represented as the product of one dimensional space (usually length) and time. The capacity of QCs, TRs, and YCs are measured in QC times, TR times, and YC times, respectively. If all QCs have the same capacity, we can evaluate the capacity of QCs by multiplying the number of QCs by their available time. In a similar way, the capacity of other resources can be evaluated. Tab. 1 summarizes units to represent the capacity of each different type of resources.

Tab. 1. Resources and units

Resources	Units
Berth (H)	Length of the berth × berthing duration
QC (C)	Number of QCs × operation time
TR (R)	Number of TRs × operation time
YC (Y)	Number of YCs × operation time
TA (A)	Number of TRs passing the TA × operation time
SY (S)	Number of slots (in TEU) × storage duration

All planning activities for operations must check the availability of resources required for the operations. An amount of resources required for an operation can be estimated as follows: berthing a vessel requires the resource of berths based on the length of a vessel multiplied by the occupation time. Unloading or loading containers consume the resource of QCs by the number of containers multiplied by the standard handling time per container. The workload in unloading and loading operations on TRs can be evaluated by multiplying the number of containers with the average transportation time per container including empty travels. The workload of unloading and loading operations on YCs can be calculated by multiplying the number of containers with the standard handling time of a YC per container. The workload on TAs represents the expected future occupation of TAs by TRs. The storage space of a SY requires a certain amount of reservation before the storage of containers and actual occupation by containers. Fig. 1 shows a planning procedure in container terminals. We classified this procedure as long-term, mid-term, and short-term according to the planning horizon.
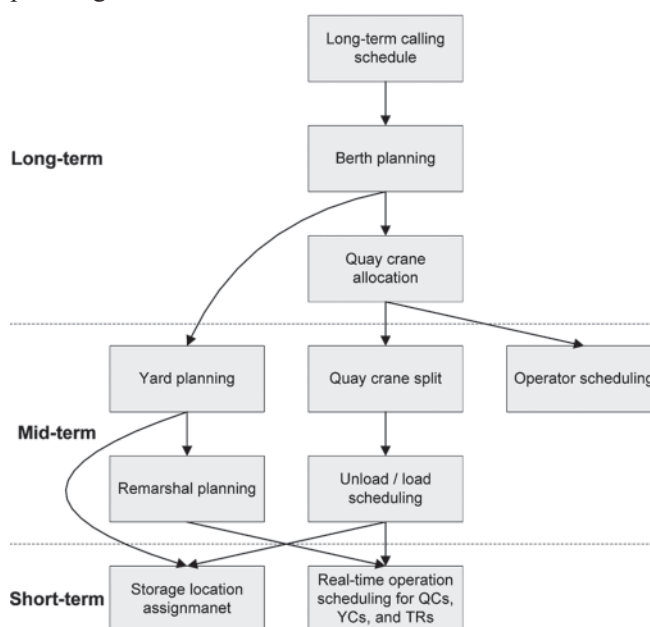
Fig. 1. Framework of the planning process

Every planning process must consider the availability of related resources. Fig. 2 shows several key planning processes and their related resources that must be checked before commitment. The berth planning is a decision process on the berthing location and time for ships. A certain zone in a berth is assigned to a ship for loading and unloading containers for a certain period of time. Scheduling of QC works (split) is a decision process on a service sequence of bays in a ship by each QC and time schedule for services. Several QCs are usually assigned to one ship. Yard planning is a decision process on storage locations for containers during unloading operation, receiving operation, and remarshalling operation. Scheduling of unloading is a decision process on a work sequence and time for inbound containers that are discharged from a ship to storage locations in a SY. Scheduling of loading is a decision process on a work sequence and time for outbound containers that are loaded from a SY to storage locations in a ship. Remarshal planning is a decision process on movements of containers from a storage block to another and time of movements.
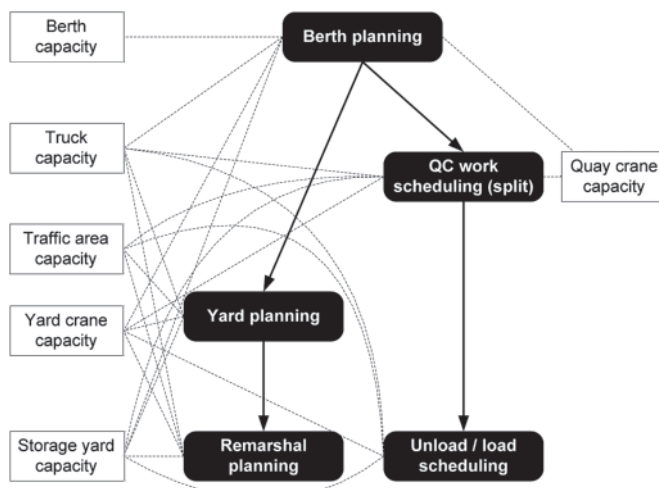
Fig. 2. *Various operational plans and their related resources*

Decisions to be made by each planning process are summarized in Tab. 2. The first line of each planning process represents the activity or activity unit on which a decision will be made. The second line represents the reference moment of the activity from which the time-phased consumption of resources resulting from the decision will be estimated. The third line represents contents of the decision to be made by each planning process.

The following sections will discuss the resource profile in major decision processes for long-term and mid-term plans in container terminals: berth planning, scheduling of QC works, and yard planning. This study considers six resources: berths, QCs, TRs, YCs, TAs, and SY. The operation time applied in resources is configured as berthing time, handling time by QCs, transportation time by TRs, handling time by YCs, occupation time of TAs, and storage time of SY. For describing the resource profile and plan, the following notations are used:

Tab. 2. *Contents of the decision for various operational plans*

Long-term	
Berth planning (B)	
Activity to be planned	Berthing of each vessel
Reference moment of the activity	Beginning of the berthing
Contents of the decision	Berthing position and time of each vessel
Mid-term	
QC work scheduling (Q)	
Activity to be planned	Loading or unloading task on deck or in hold of a bay by a QC
Reference moment of the activity	Beginning of each task
Contents of the decision	Schedule for QCs to discharge (or load) containers from (or onto) vessels
Yard planning (P)	
Activity to be planned	Receiving outbound containers for a vessel or unloading inbound containers by a QC for a vessel for a period
Reference moment of the activity	Starting of arrivals of outbound containers at a gate or unloading of inbound containers from a vessel
Contents of the decision	Storage positions for outbound containers for a vessel arriving during a period or inbound containers discharged from a vessel
Remarshal planning (M)	
Activity to be planned	Moving a set of containers from a block to another for a period
Reference moment of the activity	Starting of movements
Contents of the decision	Containers to be moved and their sources and destination positions for a period
Short-term	
Unload scheduling (U)	
Activity to be planned	Unloading containers on deck or in hold of a bay
Reference moment of the activity	Starting of unloading
Contents of the decision	Discharging sequence of individual inbound containers
Load scheduling (L)	
Activity to be planned	Loading containers onto deck or into hold of a bay
Reference moment of the activity	Starting of loading
Contents of the decision	Loading sequence of individual outbound containers

Indices

r – index used in resources where $r = H$ (berth), C (QC), R (TR), Y (YC), A (TA), and S (SY)

t – index used in periods where $t = 1, 2, …, m$

a – index used in activities where $a = 1, 2, …, n$.

Problem data

s_{ar}^t – a unit amount of resource **r** that must be used with the time offset of **t** for carrying out activity **a**. In a berth planning, for example, if a vessel is decided to berth at a quay at period p (let this be activity "B"), the operation time of QCs at period (p + t) will be required by the amount of s_{BC}^t.

Sets

T_{ar} – a set of time offsets in which resource r is consumed by activity **a**

B – a set of activities related to berth plans. Each activity corresponds to a decision on the berthing of a vessel

Q – a set of activities related to QC work schedules. Each activity corresponds to a decision on the work for a vessel by a QC

P – a set of activities related to yard plans.

Decision variables

X_a – a decision vector for activity **a**. As an illustration, a decision vector in a yard plan for outbound containers is a set of storage blocks for the arriving outbound containers to be stacked and the amount of containers to be stored at each storage block.

BERTH PLANNING

A berth planning determines the berthing position and time of a vessel. Tab. 3 shows input parameters, decision variables, objectives, and constraints for the berth planning. A berth planning requires such input data as a calling schedule, favorable berthing location, length of a vessel, required draft of each vessel, required unloading and loading time for each vessel, and various constraints and priorities for locating and sequencing a vessel. One of the objective in a berth planning is to locate vessels at the most favorable position on the quay that will reduce the container delivery time between the marshaling yard and QCs and also to make vessels to depart the port before their committed due times. Also, the waiting time of vessels at a port must be minimized.

Tab. 3. Definition of problems in a berth planning

Input parameters	Calling schedule of vessels Favorable berthing location of each vessel Length of each vessel Draft required for each vessel Number of unloading and loading containers of each vessel Resource profiles
Decision variables	Berthing position of each vessel Berth time of each vessel
Objectives	To minimize delays in the departure of a vessel To minimize the travel distance between the shore and the yard for all containers in a vessel To minimize the waiting time of a vessel at a port
Constraints	Depth of water for berths Arrival time of a vessel at a port Availability of resources

Resource requirements depend on the number of unloading and loading containers and are evaluated by using the load profile of each resource in a berth planning. The requirement of each resource can be determined as a time-phased way with respect to the berth time of a vessel. Decision variables in a berth planning consist of the berthing position and berthing time of each vessel. By adding the schedule of a vessel in a berth plan, various resources are required as shown in Figs 3-(a) and (b). Figs 3-(a) and (b) show the resource profile for outbound and inbound flows, respectively.

A resource profile can be evaluated by using several different ways: s_{BH}^0 indicates the amount of berths required in the berth plan B at a day when a vessel arrives at a berth. It can be evaluated by using (the length of a vessel plus the allowance between adjacent vessels) × (the expected berthing duration of a vessel). s_{BC}^0 can be evaluated by using {(the time for a QC to transfer an outbound container to a slot of a vessel) × (the percentage of loading containers among all containers for a vessel) + (the time for a QC to transfer an inbound container to a TR) × (the percentage of unloading containers among all containers for the vessel)}. Standard time that includes not only pure operation time but also unavoidable delays and personal and fatigue allowances must be used.

Because TRs are required for loading and unloading operations, s_{BR}^0 can be evaluated in the similar way as s_{BC}^0. s_{BY}^t for $t < 0$ can be evaluated by using (the time for a YC to receive an outbound container from an external road truck) × (the percentage of containers, among all the outbound containers, arriving at a SY on the tth day before the berthing of a vessel). s_{BY}^t for $t > 0$ can be evaluated by using (the time for a YC to transfer an inbound container to an external road truck) × (the percentage of containers, among all the inbound containers, leaving a terminal on the tth day after the departure of a vessel). s_{BY}^t for $t = 0$ can be evaluated by using {(the time for a YC to transfer an outbound container to a TR) × (the percentage of loading containers among all containers for a vessel) + (the time for a YC to receive an inbound container from a TR) × (the percentage of unloading containers among all containers for a vessel)}. s_{BS}^t for $t \leq 0$ can be evaluated by using (the cumulative percentage of containers, among all the outbound containers, having arrived at a SY until the tth day before the arrival of a vessel) × (the length of a period). s_{BS}^t for $t \geq 0$ can be evaluated by using {(1 – the cumulative percentage of containers, among all the inbound containers, having left the terminal until the $(t – 1)^{th}$ day after the departure of a vessel) × (the length of a period)}.

As an example, we illustrate how s_{BY}^t for $t < 0$ can be estimated as follows. In order to evaluate s_{BY}^t for $t < 0$, we must have the following two data: the operation time for a YC to receive an outbound container from an external truck; and the percentage of containers, among all the outbound containers, arriving at a SY on the tth day before the arrival of the vessel. Tab. 4 shows an example of s_{BY}^t, for $t < 0$. The expected handling time for a receiving operation by a YC used in the example is 1.521 minutes.

Tab. 4. Example of s_{BY}^t for $t < 0$

t (day)	-6	-5	-4	-3	-2	-1
Percentage of containers [%]	2	5	6	10	12	65
s_{BY}^t (minutes)	0.030	0.076	0.091	0.152	0.183	0.989

Tab. 5 summarizes the data used for calculating a resource profile. Tabs 4 and 6 show the percentage of containers

arrived at a SY on the days before loading and of containers left the terminal on each day after the departure of a vessel, respectively. Tab. 7 illustrates the resource profile for berthing of a vessel.
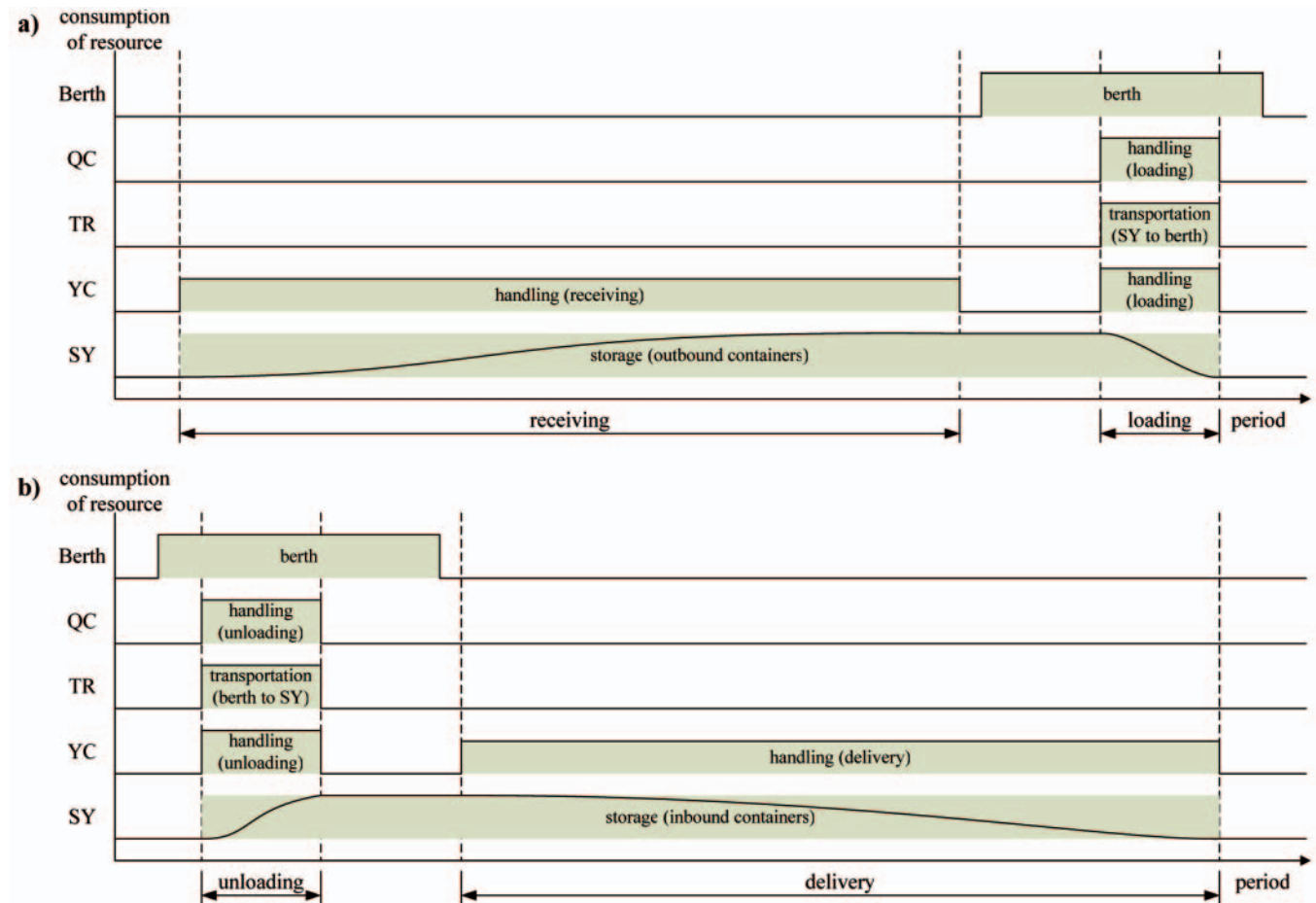
Fig. 3. *Resource profile for berthing a vessel.* ***a)*** *resource profile for outbound containers,* ***b)*** *resource profile for inbound containers*

Tab. 5. *Data used for calculating the resource profile for a vessel in a berth planning*

Length of the vessel plus the allowance between adjacent vessels	300 m
Berthing duration of the vessel	18 hrs
Number of loading containers for the vessel	540
Number of unloading containers for the vessel	560
Time for a QC to transfer an outbound container to a slot of the vessel	1.9 min.
Time for a QC to transfer an inbound container to a TR	1.9 min.
Turnaround time for a TR to the travel between the shore and the yard	10 min.
Time for a YC to receive an outbound container from an external truck	1.521 min.
Time for a YC to transfer an inbound container to an external truck	2.242 min.
Time for a YC to transfer an outbound container to a TR	1.134 min.
Time for a YC to receive an inbound container from a TR	1.114 min.
Storage duration of a container during a period (the length of a period)	24 hrs

Tab. 6. *Percentage of inbound containers left the terminal on the nth day after unloading*

n	1	2	3	4	5	6
Percentage (%)	34	22	15	14	11	4

Tab. 7. *Resource profile for berthing a vessel (s_{Br}^{t}) (unit: minute)*

t	-6	-5	-4	-3	-2	-1	0	1	2	3	4	5	6
r													
H	–	–	–	–	–	–	324,00	–	–	–	–	–	–
C	–	–	–	–	–	–	1.9	–	–	–	–	–	–
R	–	–	–	–	–	–	10	–	–	–	–	–	–
Y	0.030	0.076	0.091	0.152	0.183	0.989	1.124	0.762	0.493	0.336	0.314	0.247	0.090
S	28.8	100.8	187.2	331.2	504	1,440	1,440	1,440	950.4	633.6	417.6	216	57.6

A numerical example is provided to illustrate a resource profile for a berth planning. We assume that the length of one period is 1 day, and the planning horizon is 14 days. Also, let us suppose that a vessel is scheduled to berth at the quay during period 7, 01:00~19:00. The total length of the quay is 1,500 m and thus the capacity of the berth is $1,500 \times 1,440$ m-min per period. The total number of slots in the SY is 21,000 slots. The SY consists of 20 storage blocks in which a storage block consists of 5 tiers, 6 rows, and 35 bays. Thus, the capacity of the SY becomes $21,000 \times 1,440$ slot-min per period. The number of QCs, TRs, and YCs is 15, 40 and 20 respectively. However, a QC has a schedule for preventive maintenances on periods 6, 7, and 8, and five TRs are expected to enter a maintenance shop for such preventive maintenances in periods 12, 13 and 14. The capacity of QCs, TRs, and YCs in a period can be evaluated by multiplying the total number of equipments with the length of a period, namely 21600, 57600 and 28800 machine-minutes, respectively. In the periods of 6, 7 and 8, the capacity of QCs becomes 20160 machine-minutes. In the periods of 12, 13 and 14, the capacity of TRs becomes 50400 machine-minutes.

Tab. 8 shows a part (periods 4 – 10) of an example in a capacity plan for the berthing of a vessel in the 7th day. The notations 'CP (capacity)', 'RS (reserved)', 'AV (available)', and 'RQ (requirement)' represent the total capacity of each resource during a period, the amount of the resource already reserved by other plans, the amount of available resource that is CP subtracted by RS, and the amount of the resource that will be reserved by the berthing of the vessel under consideration, respectively. Values in the 'RQ' are calculated by using the resource profile noted in Tab. 7 and the number of loading and unloading containers for the vessel noted in Tab. 5.

In Tab. 8, note that the resource requirements for the QCs and SY exceed their available capacities in the period of 7. Thus, we have to prepare extra QCs and storage spaces for containers in the period of 7 or reject the berthing of this vessel. Because a QC has a schedule for preventive maintenances in the period of 7, changes in a maintenance schedule for the QCs may solve these problems. Also, leasing the outside of SY (e.g. off-dock container yard) or reducing the dwell time of containers may increase in storage spaces for containers.

SCHEDULING OF QC WORKS (SPLIT)

Scheduling of QC works determines a schedule for each QC to discharge and load containers on a specific deck or in a specific hold of a vessel. We assume that a related berth plan has already been constructed. Tab. 9 shows the input parameters, decision variables, objectives, and constraints for scheduling of QC works.

For constructing a QC work schedule, a stowage plan for vessels and yard map in a SY must be provided. A stowage plan indicates the location of slots which containers must be discharged from or to be loaded in. A yard map shows storage locations of containers bound for a vessel. There may be some precedence relationships to be satisfied in unloading and loading tasks. For example, when a discharging operation is performed at a bay in a vessel, operations on a deck must be performed before the operations in hold of the same bay start. Also, loading operations in a hold must precede the loading operation on a deck of the same bay in a vessel. Because QCs travel on the same rail, two adjacent QCs must be apart from each other by at least a certain distance for them to simultaneously perform

Tab. 8. Example of a capacity plan in a berth planning

t	4	5	6	7	8	9	10
Berth							
CP	2,160,000	2,160,000	2,160,000	2,160,000	2,160,000	2,160,000	2,160,000
RS	1,857,600	1,978,560	1,918,080	1,797,120	–	–	–
AV	302,400	181,440	241,920	362,880	2,160,000	2,160,000	2,160,000
RQ	–	–	–	324,000	–	–	–
QC							
CP	21,600	21,600	20,160	20,160	20,160	21,600	21,600
RS	20,403	20,613	19,068	18,312	–	–	–
AV	1,197	987	1,092	1,848	21,600	21,600	21,600
RQ	–	–	–	**2,090**	–	–	–
TR							
CP	57,600	57,600	57,600	57,600	57,600	57,600	57,600
RS	46,890	47,340	47,115	43,185	36,540	36,240	36,075
AV	10,710	10,260	10,485	14,415	21,060	21,360	21,525
RQ	–	–	–	11,000	–	–	–
YC							
CP	28,800	28,800	28,800	28,800	28,800	28,800	28,800
RS	24,900	25,380	24,960	23,610	22,140	22,020	21,540
AV	3,900	3,420	3,840	5,190	6,660	6,780	7,260
RQ	82	99	534	1,236	427	276	188
SY							
CP	30,240,000	30,240,000	30,240,000	30,240,000	30,240,000	30,240,000	30,240,000
RS	28,800,000	29,160,000	29,088,000	28,800,000	28,080,000	27,720,000	27,360,000
AV	1,440,000	1,080,000	1,152,000	1,440,000	2,160,000	2,520,000	2,880,000
RQ	178,848	272,160	777,600	**1,584,000**	806,400	532,224	354,816

their operations without any interference. Planners attempt to construct in a way of minimizing the makespan in ship operations.

Input parameters	Stowage plan of a vessel Available time window of each QC Yard map Resource profiles
Decision variables	Work schedule for QCs assigned to a vessel
Objectives	To minimize a make-span in ship operations
Constraints	Precedence relationships in operations Interference among QCs Availability of resources

Like in the berth planning, resource requirements depend on the number of unloading and loading containers and are evaluated by using a load profile for the scheduling of QC works. Requirements for each resource can be represented as shown in Figs 4-(a) and (b) that illustrate the resource profiles applied in inbound and outbound flows, respectively.
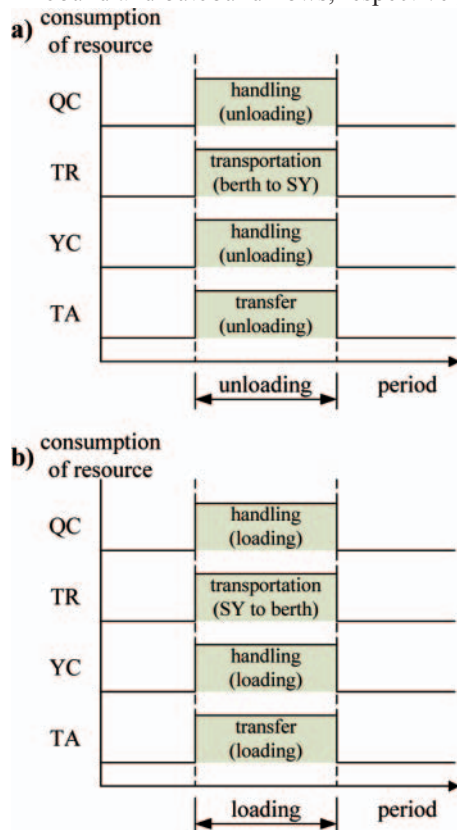

Fig. 4. *Resource profile for unloading and loading operations in a vessel.*
a) resource profile for inbound containers,
b) resource profile for outbound containers

During the process of the scheduling of QCs in advanced container terminals, blocks where inbound containers are unloaded and outbound containers are picked from each ship-bay are simultaneously determined. The availability of the resources in each corresponding block must be checked before the decision on the blocks is fixed. The resources in each block are YCs, TAs, and SY of each block. However, because the fleet of TRs may be operated in a pool for all QCs, the capacity of all TRs in a terminal are compared with the required amount of TRs during the ship operation.

Let $s^0_{QY_u}$ and $s^0_{QY_l}$ be the unit amount of the YC capacity required for transferring a container for unloading and loading operations that is required at the period when the ship operation occurs, respectively. $s^0_{QA_u}$ and $s^0_{QA_l}$ can be defined in the same way as previously mentioned ways. A resource profile can be evaluated as follows: s^0_{QC} can be evaluated by using {(the time for a QC to transfer an outbound container to a slot of a vessel) × (the percentage of loading containers among all containers for a QC) + (the time for a QC to transfer an inbound container to a TR) × (the percentage of unloading containers among all containers for a QC)}. Because TRs are required in loading and the unloading operations, s^0_{QR} can be evaluated in the similar way as s^0_{QC}. $s^0_{QY_u}$ and $s^0_{QY_l}$ can be evaluated by using the time for a YC to receive an inbound container from a TR and time for a YC to transfer an outbound container to a TR, respectively. Because TAs are consumed at the same period when YCs are required, $s^0_{QA_u}$ and $s^0_{QA_l}$ can be evaluated in the similar way as $s^0_{QY_u}$ and $s^0_{QY_l}$, respectively.

Tab. 10 summarizes data used for calculating the resource profile. For the transfer time of a QC, cycle time of a TR, and handling time of a YC, we used those in Tab. 5. Tab. 11 illustrates a resource profile in ship operations by QCs.

Number of loading containers for a QC	15 during period 3
Number of unloading containers for a QC	16 during period 3
Time for a TR to transfer a loading container in a TA	3 min
Time for a TR to transfer an unloading container in a TA	3 min

r	R	Y_u	Y_l	A_u	A_l
	10	1.114	1.134	3	3

We will introduce a numerical example to illustrate the resource profile applied to the scheduling of QC works. We assume that the length of one period is 1 hour, and a planning horizon is 12 hours. Also, let us suppose that a QC is scheduled to handle the containers during the period of 3. The capacity of a QC is 60 machine-minutes, the capacity of TRs is 2,400 machine-minutes, and the capacity of YCs in a storage block is 60 machine-minutes (refer to Section 3.1). Assuming that a storage block has 9 TAs and average occupation time of a TR in the TA is 3 minutes, the capacity of TAs in a storage block for a period can be obtained by multiplying the number of TAs in a storage block with the maximum number of TRs passing the TA for a period, namely, 180 machine-minutes.

The containers to be discharged or loaded by the QC will be located or are located in four different storage blocks as shown in Tab. 12. Tab. 13 shows an example of a capacity plan for the scheduling of QC works. Entries of 'RQ (requirement)' of each resource are calculated by using the resource profile in Tab. 11, number of loading and unloading containers for the QC in Tab. 10, and storage distribution of the containers for the QC in Tab. 12.

Storage block	1	2	3	4
Number of unloading containers	11	5	–	–
Number of loading containers	–	3	4	8

Tab. 13. Example of a capacity plan for the scheduling of QC works

a) TR

t	1	2	3	4	5	6	7	8	9	10	11	12
TR												
CP	2,400	2,400	2,400	2,400	2,400	2,400	2,400	2,400	2,400	2,400	2,400	2,400
RS	1,967	1,963	1,800	1,523	1,517	1,511	1,509	1,503	1,503	1,501	1,500	1,359
AV	433	437	600	877	883	889	891	897	897	899	900	1,041
RQ	–	–	310	–	–	–	–	–	–	–	–	–

b) YC and TA in storage block 1

t	1	2	3	4	5	6	7	8	9	10	11	12
YC1												
CP	60	60	60	60	60	60	60	60	60	60	60	60
RS	53	52	50	46	46	46	46	45	45	45	45	44
AV	7	8	10	14	14	14	14	15	15	15	15	16
RQ	–	–	12	–	–	–	–	–	–	–	–	–
TA1												
CP	180	180	180	180	180	180	180	180	180	180	180	180
RS	107	103	128	133	133	133	132	130	129	129	129	126
AV	73	77	52	47	47	47	48	50	51	51	51	54
RQ	–	–	12	–	–	–	–	–	–	–	–	–

c) YC and TA in storage block 2

t	1	2	3	4	5	6	7	8	9	10	11	12
YC2												
CP	60	60	60	60	60	60	60	60	60	60	60	60
RS	53	51	50	46	46	46	46	45	45	45	45	44
AV	7	9	10	14	14	14	14	15	15	15	15	16
RQ	–	–	9	–	–	–	–	–	–	–	–	–
TA2												
CP	180	180	180	180	180	180	180	180	180	180	180	180
RS	108	103	88	125	125	125	125	123	122	122	121	120
AV	73	77	92	55	55	55	55	57	58	58	59	60
RQ	–	–	9	–	–	–	–	–	–	–	–	–

In Tab. 13 note that the resource requirements for the YCs in the storage block of 1 exceed the available capacity in the period of 3. Therefore, we have to deploy additional YCs in the period of 3. If other storage blocks can be used for unloading and loading containers in the period of 3, then the planner may modify the original schedule. Of course, the availability of the YCs and TAs must be checked again after the modification. Unfortunately, if a terminal cannot provide additional YCs in the period of 3, a certain part of work schedule in the period of period 3 must be moved to other periods.

YARD PLANNING

There are different types of yard plans depending on the handling facilities in a yard. However, most of yard plans specify, at least, the number of inbound containers to be discharged from each vessel and then stacked at each block, and the number of outbound containers bound for each vessel to be stacked at each block. Some yard plans may provide more detailed decisions on the storage, such as plans on storage layouts of outbound containers in each block. This paper assumes that a yard plan is constructed before containers bound for or discharged form a vessel start to arrive at a specific yard.

The decision on the exact storage location of an individual container is made in real time whenever a container arrives at a yard. Tab. 14 shows input parameters, decision variables, objectives, and constraints for a yard planning. For making a good yard plan, planners attempt to balance the workload in storage blocks and to minimize the travel distance for TRs to transport the containers between their storage blocks and berthing locations of the corresponding vessels.

Tab. 14. Definition of the problem in a yard planning

Input parameters	Number of outbound containers of each group that are bound for a vessel and will arrive at a terminal during each period
	Number of inbound containers discharged from a vessel during each period
	Resource profiles
Decision variables	Storage amounts for each group of containers to be stored in each storage block
Objectives	To balance workloads among storage blocks
	To minimize travel distances for TRs to transport containers between storage blocks and vessel berthing locations
Constraints	Availability of resources
	Storage capacity of each storage block
	Handling capacity of each storage block

The requirement of each resource can be determined as a time-phased way with respect to the arrival time of an
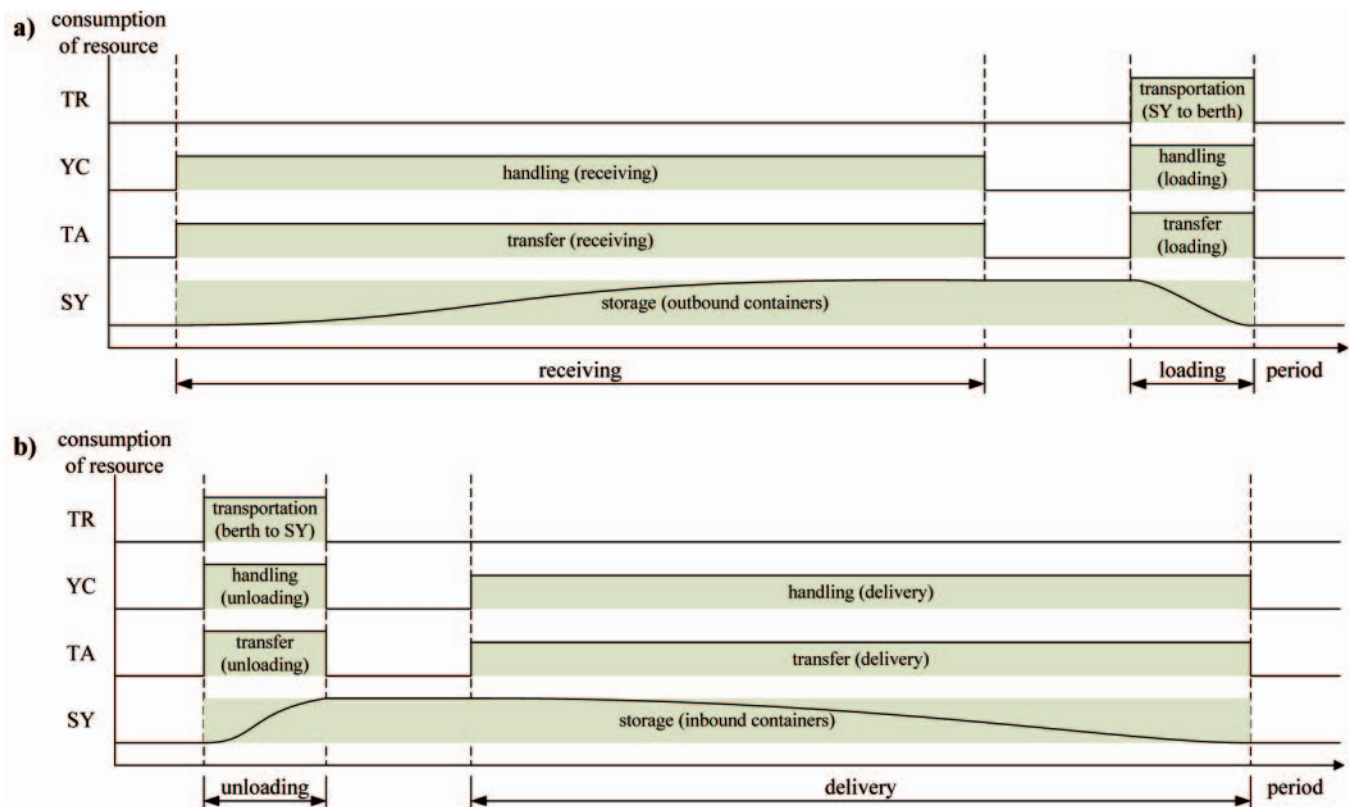
Fig. 5. *Resource profile for inbound and outbound containers.* **a)** *resource profile for outbound containers,* **b)** *resource profile for inbound containers*

outbound container or the discharging time of an inbound container. Figs 5-(a) and (b) illustrate a resource profile for outbound and inbound flows, respectively. As in the case of the scheduling of QC works, it is necessary to consider the YCs, TAs and storage spaces by each storage block and all TRs in a terminal. Decision variables in a yard planning are the number of outbound or inbound containers to be stacked at each block in each time period.

A resource profile for outbound containers can be evaluated as follows: s_{PR}^t for $t \geq 0$, can be evaluated by using the turnaround time for a TR to the travel between the shore and the yard. s_{PY}^t for $t \geq 0$ can be evaluated by (the transfer time for a YC to receive an outbound container) × (the percentage of containers, among all the outbound containers, arriving at the SY on the $(t + 1)^{th}$ period from the starting period of arrivals). s_{PY}^t for $t \geq 0$ can be evaluated by using the time for a YC to transfer an outbound container from a TR. Because TAs are required at the same period when YCs are required, s_{PA}^t for $t \geq 0$ can be evaluated in the similar way as s_{PY}^t for $t \geq 0$. s_{PS}^t for $t \geq 0$ can be evaluated by (the cumulative percentage of containers, among all the outbound containers, arriving at the SY until $(t + 1)^{th}$ period from the starting period of arrivals) × (the length of a period).

Second, a resource profile for inbound containers can be explained as follows: s_{PR}^t for $t = 0$ can be evaluated by using the time for a TR to the travel between shore and yard. s_{PY}^t for $t = 0$ can be evaluated by using the time for a YC to receive an inbound container from a TR. s_{PY}^t for $t > 0$ can be evaluated by using (the time for a YC to transfer an inbound container to an external truck) × (the percentage of containers, among all the inbound containers, leaving the terminal on the tth period after unloading). Because TAs are consumed at the same period when YCs are required, s_{PA}^t for $t > 0$ can be evaluated in the similar way as s_{PY}^t for $t > 0$. s_{PS}^t for $t = 0$ can be evaluated by using the storage duration of the container for a period. s_{PS}^t for $t > 0$, can be evaluated by {(1 – the cumulative percentage of

containers, among all the inbound containers, having left the terminal until the $(t – 1)^{th}$ period after unloading) × (the length of a period)}.

Tab. 15 summarizes data used for calculating the resource profile. For the cycle time of a TR, handling time of a YC, and transfer time of a TR, we used ones in Tabs 6 and 11. Tabs 16 and 17 illustrate the resource profile for receiving and discharging of containers, respectively.

Tab. 15. *Data used for calculating a resource profile in a yard planning*

Number of receiving containers for a vessel	540
Number of unloading containers for a vessel	560
Time for an external truck to transfer a receiving container in a TA	3 minutes
Time for an external truck to transfer a delivery container in a TA	3 minutes
Storage duration of the container for a period	24 hours or 1,440 minutes

Tab. 16. *Resource profile for receiving an outbound container (s_{Pr}^t) (unit: minute)*

t	0	1	2	3	4	5	6
r							
R	–	–	–	–	–	–	10
Y	0.030	0.076	0.091	0.152	0.183	0.989	1.134
A	0.06	0.15	0.18	0.3	0.36	1.95	3
S	28.8	100.8	187.2	331.2	504	1,440	1,440

t	0	1	2	3	4	5	6
r							
R	10	–	–	–	–	–	–
Y	1.114	0.762	0.493	0.336	0.314	0.247	0.090
A	3	1.02	0.66	0.45	0.42	0.33	0.12
S	1,440	1,440	950.4	633.6	417.6	216	57.6

The following introduces a numerical example to illustrate a resource profile in a yard planning. We assume that the length of one period is 1 day and the planning horizon is 9 days. Let us suppose that a yard is scheduled to receive outbound containers from period 2 to 7 and to discharge inbound containers during the period of 2. The capacity of a storage block in the SY becomes 1,050 × 1,440 slot-minutes − a storage block with 5 tiers, 6 rows, and 35 bays. The capacity of TRs is 57,600 machine-minutes, the capacity of YCs in a storage block is 1,440 machine-minutes, and the capacity of TAs in a storage block is 4,320 machine-minutes.

Planners decide that inbound containers are stacked in 3 storage blocks, and outbound containers are stacked in 5 storage blocks as shown in Tab. 18. Tab. 19 illustrates an example of a capacity plan in a yard planning. Entries of 'RQ (requirement)' of each resource correspond to the amounts of the resources that are required for the storage in Tab. 18. The values in 'RQ' are calculated by using the resource profile in Tabs 16 and 17, the number of inbound and outbound containers that are planned to be stacked at the block 1 and 3 as shown in Tab. 18.

Tab. 18. *Storage plans for inbound and outbound containers*

Storage block	1	2	3	4	5	6	7
Number of inbound containers	220	200	140	–	–	–	–
Number of outbound containers	–	–	90	120	111	102	117

In Tab. 19 note that the resource requirements for the YCs and TAs in the storage block 1 exceed their available capacities in the period of 2. Therefore, we have to prepare extra YCs and TAs in other periods.

CONCLUSIONS

− For constructing an efficient operational plan in container terminals, a large number of factors must be considered for decision-making. Although various planning activities are mutually related with each other, they have been treated as independent decision-making processes. Furthermore, they often share the same resource that they have to compete with each other to secure.

− This study proposed a unified framework for integrating various planning activities in container terminals and defined decision-making problems in each planning

Tab. 19. *Example of a capacity plan in a yard planning*

a) TR

t	1	2	3	4	5	6	7	8	9
TR									
CP	57,600	57,600	57,600	57,600	57,600	57,600	57,600	57,600	57,600
RS	47,160	43,200	36,540	36,240	36,075	36,015	32,610	32,610	
AV	10,440	14,400	21,060	21,360	21,525	21,585	24,990	24,990	57,600
RQ	–	5,600	–	–	–	–	–	–	–

b) YC, TA, and SY in the storage block 1

t	1	2	3	4	5	6	7	8	9
YC1									
CP	1,440	1,440	1,440	1,440	1,440	1,440	1,440	1,440	1,440
RS	1,255	1,200	1,108	1,100	1,090	1,050	1,070	1,050	–
AV	185	240	332	340	350	390	370	390	1,440
RQ	–	**245**	168	108	74	69	54	20	–
TA1									
CP	4,320	4,320	4,320	4,320	4,320	4,320	4,320	4,320	4,320
RS	3,010	3,770	3,700	3,600	3,500	3,400	3,300	3,200	–
AV	1,310	550	620	720	820	920	1,020	1,120	4,320
RQ	–	**660**	224	145	99	92	73	26	–
SY1									
CP	1,512,000	1,512,000	1,512,000	1,512,000	1,512,000	1,512,000	1,512,000	1,512,000	1,512,000
RS	1,157,000	1,140,000	1,104,000	1,103,000	1,102,000	1,101,000	1,100,000	1,099,000	–
AV	355,000	372,000	408,000	409,000	410,000	411,000	412,000	413,000	1,512,000
RQ	–	316,800	316,800	209,088	139,392	91,872	47,520	12,672	–

Tab. 19. Example of a capacity plan in a yard planning

c) YC, TA, and SY in the storage block 3

t	1	2	3	4	5	6	7	8	9
YC3									
CP	1,440	1,440	1,440	1,440	1,440	1,440	1,440	1,440	1,440
RS	635	640	520	510	500	490	480	470	–
AV	805	800	920	930	940	950	960	970	1,440
RQ	–	159	114	77	61	60	124	115	–
TA3									
CP	4,320	4,320	4,320	4,320	4,320	4,320	4,320	4,320	4,320
RS	3,450	1,900	4,000	3,900	3,800	3,700	3,600	3,500	–
AV	870	2,420	320	420	520	620	720	820	4,320
RQ	–	665	238	161	126	125	248	296	–
SY3									
CP	1,512,000	1,512,000	1,512,000	1,512,000	1,512,000	1,512,000	1,512,000	1,512,000	1,512,000
RS	1,139,000	1,140,280	1,102,000	1,101,000	1,100,000	1,090,000	1,080,000	1,070,000	–
AV	373,000	371,720	410,000	411,000	412,000	422,000	432,000	442,000	1,512,000
RQ	–	2,592	9,072	16,848	29,808	45,360	129,600	129,600	–

activity. Input parameters, decision variables, objectives, constraints, time buckets, and planning horizon for each decision activity were identified. The concept of a resource profile was suggested that should be utilized to check the feasibility of a plan with respect to the constraint on the resource availability. Numerical examples were also provided to illustrate capacity planning procedures for a berth planning, scheduling of quay crane operations, and yard planning.

− The concept proposed in this study may be utilized for developing operational software for container terminals. Also, methods for optimizing various operational decisions by utilizing the concepts proposed in this study may be developed in future studies.

BIBLIOGRAPHY

1. Bontempi G., Gambardella L. M. and Rizzoli A. E.: *Simulation and optimisation for management of intermodal terminals*. Proceedings of the 1997 European Simulation Multiconference, Istanbul, Turkey, June 1-4, Society for Computer Simulation International, 1997
2. Crainic T. G. and Kim K. H.: *Intermodal transportation, Handbooks in Operations Research and Management Science*: Vol. 14, Transportation (edited by Barnhart C. and Laporte, G.., Chapter 8), North-Holland, Amsterdam, Netherlands, 2007
3. Günther H. O. and Kim K. H.: *Containerterminals and terminal operations*, OR Spectrum, 28(4), 2006
4. Kim K. H. and Bae J. W.: *Re-marshaling export containers in port container terminals*, Computers and Industrial Engineering, 35(3-4), 1998
5. Kim K. H. and Moon K. C.: *Berth scheduling by simulated annealing*, Transportation Research Part B, 37(6), 2003
6. Kim K. H. and Park K. T.: *A note on a dynamic space-allocation method for outbound containers*, European Journal of Operational Research, 148(1), 2003
7. Kim K. H. and Park Y.M.: *A cane scheduling method for port container terminals*, European Journal of Operational Research, 156(3), 2004
8. Meersmans P. J. M. and Dekker R.: *Operations research supports container handling*, Econometric Institute Report EI 2001-22, Erasmus University Rotterdam, Rotterdam, The Netherlands, 2001.
9. Moorthy R. and Teo C.-P.: *Berth management in container terminal: the template design problem*, OR Spectrum, 28(4), 2006
10. Murty K. G., Liu J., Wan Y.W. and Linn R.: *A decision support system for operations in a container terminals*, Decision Support Systems, 39(3), 2005
11. Ramani K. V.: *An interactive simulation model for the logistics planning of container operations in seaports*, Simulation, 66(5), 1996
12. Steenken D., Voß S. and Stahlbock R.: *Container terminal operation and operations research – a classification and literature review*, OR Spectrum, 26(1), 2004
13. Taleb-Ibrahimi M., de Castilho B. and Daganzo C. F.: *Storage space vs handling work in container terminals*, Transportation Research Part B, 27(1), 1993
14. Vis I. F. A. and de Koster R.: *Transshipment of containers at a container terminal: an overview*, European Journal of Operational Research, 147(1), 2003
15. Vollmann T. E., Berry W. L. and Whybark D. C.: *Manufacturing Planning and Control Systems*, 4th Edition, McGraw-Hill, New York, 1997
16. Won S. H. and Kim K. H.: *Allocating storage spaces for temporary inventories considering handling, transportation, and storage capacities*, Journal of Korean Operations Research and Management Science Society, 31(3), 2006
17. Zhang C., Liu J., Wan Y.-W., Murty K. G. and Linn R. J.: *Storage space allocation in container terminals*, Transportation Research Part B, 37(10), 2003
18. Zhang C., Wan Y.-w., Liu J. and Linn R. J.: *Dynamic crane deployment in container storage yards*, Transportation Research Part B, 36(6), 2002

CONTACT WITH THE AUTHORS

Seung Hwan Won,
Kap Hwan Kim,
Dept. of Industrial Engineering
Pusan National University, South Korea
Jangjeon-dong, Kumjeong-ku, Busan 609-735, Korea
phone: 82-51-510-2419, fax: 82-51-512-7603
e-mail: kapkim@pusan.ac.kr

Occurrence probability of maximum sea levels in Polish ports of Baltic Sea coast

Bernard Wisniewski, Prof.
Tomasz Wolski, Ph. D.
University of Szczecin

ABSTRACT

In this work long-term probability of occurrence of maximum sea levels in some points of Polish Baltic Sea coast, was determined. Use was made of multi-year series of measurement data on maximum yearly sea levels, and their probability distributions were determined. To the analysis Gumbel's distribution and Pearson distribution of 3rd type as well as quantile methods and the highest credibility method, were applied. Kolmogorov test was used to examine conformity of the theoretical distributions with real random variable distribution. As results from the analysis, the highest sea levels of 1000- year return period can be expected in Polish ports of the west part of the coast , i.e. Kolobrzeg (750, 2 cm , i.e. 2,5 m above the average sea level) and Swinoujscie (723,6 cm) . Lower sea levels of the same return period can be expected in Ustka (720,2 cm), Wladyslawowo (709,7 cm) and Gdansk (716, 7 cm), respectively.

INTRODUCTION

This work is aimed at determination of long-term probabilistic prediction of maximum yearly sea levels in five Polish Baltic Sea coast observation stations: Swinoujscie, Kolobrzeg, Ustka, Wladyslawowo and Gdansk. Knowledge of sea levels of a given occurrence probability is necessary in designing the marine hydro-engineering buildings as well as in determining the characteristics of storm swellings.

The most important is to know high water level stages which can happen once a determined number of years, e.g. once 50, 100, 150 or 200 years. This period is called the return period **T.** It is expressed as follows:

$$T = \frac{100}{p\%} \ [\text{years}] \qquad (1)$$

where:
T – mean return period
p – probability [%.].

Empirical probability is defined by Weibull's function [1]:

$$p(m, N)\% = \frac{100m}{N+1} \qquad (2)$$

or Czegodajew formula used in hydro-engineering [7]:

$$p(m, N)\% = \frac{m - 0.25}{N+0.50} * 100\% \qquad (3)$$

where:
m – successive term of distribution series
N – size of series.

To estimate a probable water level, available measurement data series from previous years should be used. Credibility of such estimation depends both on length of water level observation series and representativeness of a chosen theoretical probability distribution function. In determining probability of the yearly highest sea levels a random sample covering a few dozen years of measurements is usually at one's disposal. Hence for Kolobrzeg the observed water levels from the years of 1867 ÷ 2006 were at one's disposal, for Swinoujscie – from the years of 1901 ÷ 2006, for Gdansk – from the years of 1886 ÷ 2006, for Ustka – from the years of 1946 ÷ 2006 and for Wladyslawowo – from the years of 1947 ÷ 2006.

Calculations of exceedance probability of water levels consist in appropriate selection of theoretical probability distributions and next in assumption of estimation methods of parameters of a selected distribution, with the use of statistical data. Confirmation of the fact whether the distribution has been properly selected can be obtained by using the tests of goodness of fit, proposed in the literature. Calculation results are given together with a confidence interval within which real variable value can be found with a given probability.

In probability theory the random variable X is such quantity which - due to random coincidence of various factors – can achieve different numerical values with a given probability. In this work the series of yearly maximum water levels observed at the stations of Swinoujscie, Kolobrzeg, Ustka, Wladyslawowo and Gdansk, are taken as the random variable X. A function which determines how large is occurrence

probability of the event that the random variable X takes one of the values contained within the numerical interval S on the x - variable axis is called the probability distribution of the random variable X.

In hydrology and oceanology the distributions:
– log-normal distribution (Gauss – Laplace)
– Pearson's distribution of type III
– Debski's distribution
– Gumbel's distribution of extreme values (Fisher-Tippett, type I) are most often used [1, 6, 8].

Every theoretical distribution density function has a number of parameters $g_1,...,g_k$, on which its graphical form depends. One of the crucial tasks is, on the basis of random sample, to estimate values of the paramters $g_1,...,g_k$, in such a way as random features of general population to be represented as best as possible by the function $f(x, g_1,...,g_k)$. In statistics to this end serve the methods of estimation of probability distribution parameters. Usefulness of particular estimation methods is dependent first of all on random sample size as a well as on a required degree of approximation of estimated values to theoretical ones. To large random samples simpler methods which provide lower estimation accuracy, can be applied [7].

In practice it is not possible to fully confirm how far a theoretical distribution fits actual distribution of random variable, i.e. that empirically elaborated on the basis of statistical observation series. In such situation consistency of theoretical distribution and observation results should be examined. To this end serve statistical consistency tests which determine occurrence probability of differences between theoretical distribution and empirical one. The λ point test of Kolmogorow and the χ^2 linear test of Pearson belong to the most often used [1, 8].

A few calculation methods of water levels with a given exceedance probability can be distinguished depending on an assumed type of probability distribution curve as well as estimation method of parameters. Among the most frequently applied the following methods can be numbered:
– quantile method (of position characteristics)
– maximum likelihood method and
– method of statitstical moments.

In this work Pearson's distribution and Gumbel's one was used and from among the applied methods the quantile one and that of highest likelihood was selected as recommended for the determining of occurrence probability of extreme hydrological phenomena such as water flow rates and water levels [6], [7].

Quantile method

The method is based on determined specific values of the variable X called quantiles. The p – order quantile is called such value of the variable x_p for which the exceedance probability is equal to p. Distribution quantiles are compared to sample quantiles. To determine quantiles from random sample its elements should be ordered according to their values to form the so called distribution series. The following quantiles are usually determined:
– $x_{50\%}$ – a value corresponding to the middle of series, equivalent of median
– x_p, $x_{100\%-p}$ – two symmetrical quantiles, equally distant from the middle of series, where: p = 10% or p = 5% is selected most frequently
– $x_{100\%}$, $x_{0\%}$ – two quantiles equivalent to lower and upper limit values of random variable.

If distribution series is long nad regular then values of symmetrical and middle quantiles can be determined by using interpolation between terms of the series. In the case of short and irregular series the searched - for quantiles are read from the equalized diagram of summed-up frequencies. However the values $x_{100\%}$ and $x_{0\%}$ are usually determined subjectively as they are located beyond the range of values of sample elements [1, 8].

Maximum likelihood method

The basic notion of the method is the likelihood function:

$$L = f(x_1, g_1,...,g_n) * f(x_2, g_1,...,g_n) * ... f(x_N, g_1,...,g_n) = = \prod_1^N f(x_i, g_1,...,g_n) \qquad (4)$$

where:
$f(x_i, g_1,...g_n)$ – probability density function of the random variable x_i in a given mathematical form and having unknown distribution parameters $g_i,(g_1,g_2...g_n)$

The function can be approximately interpreted as probability of obtaining the random sample $Z_N(x_i)$ exactly the same as that really observed. For calculation reasons to use the logarithm of likelihood function is more convenient:

$$\ln L = \ln f(x_1, g_1,..., g_n) + ... \ln f(x_N, g_1,..., g_n) = = \sum_i^N \ln f(x_i, g_1,..., g_n) \qquad (5)$$

Estimation of distribution parameters consits in finding such system of the values g_1, $g_2,...g_n$ at which probability of observing the given random sample $Z_N(xi)$ is the greatest. The discussed method is equivalent to searching for maximum value of the function L respective to g_1 value, i.e. to solving the set of equations:

$$\frac{\partial L}{\partial g_i} = 0 \quad \text{or} \quad \frac{\partial \ln L}{\partial g_i} = 0 \qquad (6)$$

where:
$i = 1,2,...g_n$.

The maximum likelihood method involves great troubles in the case when one of the estimated parameters is lower or upper variability range limitation of the random variable X. In such cases to use other methods is proposed for estimating the limitations [1, 8].

APPLIED METHODS

Determination of theoretical probable maximum sea levels by means of the quantile method with the use of Gumbel's distribution

The Gumbel's distribution density function is based on statistical distributions of extreme values which occur in certain larger sets of values. For instance it can be maximum values of sea levels considered in this paper. The Gumbel's distribution density function is double exponential and described by the formula [2]:

$$f(x) = \frac{1}{\hat{a}} e \left[- \frac{x - \hat{b}}{\hat{a}} - e\left(-\frac{x - \hat{b}}{a}\right) \right] \qquad (7)$$

where:
$\hat{a}$ – scale parameter (it determines dispersion of the distribution along x-axis)
$\hat{b}$ – location parameter (it determines location of the distribution on x-axis)
e – Napierian base.

Essence of estimation of the assumed distribution against given measurement data is to determine estimators of the distribution parameters $\hat{a}$ and $\hat{b}$.

After finding logarithms and simplifying the above given formula the following was obtained:

$$X_{p\%} = \hat{b} - 1/\hat{a} * \ln[-\ln(1 - f(x))] \qquad (8)$$

To estimate the parameters $\hat{a}$ and $\hat{b}$, formulas for the three quantiles: upper one X_p, middle one $X_{50\%}$ and lower one X_{1-p}, were preliminarily determined. Here the following values were assumed: p = 5% and 1-p = 95%.

In compliance with the formula (8) for $X_{p\%}$ the following was achieved [7]:

$$X_{5\%} = \hat{b} - 1/\hat{a}(-2.9702) \qquad (9)$$

$$X_{50\%} = \hat{b} - 1/\hat{a}(-0.36651) \qquad (10)$$

$$X_{95\%} = \hat{b} - 1/\hat{a}(1.097189) \qquad (11)$$

Next the variability measure was determined form the formula:

$$V = (X_p - X_{1-p})/2 \qquad (12)$$

By substituting relevant expressions from Eqs (9) and (11) for X_p and X_{1-p}, respectively, the following was obtained:

$$V = 4.0672/2\hat{a} \rightarrow \hat{a} = 2.0336/V \qquad (13)$$

Then, on the basis of distribution series of maximum water levels for each of the considered stations the water levels were read or interpolated by using the empirical probability from the formula (2), for X_p and X_{1-p} at p = 5%. The obtained values were used for determining the distribution parameters $\hat{a}$ and $\hat{b}$ from Eqs. (12), (13) and (10), respectively. The so achieved distribution parameters $\hat{a}$ and $\hat{b}$ were introduced to Eq. (8) for $X_{p\%}$ and the theoretical sea levels for selected probability quantiles were calculated for each of the observation stations (Tab. 1, 2, 3, 4 and 5)

Tab. 1. Theoretical maximum sea levels and probability of their occurrence at Swinoujscie observation station in the period of 1901÷2006 years

T (years)	F(X)	Sea level [cm]			
		Gumbel's distribution		Person's distribution	
		Quantile method	Maximum likelihood method	Quantile method	Maximum likelihood method
1000	0.1%	717.9	723.6	695.1	715.0
200	0.5%	686.3	690.9	671.4	679.1
100	1%	672.6	676.8	661.2	674.7
50	2%	658.9	662.6	650.6	662.0
20	5%	640.6	643.7	635.8	644.3
10	10%	626.5	629.1	623.8	630.1
5	20%	611.7	613.9	610.6	614.7
2	50%	589.5	590.9	589.5	590.5
1.33	75%	575.9	576.7	576.1	575.7
1.11	90%	565.9	566.5	566.7	565.6

Tab. 2. Theoretical maximum sea levels and probability of their occurrence at Kolobrzeg observation station in the period of 1867÷2006 years

T (years)	F(X)	Sea level [cm]			
		Gumbel's distribution		Person's distribution	
		Quantile method	Maximum likelihood method	Quantile method	Maximum likelihood method
1.05	95%	560.8	560.2	562.1	560.8
1.01	99%	552.3	555.3	555.0	554.2
1.00	100%	544.3	544.3	544.3	544.3

Tab. 3. Theoretical maximum sea levels and probability of their occurrence at Ustka observation station in the period of 1946÷2006 years

T (years)	F(X)	Sea level [cm]			
		Gumbel's distribution		Person's distribution	
		Quantile method	Maximum likelihood method	Quantile method	Maximum likelihood method
1000	0.1%	740.1	750.2	749.8	739.0
200	0.5%	704.1	711.5	713.8	708.1
100	1%	688.5	694.8	698.8	692.0
50	2%	672.9	678.0	683.0	677.0
20	5%	652.1	655.7	660.7	656.3
10	10%	636.1	638.4	643.3	639.6
5	20%	619.3	620.4	623.9	621.6
2	50%	594.0	593.1	593.5	593.1
1.33	75%	578.5	576.4	575.7	575.5
1.11	90%	567.2	564.2	562.3	563.5
1.05	95%	561.3	555.0	555.8	557.8
1.01	99%	551.7	546.1	547.3	549.2
1.00	100%	537.6	537.6	537.6	537.6

T (years)	F(X)	Sea level [cm]			
		Gumbel's distribution		Person's distribution	
		Quantile method	Maximum likelihood method	Quantile method	Maximum likelihood method
1000	0.1%	725.7	720.0	698.3	696.1
200	0.5%	692.3	687.5	673.5	675.1
100	1%	677.8	673.5	664.3	662.3
50	2%	663.4	659.4	654.0	651.4
20	5%	644.0	640.5	638.9	636.2
10	10%	629.1	626.0	626.2	623.8
5	20%	613.5	610.9	612.6	610.2
2	50%	590.0	588.0	590.0	588.0
1.33	75%	575.6	573.9	575.5	573.8
1.11	90%	565.1	563.7	564.3	563.6
1.05	95%	559.6	556.0	559.1	558.4
1.01	99%	550.7	550.0	550.4	550.7
1.00	100%	535.3	535.3	535.3	535.3

Tab. 4. *Theoretical maximum sea levels and probability of their occurrence at Wladyslawowo observation station in the period of 1947÷2006 years*

T (years)	F(X)	Sea level [cm]			
		Gumbel's distribution		Person's distribution	
		Quantile method	Maximum likelihood method	Quantile method	Maximum likelihood method
1000	0.1%	709.7	709.7	681.0	682.9
200	0.5%	679.4	679.1	659.4	669.4
100	1%	666.3	665.9	651.3	652.6
50	2%	653.1	652.5	642.4	642.8
20	5%	635.6	634.7	629.2	629.1
10	10%	622.0	621.0	618.1	617.9
5	20%	607.9	606.6	606.2	605.5
2	50%	586.5	585.0	586.5	585.2
1.33	75%	573.4	571.6	573.8	571.9
1.11	90%	563.9	561.9	564.1	562.2
1.05	95%	558.9	554.6	559.5	557.3
1.01	99%	550.8	549.3	551.9	549.6
1.00	100%	532.8	532.8	532.8	532.8

Tab. 5. *Theoretical maximum sea levels and probability of their occurrence at Gdansk observation station in the period of 1886÷2006 years*

T (years)	F(X)	Sea level [cm]			
		Gumbel's distribution		Person's distribution	
		Quantile method	Maximum likelihood method	Quantile method	Maximum likelihood method
1000	0.1%	716.9	716.7	695.5	695.3
200	0.5%	684.9	683.9	670.7	670.8
100	1%	671.1	669.8	661.4	660.2
50	2%	657.2	655.6	651.2	648.9
20	5%	638.7	636.6	636.0	633.2
10	10%	624.4	622.0	623.3	620.4
5	20%	609.5	606.7	609.6	606.4
2	50%	587.0	583.7	587.0	583.8
1.33	75%	573.2	569.5	572.4	569.3
1.11	90%	563.2	559.2	561.3	559.1
1.05	95%	557.9	550.6	556.0	557.5
1.01	99%	549.4	544.9	547.3	549.1
1.00	100%	532.3	532.3	532.3	532.3

Determination of theoretical probable maximum sea levels by means of the quantile method with the use of Pearson's distribution of type III

In hydrology Pearson's distribution is used most often. Its type III has found the widest application to equalization of series of numerical features of hydrological phenomena. The density function of Pearson's 3rd type distribution is of the following form [5, 6]:

$$f(x) = \frac{\alpha^\lambda}{\Gamma(\lambda)} e^{-\alpha(x-\varepsilon)}(x-\varepsilon)^{\lambda-1} \qquad (14)$$

where:

$\alpha, \varepsilon, \lambda$ – distribution parameters which should satisfy the following conditions: $x \geq \varepsilon$ (lower limitation of the distribution), $\alpha > 0$, $\lambda > 0$

$\Gamma(\lambda)$ – gamma function of the variable λ.

In this work the simplified form of the function which determines Pearson's 3rd type probability distribution, was used [5, 6]:

$$X_{p\%} = X_{50\%} * [1 + \Phi(p, s) * C_v] \qquad (15)$$

where:

$X_{50\%}$ – value of the middle quantile,

C_v – variability coefficient,

$\Phi(p,s)$ – function of exceedance probability and skewness (asymmetry).

The following are parameters of the distribution:
- the variability measure

$$V = (X_{10\%} - X_{90\%})/2$$

- the variability coefficient

$$C_v = V/X_{50\%} \qquad (16)$$

- the skewness coefficient *s* determined from an auxiliary table depending on value of the expression:

$$C_p = (C_v * X_{50\%})/(X_{50\%} - X_{100\%}) \qquad (17)$$

Like in the Gumbel's distribution, on the basis of the distribution series of maximum water levels for each of the observation stations the water levels were read or interpolated by using the empirical probability from Weibull's formula (2), for X_p and X_{1-p} at p = 10% (the quantiles: $X_{10\%}$, $X_{50\%}$, $X_{90\%}$, $X_{100\%}$). The obtained values of quantiles were used for determining the distribution parameters: V, C_v and *s* from Eqs. (12) and (16) as well as (17) and the auxiliary table, respectively [5]. The calculated distribution parameters and the function $\Phi(p,s)$ read from the above mentioned auxiliary table, were introduced to the successive formula, (15), for X_p, and the theoretical sea levels for the selected probability quantiles for each of the observation stations were calculated (Tabs 1, 2, 3, 4 and 5).

Determination of theoretical probable maximum sea levels by means of the maximum likelihood method with the use of Pearson's distribution of type III

In this method the form of Pearson's distribution function, proposed by Foster, was applied [6, 1]:

$$X_p = \varepsilon + 1/\alpha * tp \qquad (18)$$

where:

ε – lower limitation of the distribution, equivalent of the quantile $X_{100\%}$

t_p – value of exceedance probability function and parameter λ, read from the auxiliary tables [6, 9]

α – the second parameter of the distribution, determined from the formula:

$$\alpha = \lambda/x_{sr} \qquad (19)$$

where:

x_{sr} – arithmetic mean of the values x_i, where x_i - the substitute variable determined from the formula:

$$x_i = x\, max - \varepsilon \text{ for } i = 1, 2, 3, ...N \qquad (20)$$

where:

x_i – maximum sea levels in distribution series as well as the parameter λ determined from the formula:

$$\lambda = 1/(4*A) * [1 + (1 + 4/3 * A)^{0.5}] \quad (21)$$

where:

A – function defined by the formula:

$$A = \ln(x_{sr}) - (\ln x)_{sr} \quad (22)$$

where:

$\ln x_{sr}$ – logarithm taken from the arithmetic mean of the values x_i

$(\ln x)_{sr}$ – arithmetic mean of the values lnx.

In the maximum likelihood method, on the basis of the distribution series of maximum water levels, for each of the observation stations the substitute variable x_i, acc. Eq. (20), and its arithmetic mean x_{sr}, as well as the logarithm of the mean, $\ln x_{sr}$, and the arithmetic mean of the logarithm values, $(\ln x)sr$, then also the functions A, acc. Eq. (22), and the parameter ë, acc. Eq. (21), which was used to calculate the second parameter of Pearson's distribution, α, acc. Eq. (19), were determined. The lower limitation of the distribution, Í, was determined from the equation of the trend-line of maximum sea levels, depicted on the quantile - quantile diagram (by using *Statistica* software).

The functions t_p were read from the auxiliary tables [6, 9]. Having all the Pearson's distribution parameters one made use of the Foster's formula, acc. Eq. (18), and calculated theoretical sea levels for selected probability quantiles for each of the observation stations (Tab. 1, 2, 3, 4 and 5).

Test of consistency of the assumed theoretical probability distribution with empirical distribution

In this work consistency of the assumed theoretical distribution with empirical one (observation series of sea levels) was examined with the use of Kolmogorow consistency test. The testing consists in checking the following condition [1, 8]:

$$D_{max}[p/m, N/\% - p\%] < \lambda_{kr}/\sqrt{N} \quad (23)$$

where:

$p/m, N/\%$ – empirical occurrence probability of *m*-th term of distributive series

$p\%$ – theoretical occurrence probability of sea level value corresponding with *m*-th term of distributive series

λ_{kr} – critical value of the Kolmogorow distribution (at $\alpha = 5\% \rightarrow \lambda_{kr} = 136$, at $\alpha = 1\% \rightarrow \lambda_{kr} = 163$)

N – size of distributive series.

The condition of the Kolmogorow test was checked for all the methods of determination of theoretical probable maximum sea levels for each of the observation stations. Results of the test are given in Tab. 6.

Calculation of estimation error and confidence interval

Confidence interval is a range within which real value of quantile will occur with the assumed probability P_α (confidence level). In this work the confidence interval limit x_p was determined on the level $P_\alpha = 68.3\%$ as well as $P_\alpha = 95\%$ by means of the following formula [1, 4]:

for the upper confidence interval:

$$x_p^\alpha = x_p + t_\alpha * \sigma(x_p) \quad (24)$$

for the lower confidence interval:

$$x_p^\alpha = x_p - t_\alpha * \sigma(x_p) \quad (25)$$

where:

$t_\alpha = 1$ – for the confidence level = 68.3%

$t_\alpha = 2$ – for the confidence level = 95%

$\sigma_{(xp)}$ – estimation error determined according to the following formula:

$$\sigma_{x_p} = F(s, p) * C_v * x_{50\%}/\sqrt{N} \quad (26)$$

where:

F(s,p) – function of probability and assymetry measure, read from the auxiliary tables [4]

The determined confidence interval limits for the confidence levels $P_\alpha = 68.3\%$ and $P_\alpha = 95\%$ are given in Tab. 7.

ESTIMATION RESULTS OF THEORETICAL MAXIMUM WATER LEVELS FOR PARTICULAR OBSERVATION STATIONS AND OCCURRENCE PROBABILITY OF THE LEVELS

In this work the sea levels with assumed occurrence probability were determined on the basis of Gumbel's distribution and Pearson's distribution by applying both the quantile and maximum likelihood methods. To check consistency of the assumed theoretical distributions with empirical ones the Kolmogorow test was used (Tab. 6). Results of the test calculations do not lead to rejection of the in-advance-assumed hypothesis on consistency of the distributions.

The best adjusted to long-term observation series are the theoretical maximum sea levels and their occurence probability determined by means of the Gumbel's distribution and maximum likelihood method, that is confirmed by description given in the chapter „Applied methods" and the diagrams presented in Fig. 1 through 5. The so-calculated highest theoretical sea

Tab. 6. *Results of Kolmogorow test for various methods of determination of theoretical sea levels at particular observation stations*

Observation stations	$\lambda_{kr}/\sqrt{N}$ for $\alpha = 1\%$	$\lambda_{kr}/\sqrt{N}$ for $\alpha = 5\%$	D_{max}			
			Gumbel's distr., quantile method	Gumbel's distr., method of maximum likelihood	Pearson's distr., quantile method	Pearson's distr., method of maximum likelihood
Swinoujscie (1901÷2006)	15.83	13.21	0.30	0.04	0.73	0.43
Kolobrzeg (1867÷2006)	13.88	11.58	-0.26	0.03	0.12	0.22
Ustka (1946÷2006)	20.87	17.41	-3.78	0.07	-2.89	-2.39
Wladyslawowo (1947÷2006)	21.04	17.56	-1.26	0.08	-0.16	-0.36
Gdansk (1886÷2006)	14.82	12.36	-1.38	0.06	-0.68	-0.28

P (%)		99.9-50	10	5	1	0.1	0.01
Swinoujscie	$P_\alpha = 68.3\%$	± 2.7	± 5.3	± 7.6	± 14.3	± 25.3	± 37.2
	$P_\alpha = 95.0\%$	± 5.4	± 10.6	± 15.3	± 28.6	± 50.6	± 74.3
Kolobrzeg	$P_\alpha = 68.3\%$	± 3.4	± 6.8	± 9.7	± 18.4	± 34.5	± 47.6
	$P_\alpha = 95.0\%$	± 6.7	± 13.7	± 19.3	± 36.9	± 69.0	± 95.2
Ustka	$P_\alpha = 68.3\%$	± 3.9	± 7.2	± 10.5	± 19.7	± 35.0	± 51.3
	$P_\alpha = 95.0\%$	± 7.7	± 14.5	± 20.9	± 39.5	± 70.0	± 102.7
Wladyslawowo	$P_\alpha = 68.3\%$	± 3.4	± 6.4	± 9.2	± 17.4	± 30.8	± 45.2
	$P_\alpha = 95.0\%$	± 6.8	± 12.8	± 18.4	± 34.7	± 61.6	± 90.3
Gdansk	$P_\alpha = 68.3\%$	± 2.8	± 5.2	± 7.4	± 14.0	± 24.9	±36.5
	$P_\alpha = 95.0\%$	± 5.5	± 10.3	± 14.9	± 28.1	± 49.8	± 73.0

levels which can occur once a 1000 years, 200 years, 100 years and 50 years are given in detail in Tab. 1 through 5. From the results it can be concluded that the highest of them will occur and did really occur in Polish west - coast ports, i.e. Kolobrzeg and Swinoujscie. The lowest of them will occur in the port of Wladyslawowo which belongs to the Polish middle coast of Baltic Sea and is directly exposed to sea. The remaining ports are located in river estuaries and water level indicators installed in them are about 1 km distant from sea coast line. For instance in the port of Kolobrzeg the water level of 750.2 cm, i.e. 2.5 m above the average mean sea level, should be expected once a 1000 years (zero points of Polish water level indicators are based on the Amsterdam's zero-level equal to -500 N.N.). Swinoujscie (with 723.6 cm), Ustka (with 720.2 cm),
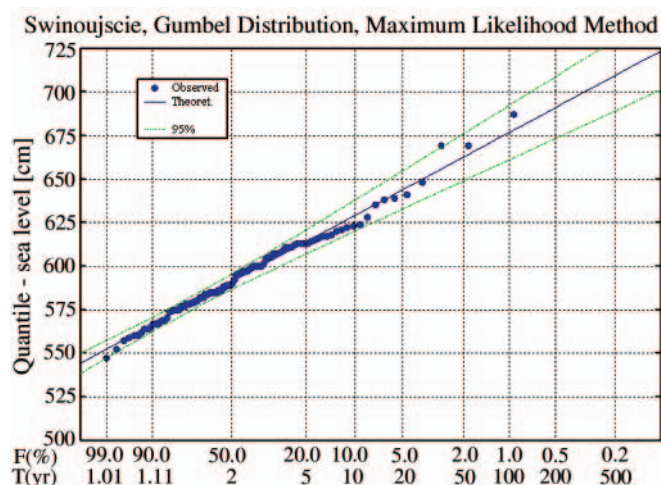

Fig. 1. *Occurrence probability of maximum yearly sea levels at Swinoujscie in the period of 1901÷2006 years (Gumbel's distribution, maximum likelihood method)*
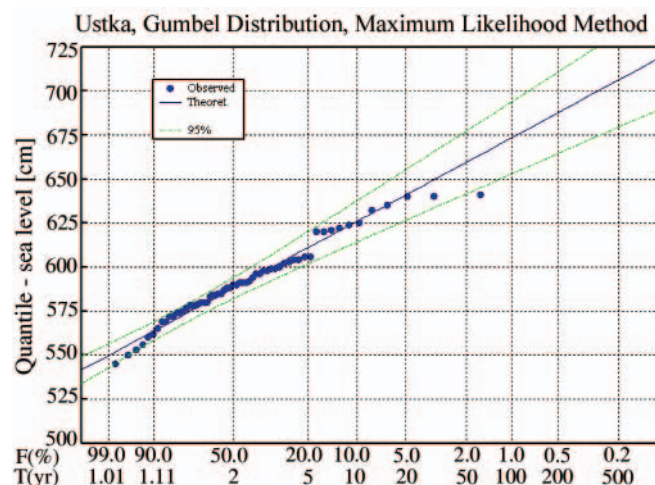

Fig. 3. *Occurrence probability of maximum yearly sea levels at Ustka in the period of 1946÷2006 years (Gumbel's distribution, maximum likelihood method)*
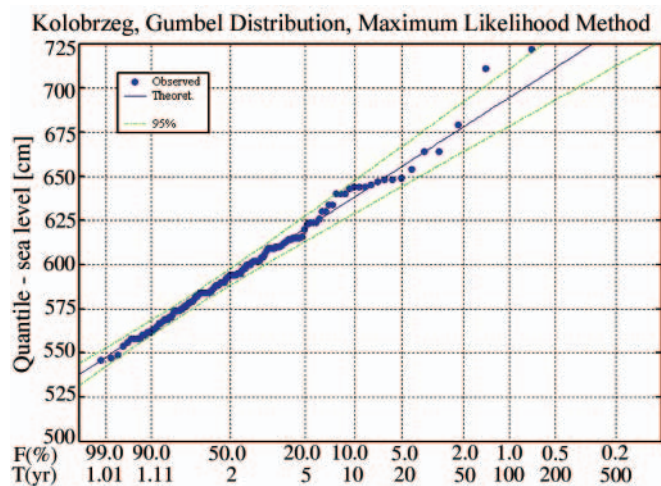

Fig. 2. *Occurrence probability of maximum yearly sea levels at Kolobrzeg in the period of 1867÷2006 years (Gumbel's distribution, maximum likelihood method)*
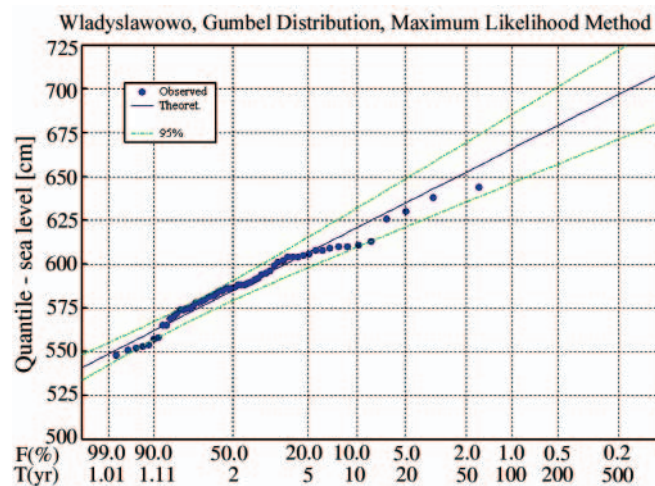

Fig. 4. *Occurrence probability of maximum yearly sea levels at Wladyslawowo in the period of 1947÷2006 years (Gumbel's distribution, maximum likelihood method)*

Gdansk (with 716.7 cm) and Wladyslawowo (with 709.7 cm) are the successive ports in which the maximum thousand-year levels can be expected. Other occurrence probabilities can be also considered. Graphical representation of the relations is presented in Fig. 1 through 5 for particular Polish ports of Baltic Sea coast.
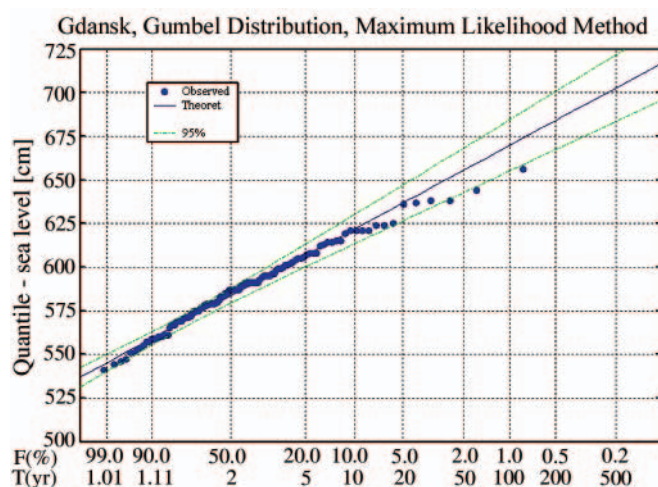

Fig. 5. Occurrence probability of maximum yearly sea levels at Gdansk in the period of 1886÷2006 years (Gumbel's distribution, maximum likelihood method)

DISCUSSION OF THE RESULTS

As already mentioned, due to its characteristics Gumbel's distribution has been considered the closest to empirical one. Its advantage results from lack of lower limitation of variability range of the random variable X, among estimated parameters. Estimation of lower or upper limitation of Pearson's distribution ($x_{100\%}$, or $x_{0\%}$) faces serious difficulty due to a subjective way of its determination [1], [8].

On the basis of comparison of both methods of estimation and determination of distribution parameters it can be concluded that the maximum likelihood method makes it possible to obtain more precise results as in this method - in contrast to the quantile method – to use interpolation of distribution parameters is not necessary.

In Polish subject-matter literature the methods of determination of probability of extreme sea levels were described in the publications of Wroblewski, A. [10, 11, 12, 13, 14] and Massel, S. [7]. Prediction of Baltic Sea extreme levels was also considered by Jednoral, T., Sztobryn, M. and Milkowska, M. [3]. This work presents the methods in question in the most complete way as it takes into account calculation approaches used by different authors. In this work, the characteristics of theoretical maximum sea levels and their occurrence probability in five repereresentative Polish ports of Baltic Sea coast, were considered. The obtained results are based on the longest observation series. From the point of view of the applied methods the most important have been so far two publications by Wroblewski [11, 13] with which to compare results of this work is deemed purposeful. In Tab. 8 can be found the comparison of results of the theoretical sea levels, determined by Wroblewski for selected quantiles, with those obtained by these authors for Gdansk observation station.

From the comparison of the results of the theoretical sea levels for Gdansk observation station, obtained by these authors by using the maximum likelihood method and Gumbel's and Pearson's distributions, with those determined by Wroblewski [11, 13], the difference from several up to a dozen or so centimeters for different quantiles, can be observed. The differences are mainly caused by a different way of determination of the lower limitation of the distribution, l. Wroblewski, determining the lower limitation of the distribution, made use of the maximum likelihood method as well as the tables of modal values. In this work the equation of the trend-line of maximum sea levels, depicted on the quantile-quantile diagram obtained from *Statistica* software, was applied. The other cause of the differences in determining the theoretical sea levels is length of observation series. In this work the series for Swinoujscie, Kolobrzeg and Gdansk are by 37 years longer than that used by Wroblewski [11, 13]

Tab. 8. Theoretical maximum sea levels and probability of their occurrence at Gdansk observation station, determined by means of both Gumbel's and Pearson's distributions with the use of the maximum likelihood method, according to Wroblewski [11, 13] and these authors, respectively

T (years)	F(X) (%)	Sea levels [cm]			
		Gumbel distr.	Pearson distr.	Gumbel distr.	Pearson distr.
		Results by these authors		Results by Wroblewski	
1000	0.1%	716.7	695.3	694	678
200	0.5%	683.9	670.8	664	-
100	1%	669.8	660.2	651	647
50	2%	655.6	648.9	639	637
20	5%	636.6	633.2	621	623
10	10%	622.0	620.4	608	612
5	20%	606.7	606.4	594	599
2	50%	583.7	583.8	573	578
1.33	75%	569.5	569.3	-	-
1.11	90%	559.2	559.1	551	555
1.05	95%	550.6	557.5	-	549
1.01	99%	544.9	549.1	538	541
1.00	100%	532.3	532.3	-	523

CONCLUSIONS

– In this work sea levels for a given occurrence probability, based both on Gumbel's and Pearson's distributions, were obtained with the use of both quantile method and maximum likewlihood method. The achieved results have been presented in Tab. 1 through 5 and partially in Fig. 1 through 5.

– For the determined theoretical sea levels the confidence intervals at the confidence levels: Pá = 68,3% i Pá = 95,0%, were calculated (Tab. 7).

– Consistency of the assumed theoretical distributions and empirical one was checked by means of the Kolmogorow test (Tab. 6). Results of the test calcultations do not lead to rejection of the assumed hypothesis on consistency of the distributions. In this work the Gumbel's distribution was considered the closest to the empirical one. Its advantage is lack of lower limitation of variability range of the random variable X, among estimated parameters.

– Among the methods applied in this work the maximum likelihood method has appeared the most accurate because of lack of necessity of interpolating the distribution parameters (in contrast to the case of using the quantile method).

– The obtained results can be considered reliable because of the long observation series of sea levels, especially those for Gdansk (1887 ÷ 2006), Swinoujscie (1901 ÷ 2006) and Kolobrzeg (1867 ÷ 2006). Large (upper) values of the observed sea level series are due to storm swellings and their impact on sea coast. The occurrence probability of high sea levels determined in this work for Swinoujscie, Kolobrzeg, Ustka, Wladyslawowo and Gdansk can be used in designing the coastal hydro-engineering buildings as well as in managing the costal zone and inudation areas during storm and flood phenomena.

BIBLIOGRAPHY

1. Byczkowski A.: *Hydrology* (in Polish), Vol. I and II, Publishing House of Warsaw Agriculture University (Wydawnictwo SGGW), Warszawa 1996
2. Gumbel, E.J.: *Statistics of Extremes*. Columbia University Press 1958
3. Jednoral T., Sztobryn M., Milkowska M.: *Application of position statistics for prediction of extreme levels of Baltic Sea in Polish coastal zone* (in Polish), Inżynieria Morska i Geotechnika, no.5/2008
4. Kaczmarek Z.: *Effectiveness of estimation of maximum flow rates of a given return period* (in Polish), Archiwum Hydrotechniki, vol. 4, no. 3/1957
5. Kaczmarek Z., Trykozko E.: *Application of the method of quantiles to estimation of the Pearson distribution.* Acta Geophysica Polonica, vol. 12, no. 1/1964
6. Kaczmarek Z.: *Meteorolgical and statistical methods in hydrology and meteorology* (in Polish). Transport and Telecommunication Publishers (Wyd. Komunikacji i Lącznosci), Warszawa 1970
7. Massel S. (ed.): *Handbook on hydro-engineering. Marine environmental loads on hydro-engineering buildings* (in Polish). Maritime Publishing House (Wyd. Morskie), Gdansk 1992
8. Ozga-Zielinska M., Brzezinski J.: *Applied hydrology* (in Polish). Scientific Publishing House (Wyd. PWN), Warszawa 1997
9. Weglarczyk S.: *Statistical methods* (in Polish). Printed series of course lectures for students of Krakow University of Technology, Krakow 1993
10. Wroblewski A.: *Occurrence of minimum yearly water states in South Baltic Sea (Based on observation results in Nowy Port of Gdansk in 1886÷1939 and 1946÷1966)* (in Polish), Przegląd Geofizyczny, vol. XV, no. 1/1970
11. Wroblewski A.: *Occurrence probability of maximum yearly levels of Baltic Sea in Gdansk Nowy Port, Kolobrzeg and Swinoujscie* (in Polish). Oceanology, no. 6/1975
12. Wroblewski A.: *Occurrence probability of minimum yearly levels of Baltic Sea in Gdansk Nowy Port, Kolobrzeg and Swinoujscie* (in Polish). Archiwum Hydrotechniki, vol. 29, no. 4/1982
13. Wroblewski A.: *Analysis and forecast of long-term sea level changes along the Polish Baltic Sea coast*, Part I. Annual sea level maxima, Oceanologia, 33, 1992
14. Wroblewski A.: *Long-term prediction of sea level rise* (in Polish). Inżynieria Morska i Geotechnika, no.3/2001

CONTACT WITH THE AUTHORS

Bernard Wisniewski, Prof.
Tomasz Wolski, Ph. D.
University of Szczecin
Wąska 13
71-415 Szczecin, POLAND
e-mail: natal@univ.szczecin.pl

Development of new technologies for shipping natural gas by sea

Monika Bortnowska, Ph. D.
Szczecin University of Technology

ABSTRACT

In recent years dynamic increase of orders for ships intended for liquified natural gas (LNG) shipping has been observed with simultaneous trend of increasing their transport capability. This results from the fact that natural gas has become today the third energy source worldwide just next to crude oil and coal. The fast growth of demand for natural gas and its limited resources would cause growth of its price, therefore better solutions of natural gas transport technology with respect to economy, ecology and safety should be searched for. This paper presents various technologies for natural gas transport by sea with special attention paid to some alternative methods of transport, namely: CNG and NGH ransport technologies in contrast to LNG one.

Keywords: natural gas; LNG carriers; liquified gas; CNG carriers; compressed gas;
NGH carriers; gas hydrate; operational cost of gas transport

INTRODUCTION

Natural gas industry plays greater and greater worldwide role both in economical and political sense. Growth of gas consumption is associated with its great popularity as the most ecological source of energy. Ecological features of natural gas as well as its wide range of applications a.o. to electric power production, combustion engine driving and chemical production, make the demand for it still growing. The demand increases by about 2 % every year.

The largest natural gas resources are found in the Persian Gulf (abt. 41% of worldwide resources) and Russia (abt. 32% of worldwide resources), moreover in North Africa and the region of the Mexican Gulf and Carribbean Sea, Fig. 1, [2]
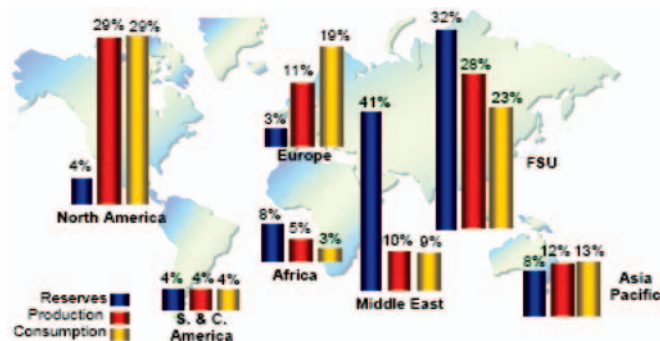

Fig. 1. Natural gas all over the world [2]

In Poland natural gas deposits are located mainly in West Pomerania, Wielkopolska region and Carpathian piedmont; rather small amounts of the gas were also found in sea-bed deposits in Polish economical zone of the Baltic Sea.

Therefore the increase of number of orders for natural gas carriers with simultaneous trend for increasing their transport capability reaching today as many as 250000 m³, is observed. The boom in production of gas carriers has contributed, due to strong competition, to the downward trend in their production costs. However it does not change the fact that gas carriers belong to very expensive ships because of difficulties in their production and operation.

Natural gas can be shipped by sea in the liquified state (LNG), compressed state (CNG), or in the form of hydrate (NGH) - the technology being still in the phase of design considerations. The CNG and NGH technologies are promising, applicable in short-range shipping up to 3000 Mm, more profitable, safe and ecological than LNG technology. Characteristic features of the natural gas shipped in the three forms are presented in Fig. 2.

A type and design of ship intended for the transporting of the raw material as well as equipment of gas loading terminal depends on a state in which it will be shipped.

For many countries, including Poland, gas shipping by sea with the use of gas carriers is really the only alternative to be independent from gas delivery from Russia and this way to greatly improve safety of energy supply to the country.

CHARACTERISTICS OF LIQUIFIED GAS TRANSPORT TECHNOLOGY

The most popular transport technology of natural gas cargo is its liquified form – by means of LNG (liquified natural gas) carriers in – 163° C temperature and a little elevated pressure of 0.17 MPa (1.7bar). Due to so low temperature LNG must be contained in a cryogenic tank. After liquefaction process
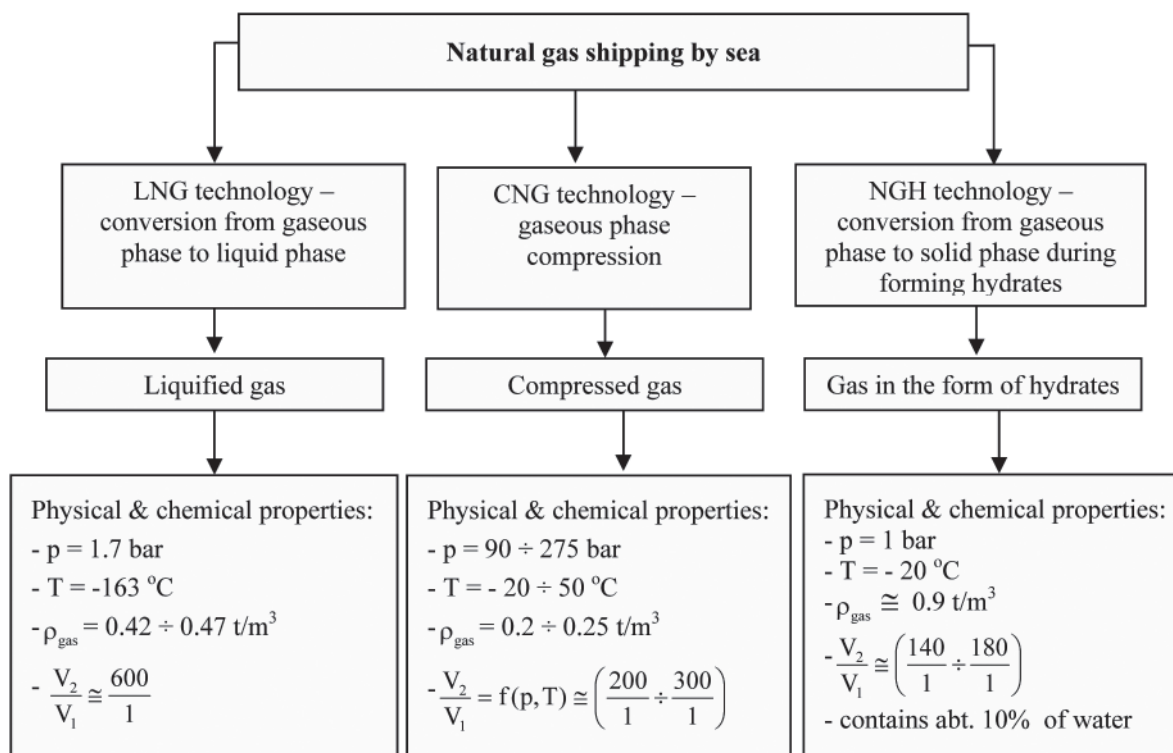
Fig. 2. *Forms of gas cargo for shipping it by sea and its main properties [the author's elaboration]*

its volume is reduced abt. 600 times against its initial state, that constitutes its main advantage for shipping and storing. In worldwide trade more than 1/4 of natural gas amount is shipped just in this state.

The LNG is called the concentrated energy as:

- after regasification, from $1m^3$ of LNG abt. 600 m^3 of network gas is obtained
- from 1 t of LNG abt. 1380 m^3 of network gas is obtained.

LNG transport chain

LNG delivery chain begins in natural gas deposits from which gas is transported through piping network to a liquefaction facility which delivers the gas to an export terminal and from this point it is transported, already in the liquefied form, by means of special LNG carriers to a import terminal and from it, after regasification, it is pumped to gas piping network to be delivered to its consumers, Fig. 3.

According to statistical data from the end of 2008 the world fleet of LNG carriers was consisted of 280 ships [10], most of which were of over 100 000 m^3 capacity. During two last years number of built Q-flex and Q-max ships of capacity greater than 200 000 m^3 each, has increased.

LNG carriers can be divided with respect to their size as follows:

- medmax LNG carriers of the cargo capacity $V_Ł = 75\ 000\ m^3$
- conventional LNG carriers of the cargo capacity $V_Ł = 125\ 000 \div 145\ 000\ m^3$
- new LNG carriers of the cargo capacity $V_Ł = 155\ 000 \div 170\ 000\ m^3$
- Q-flex LNG carriers of the cargo capacity $V_Ł = 216\ 000\ m^3$
- Q-max LNG carriers of the cargo capacity $V_Ł = 265\ 000\ m^3$.

LNG carriers belong to the group of very specialized ships, that results mainly from the applied cargo transport technology. The crucial problem is to ensure continuous cooling the cargo as well as to avoid its evaporation to the atmosphere. Therefore LNG transportation requires application of very effective insulation of tanks.

Among merchant ships LNG carriers are of the highest speed, their average service speed varies usually in the range of $19 \div 21$ knots. LNG shipping specificity consisting in continuous loss of the cargo during voyage to some extent forced voyage period shortening to a minimum. The daily Boil-Off-Rate (BOR) amounts on avarage to $0.15 \div 0.2$ % of gas cargo mass and the amount depends mainly on degree of insulation effectiveness. The evaporated cargo can be discharged to the atmosphere, again liquified or utilized onboard as fuel for main propulsion diesel engines, gas turbines or boilers delivering steam to turbines.

The largest LNG carrier („Mozah") built nowadays, fitted with five membane tanks is of 266 000 m^3 cargo capacity. It was built by Samsung Shipyard in South Korea for QGTC company. There are a few other ships like that under construction but their size, design or specification have not been disclosed so far.

Attention should be paid to the fact that safety of cargo in tanks and ship operation safety should be also ensured along with the increased size of the ships.
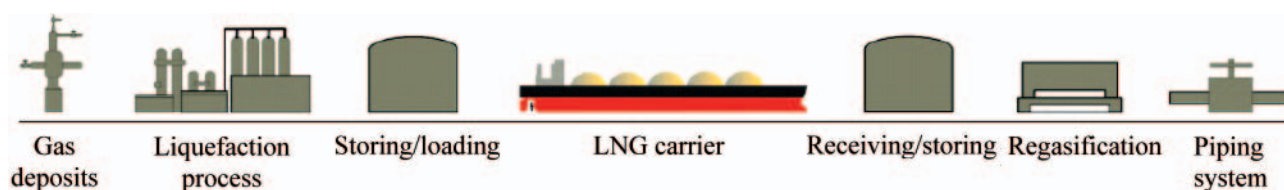

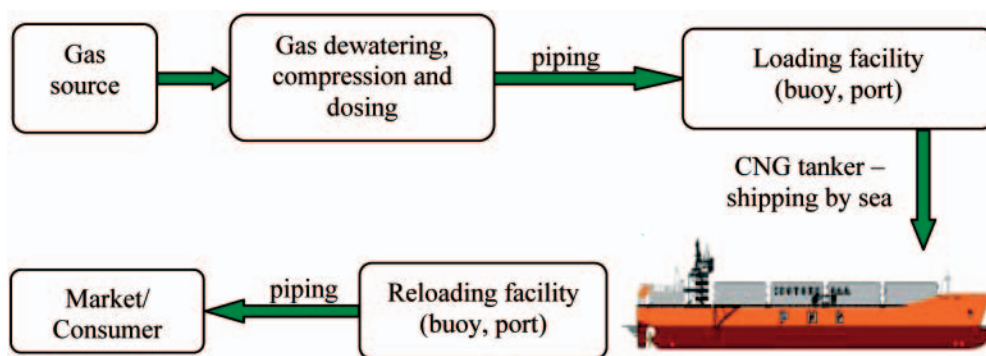**Fig. 3.** *LNG transport chain with the use of LNG carriers acc. [4]*

Fig. 4. CNG transport chain by using special gas carriers [the author's elaboration]

CHARACTERISTICS OF COMPRESSED GAS TRANSPORT TECHNOLOGY

The CNG is natural gas compressed under high pressure. The typical pressure range used to compress the gas is of 200 ÷ 250 bar. The compresion process is aimed at concentrating gas energy in unit volume. The higher pressure the greater amount of gas contained in unit volume. After the compression about 200/1 ÷ 300/1 units of gas can be achieved.

Storing and transporting the CNG is carried out in special tanks, under high pressure. Capacity of such tanks – usually cylindrical vessels – depends on working pressure, temperature as well as chemical content of natural gas. The tanks having different values of length and diameter, are made of steel or light composite materials.

CNG transport chain with application of gas carriers

CNG delivery chain begins in natural gas deposits from which the gas is sent through piping system to compression facility and next through loading system (buoy, port) to a ship which transports it in the compressed form to reloading terminal (buoy, port). In the terminal gas can be reloaded to underground stores or directly to gas piping network after passing through internal installations of the terminal [9]. Fig. 4 shows the schematic diagram of the CNG transport path.

Concept of gas transportation in the compressed form is not entirely new as the first attempts to CNG transporting for commercial purposes were made by Columbia Gas Company, in the 1960s, but it is one of alternatives for LNG transport, especially to servicing local markets and satisfying the needs without signing any delivery contracts.

According to available analyses CNG transport technology by sea within 3000 Mm delivery range becomes competitive to LNG mode of transport as well as to that by undersea piping systems. An advantage of CNG technology is avoidance of building an expensive liquefaction facility for natural gas, its storing and building tanks to its regasification which are often placed close to areas of large density of population, that impairs its safety. The new natural gas transport technology by using CNG carriers is associated only with building the facility for gas compression to over 200 bar pressure in the receiving port, that leads to large cost savings within the whole gas transport chain.

During CNG transport the cargo can be reloaded far offshore by using loading buoys anchored in a safe distance from coast.

Transport of gas in the compressed form is characterized by many advantages, a.o. the following:

- *safety nad ecology* – gas loading and reloading can be performed far offshore by using loading buoys; in the case of occurrence of a possible leakage CNG does not explode but evaporizes and disperses in the atmosphere; when combusted it emitts less contaminations to the atmosphere than oil or coal, lowering this way emission of noxious products such as: CO, CO_2, NO_x
- *flexibility of gas delivery chains* – it means a.o. possibility to adjust amount of gas delivery to current demand of the market
- *savings in transport and storage costs as well as investment cost of the reloading port* (abt. 80% of the whole investment cost is connected with CNG carrier - Fig. 8).

Concepts of CNG carriers and design solutions of cargo tanks

In recent years big gas concerns have discovered great possibilities in CNG transport technology; many of them have elaborated their own CNG transport technologies and designs of CNG carriers. The following ones belong a.o. to the most important:

- **Coselle (Williams)** – gas is transported in turns of steel, thick-walled pipes of the diameter D = 0.168 m and of l = 1700 km in length on average, winded onto the so called „carousel", in ambient temperature, under 275 bar pressure. The Coselle CNG transport system is modular and intended for extension. It means that CNG transport system may begin from delivery of gas in small amounts and then be developed by adding more and more greater number of the gas carriers. Gas cargo capacity of such ships is contained in the interval of 1.4 ÷ 56 mln m³ within 2000 Mm range of delivery [6, 8].

According to literature sources the technology is the least expensive alternative of CNG delivery which could bring 30 % cost savings.
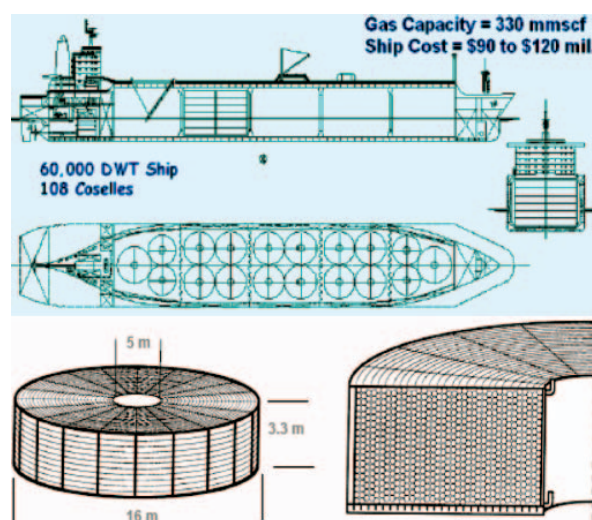
- **Knutsen OAS – PNG** (*Pressurized Natural Gas*) system characteristic of vertical cylindrical tanks (of the dimensions: h = 18 ÷ 36 m in height, D = 1.04 m in diameter) in which gas is transported in ambient temperature under 250 bar pressure. The gas cargo capacity of such ships varies in the interval of 2 ÷ 30 mln m³ of compressed gas within the 3000 Mm range of delivery [6].

Technical details of the concept have not been revealed so far hence it is not clear in which way its cargo tanks differ from other technologies.
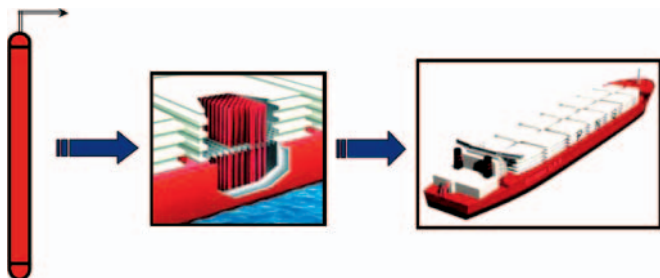

- **CETech** – a common concept elaborated by three partners: *Statoil*, *Teekay* - a Canadian firm, and *Leif Höegh & Co* – a Norwegian one. The planned ships will be equipped with steel horizontal pipes capable of transporting the CNG compressed up to about 200 ÷ 250 bar, in ambient temperature. CNG cargo capacity of the largest of them will reach 20000 t.
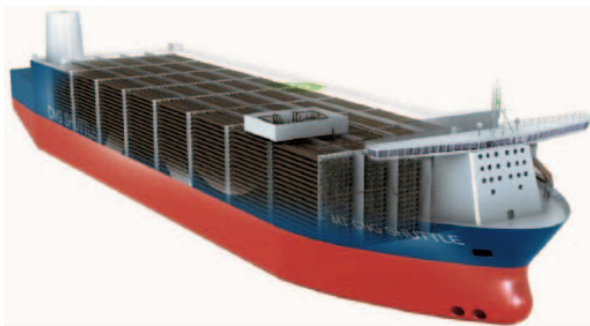
- **EnerSea – VOTRANS –** the firm has proposed a little different method of CNG transport, namely that in which gas is compressed to an appropriate pressure (90 ÷ 130 bar), and next cooled to the temperature in the range of –20 ÷ – 40 °C. The so low temperature is applied to achieve greater gas density.

CNG is transported in a set of pipes made of carbon steel, placed horizontally, or vertically in the case of smaller capacities. The pipes are insulated thermally from the surrounding, in relevant tanks. Ship's cargo compartment is consisted of 100 tank modules of the height h = 24 ÷ 36 m. Every module contains 24 longitudinal tanks of the diameter D = 1m each. The tank modules are insulated by cooled nitrogen. Cargo capacity of such ships varies in the interval of 5.6 ÷ 57 mln m³ of CNG, within the 200 ÷ 3000 Mm range of delivery [8].
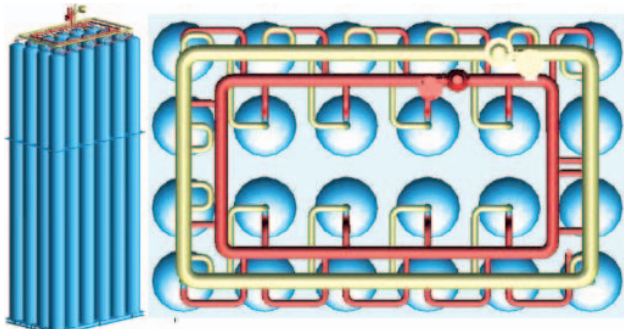
- **Trans Ocean Gas - *Cassettes*** – the firm has proposed a unique method of CNG transport consisting in using pressure tanks made of glass fibre reinforced plastic (FRP). CNG is transported in ambient temperature under 250 bar pressure. Cargo- carrying capacity of ships of the concept amounts at the most to 28 mln m³ of gas. The cargo tank is designed in the form of „cassettes" inside of which are placed 18 vertical pressure cylinders of the dimensions: the height h = 12 m and the diameter D = 1.04 m (in three groups of 6 cylinders in each). In the cassette of 12 x 12 x 3 dimensions the natural gas cargo of about 48110 m³ in volume can be stored. It is approximately equivalent to a 10-feet TEU container [1]. Weight of fully loaded cassette of standard dimensions can reach about 200 T. An advantage of such FRP pressure tanks, as compared with traditional steel ones, is their lower weight by abt. 30 % and higher resistance to corrosion and cracks. A main disadvantage of the technology in question is a very high production cost of FRP tank, greater than that of steel tank by 100%.

- **TransCanada CNG Technologies** – in such design concept natural gas is transported in long pipes of the dimensions: the length l = 12.4 ÷ 36.6 m and diameter D = 1.04 m, in a close to ambient temperature, under pressure of abt. 210 bar. The pressure tanks made of high strength steel are based on CRLP concept. Outer surface of the pipe is covered by glass fibre and resin, that contributes to a significant drop of its mass. The concept is intended to be applied to small ships/barges of cargo capacity of abt. 2.83 mln m³ of gas.
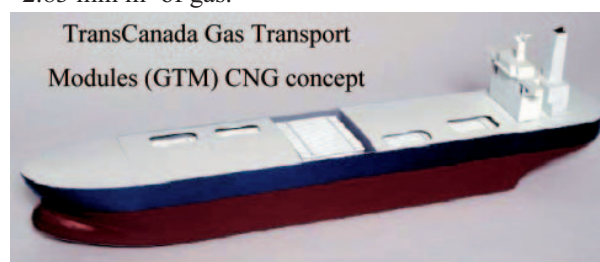
In Tab. 1 examples of the main design parameters of CNG carriers of existing concepts are presented.

CNG ships, resembling bulk carriers, can be built in large and medium shipyards as they are not so much sophisticated like LNG and LPG carriers are.

Tab. 1. Main design parameters of CNG carriers based on different transport technology concepts (acc. the author's elaboration)

Concepts of CNG carriers	Gas volume [m³]	L_{pp} [m]	B [m]	H [m]	T_{max} [m]	D_{max} [t]	DWT [t]	M_{SP} [t]	V [w]	Cylinders [units]	Propulsion power P_B [kW]
EnerSea –Votrans *)	6.226.000	191.12	34.14	20.0	8.26	42621	6431	36190	14.0	1296	22000
Knutsen OAS	20 000 compres-sed gas	260	54	29.0	13.5	-	33000	-	15.5	2672	-
EnerSea -Votrans V-800	-	267	46.9	27.6	10.4	102935	25395	77660	18.0	2184	40000
Trans Canada	2.830.000	134.0	29.0	-	9.0	-	15700	-	11	-	-
Coselle **)	9 339 000	243	38.0	28.0	10.3	-	60 000	-	15.5	108 „coselles"	-

*), **) - the ships taken to further considerations.

Tab. 2. Values of weight of the tanks and volume of gas shipped in them for two concepts of CNG ships (the author's elaboration)

CNG ship:	of EnearSea – Votrans design	of Coselle design
Characteristics of cargo tank	Modules of gas cylinders: 1 module = 24 cylinders Standard dimensions of the tank: h = 24 ÷ 36 m. D = 1.04 m wall thickness t = 0.0335 m - (assumed for calculations)	Diameter: D = 0.168 m Wall thickness: t = 0. 0055 m Length of pipe turns: l = 17702 m Total volume: V = 351 m³ Gas storing temperature: 10°C Gas storing pressure: 240 bar
Weight of steel tank/ Weight of pipe turns in one „carousel" [t]	$P_{zb} = \frac{\pi}{4}[D^2 - (D - 2t)^2] * H * \rho_S$ $P_{zb} = 19.8 \div 29.8$	$P_{zb} = 408$ Weight of „carousel": $P_{carousel} = $ abt. 40 $P_{zb} + P_{carousel} = 448$
	$\rho_s = 7.801$ [t/m³] - density of X-80 HS steel	
Volume of steel tank/ Volume of pipe turns in one „carousel" [m³]	$V_{zb} = \frac{4}{3}\pi r^3 + \pi r^2 H$ $V_{zb} = 21.0 \div 31.2$	$V_{zb} = 325$
Weight of compressed gas in cargo tank [t]	$P_{gas} = V_{zb} * \rho_{spr.\ gas}$ $\rho_{spr.\ gas} = 0.22$ [t/m³] - mean CNG density	
	$P_{gas} = 4.6 \div 6.9$	$P_{gas} = 72$
Gas weight/cylinder weight ratio	$\eta = P_{gas}/P_{zb} = 0.23$	$\eta = P_{gas}/P_{zb} = 0.18$
Weight of gas in all cargo tanks on the considered ships *),**) [t]	$P_{wg} = P_{gazu} * n_{zb}$ $P_{wg} = 4.9 * 1296 = 6350$	$P_{wg} = P_{gazu} * n_{zb}$ $P_{wg} = 72 * 108 = 7776$
Weight of all cargo tanks on the considered ships *),**) [t]	$P_{wzb} = P_{zb} * n_{zb}$ $P_{wzb} = 20.2 * 1296 = 26131$	$P_{wzb} = P_{zb} * n_{zb}$ $P_{wzb} = 408 * 108 = 44064$
Estimated compression ratio	$\frac{V_2}{V_1} = \frac{6226000}{27631} \cong \frac{230}{1}$ *)	$\frac{V_2}{V_1} = \frac{9339000}{35176} \cong \frac{270}{1}$ **)

*), **) - the main design parameters of the ships - as given in Tab. 1.
V_2 – natural gas volume (ship load-carrying capacity),
V_1 – compressed gas volume in cargo tanks (for the „Coselle" tank: equal to abt. 325.7 m³; for the gas cylinder: abt. 21.32 m³, at h = 24.4 m)

Parameters of compressed natural gas and gas cargo tanks

The greatest difficulty in CNG shipping is associated with an excessively large tank mass / shipped CNG mass ratio. As compared with LNG technology, load-carrying capacity of CNG ships is from two to three times lower. Therefore in every CNG transport technology above described attempts are undertaken to increase volume of transported gas in relation to weight of cargo tanks by improving materials used to production of the tanks (e.g. application of non-metallic composites, higher strength steel) or increasing the mass/volume ratio of gas by searching for optimum parameters in pressure-temperature relation.

To assess volume of a cargo tank and gas to be contained in it, appropriate calculations were performed; its results are presented in Tab. 2. Out of the presented design solutions of cargo tanks the two types have been selected for further analysis: the cylindrical steel tank according to the EnerSea-Votrans' concept and the steel tank in the form of thin – walled pipes according to the Coselle's concept.

As results from the preliminary calculations, despite the greater weight of the cargo tanks according to the Coselle concept its pressure and temeperature parameters of compressed gas result in the greater gas compression ratio, that makes it possible to transport the greater amount of gas.

CHARACTERISTICS OF TRANSPORT TECHNOLOGY OF GAS IN THE FORM OF HYDRATES

By using NGH (natural gas hydrate) ships natural gas in the form of hydrates can be transported in the conditions of the low temeperature T = –20 °C and atmospheric pressure.
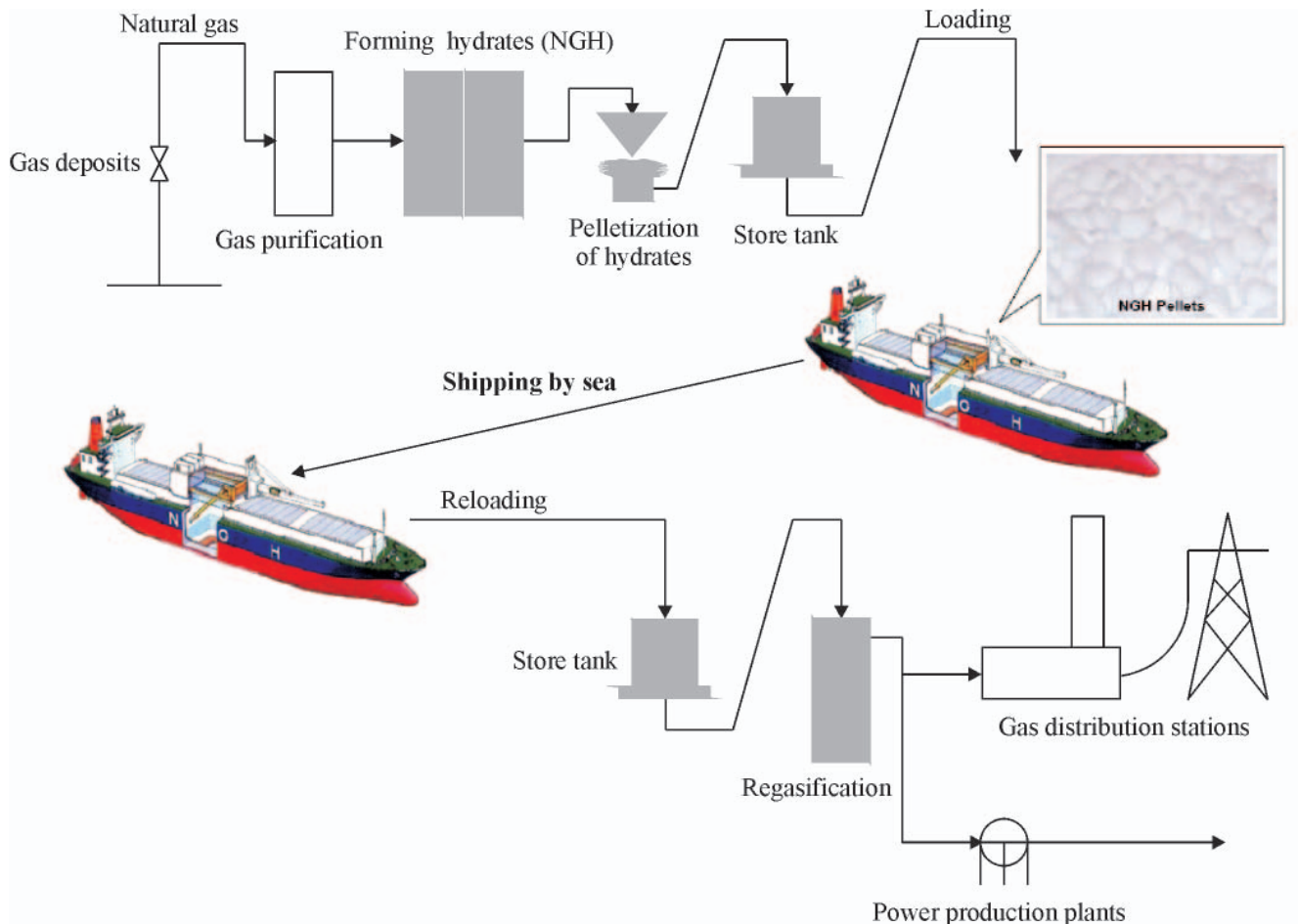
Gas hydrate is a substance consisted of frozen water particles which form cage structures (pellets) in the condition of elevated pressure and/or lowered temeperature, in which gas particles are kept.

To form hydrates, presence of water or its vapour (in equilibrium state) and hydrate building gases as well as an appropriate range of pressure and temperature is necessary.

The conditions for forming hydrates during their production and transportation are presented in Fig. 5.
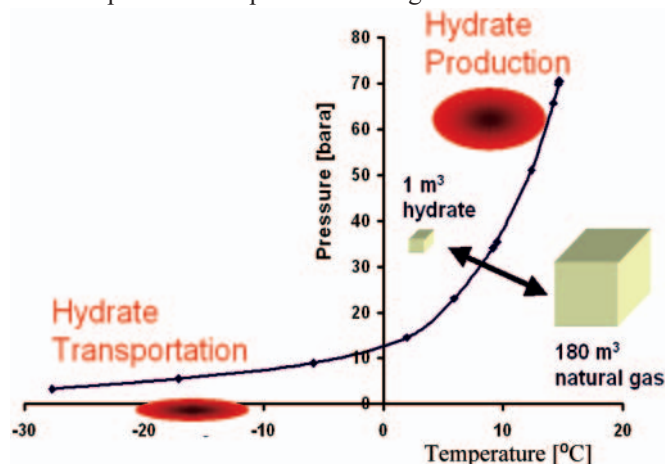

Fig. 5. Conditions for forming hydrates
during their production and transportation

Transport chain of gas in the form of hydrates

Transport of natural gas by using NGH ships can be split into the following phases, Fig. 6:

Fig. 6. NGH transport chain (the author's elaboration based on [7])

- mining
- production of NGH in the form of hydrate pulp or granulates
- preparation to transport and loading into ship
- reloading and regasification – gas recovery
- delivery to gas provider.

Design concepts of NGH carriers

As for many years the transport technology of gas in the form of hydrates by using NGH carriers has been still under study there are no built ships of such a type.

Design concepts of NGH carriers are under elaboration in a few countries, namely: Japan, Norway, USA and Great Britain. Scientific research centres operating in the countries, i.e.: *Mississippi State University* (MSU), *Mitsui Engineering & Shipbulding Co. Ltd.* (MES) or *Norwegian University of Science and Technology* (NTNU) conduct research projects on the storing and transporting of natural gas in the form of hydrates.

In 2001 the first design concept of such ship was elaborated, Fig. 7, and as results from a long-term feasibility plan, the end of the pilotage project is scheduled on the year 2009.

The NGH ship design concept resembles a traditional cargo ship in design, such as tanker or bulk carrier. The ship's hull is characterized by double side and bottom plating and subdivision into 12 holds whose tanks are insulated to prevent ice forming outside. Loading operation of the hydrate would be carried out by using the piping system leading to the tanks. During voyage the heat transferred to the cargo through tank walls would locally result in a decomposition of the hydrate into gas and ice. The so released gas could be utilized as a fuel for propelling main engine.

According to the preliminary design of NGH ship each of its 12 tanks was fitted with a mechanical self-reloading device similar to those used to reloading operations on bulk carriers. The necessity of installing such devices in every cargo tank of NGH ship contributes to a very high cost of such ship.

Transport of gas in the form of hydrates is another alternative in relation to LNG transport technology and has many advantages, a.o. such as:
- CNH is easy for storing and safe in transporting
- low transport requirements as to temperature and pressure (T = –20 ℃, at atmospheric pressure)
- low investment and operational costs – inexpensive in production and delivery
- high transported hydrate mass /tank mass ratio
- lower risk of possible explosion due to cristalline structure

- ecological – not dangerous to the environment
- possible conversion of existing ships, e.g. oil tankers
- adjustment of gas deposit resources and quality of transported gas to receiver's needs
- lower requirements as to thermal insulation of cargo tanks.

However the following is disadvantegous:
- hydrate contains abt.10% of water
- small gas volume relative to cubature
- profitable only for ships of VLCC size
- necessity of regasification.

Like in CNG transport technology, only short-range shipping up to 3000 Mm is profitable. When properties of the gas in LNG and NGH form are taken into account, size of the fleet of NGH ships should be almost four times greater as compared with that of LNG ships (under the assumption that LNG contains 600 m³ of natural gas and NGH about150 m³ of it). Therefore load-carrying capacity of NGH ships must be at least four times greater than that of LNG ships at the same transported quantity of natural gas, that detrimentally influences cost of NGH shipping by sea.

OPERATIONAL COSTS OF DIFFERENT NATURAL GAS TRANSPORT TECHNOLOGIES

The two following factors decide on which technology of gas transport by sea would be the most profitable:
- load-carrying capacity of ship
- transport range (distance).

Size of gas carriers as well as their whole fleet and especially volumetric capacity of their cargo tanks would first of all depend on:
- direction of import
- quantity of imported gas
- land infrastructure, i.e.: gas receiving terminal and gas piping network

whereas their operational costs would be dependent on:
- location of natural gas import source, i.e. choice of transport route
- fuel cost (depending a.o. on current fuel price, specific fuel consumption, ship speed etc)
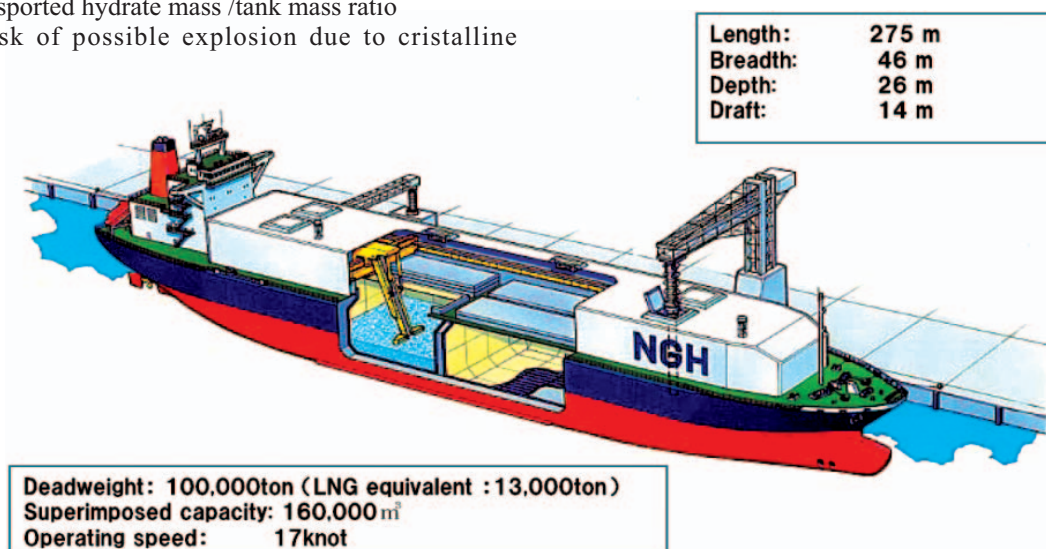
Length: 275 m
Breadth: 46 m
Depth: 26 m
Draft: 14 m

Deadweight: 100,000ton (LNG equivalent :13,000ton)
Superimposed capacity: 160,000㎥
Operating speed: 17knot

Fig. 7. NGH ship design concept [7]

- size of ship and kind of its propulsion system (it mainly concerns LNG ships)
- type and number of applied cargo tanks as well as design parameters of ship hull
- personnel cost – freight rate (long-term one)
- additional expenditures.

Moreover for calculations of the operational costs the following should be assumed:
- period of active operation of ship
- period of ship stand-by in ports during each round voyage of the ship
- number of ships angaged on a given route– depending on their load-carrying capacity and speed, as well as for LNG ships - on a gas cargo quantity evapourized during voyage.

Summing up, operational costs depend on many above mentionad factors. Knowledge of all the parameters makes it possible to perform optimization investigations to select the best variant of gas carrier together with appropriate gas transport technology, regarding gas delivery cost minimization.

Determination of exact operational cost is usually difficult and complicated because of lack of reliable data, as well as due to commercial secret policy from the side of firms competing on the market.

In Fig. 8, on the basis of literature sources and available knowledge, a comparison of component costs of LNG and CNG transport technologies is presented, and in Tab. 3 – a comparison between costs of LNG and NGH transport technologies.
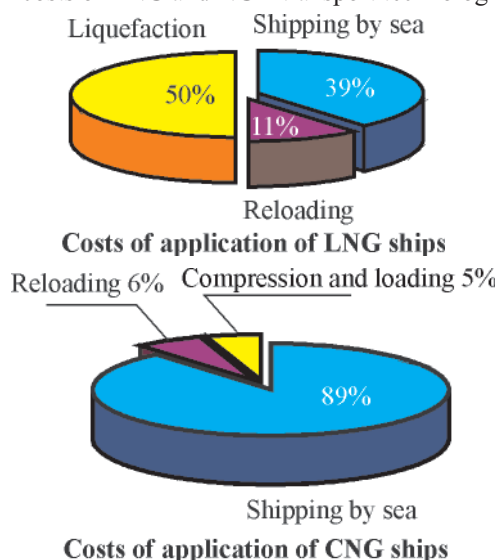

Fig. 8. *Comparison of component costs of application of CNG and LNG ships [3]*

As results from an economic analysis performed in 2002, the costs of the NHG transport chain are lower by 12% in relation to those of LNG transport chain. Shipping costs are similar, but the option of NGH transport technology is more expensive by 2% only, like the difference of their regasification costs which amounts to 1% only, Tab. 3, acc. [5].

CONCLUSIONS

– Fast growing demand on natural gas and its limited resources will cause increasing prices, therefore new, better solutions of natural gas transport technology should be searched for economical and ecological reasons. Limited possible application of piping systems to its transportation forced to an extent the development of mass transport technologies of natural gas in the liquid or compressed form.
– Long-range transport of liquified gas is (despite its complexity and high cost) the most profitable transport method, whereas CNG and NGH transport technologies are the best for transportation of medium and small amounts of gas over short distances, up to 3000 Mm. Therefore economic merits of the two transport alternatives should be taken into consideration in planning natural gas transport to Poland, especially in the case of its delivery from Norway. Expected delivery distance (from Barents Sea to Swinoujscie) equal to abt. 2600 km indicates large possible savings in investment cost, mainly for transport operation.
– As above mentioned, transport of gas in the form of hydrates is still in the research phase hence its practical application would be a more distant alternative. For the time being, it could be considered a potential, future alternative of gas delivery to Poland.
– Research on development of design and production technology of ships intended for natural gas shipping are currently carried out in the Department of Ocean Engineering and Design of Sea-going Ships, West-Pomeranian University of Technology, ZUT in the frame of the research project No. 507-09-022-9718/7, titled: „*METAN – Research on development natural gas shipping with special attention paid to the state of transported gas, optimum size of ship, type of power plant as well as logistic and technolgical problems*".

NOMENCLATURE

B	–	ship breadth [m]
D	–	outer diameter of cylinders or pipe turn [m]
D_{max}	–	maximum ship displacement [t]
DWT	–	ship deadweight [t]
h	–	height of cylindrical tanks [m]
H	–	ship hull depth [m]

Tab. 3. *Costs of transport chain based on NGH or LNG technology, acc. [5]*

Transport chain	LNG [%] mln $ ([%])	NGH [%] mln $ ([%])	Difference mln $ ([%])
Production	1144 (55%)	992 (54%)	152 (13%)
Shipping by sea with the use of ships	660 (32%)	628 (34%)	32 (5%)
Regasification	285 (13%)	218 (12%)	57 (24%)
Total	2089 (100%)	1838 (100%)	**251 (12%)**

Note: Calculations were perfromed under the assumption that the yearly amount of gas transported in the delivery range of abt. 6000 km is equal to 11320000 m³.

l   − length of turn of pipes acc. to Coselle technology [m]
L_{pp} − ship length b.p. [m]
M_{SP} − light ship mass [t]
n_{zb} − number fo cargo cylinders / number of carousels with pipe turns [pieces]
r   − cylindrical tank diameter [m]
t   − cylindrical tank wall thickness [m]
T_{max} − maximum ship draught [m]
V   − ship speed [m/s]
$V_{Ł}$ − load-carrying capacity of ship [m^3]
V_1 − volume of compressed gas in cargo tanks [m^3]
V_2 − volume of natural gas [m^3]
$\rho_{spr.gas}$ − density of compressed natural gas [t/m^3]

BIBLIOGRAPHY

1. Abdi M. A.: *Design and Operations of Natural Gas Handling Facilities*, Faculty of Engineering and Applied Science, Memorial University of Newfoundland
2. Chairperson Ch. M. R.: *Liquefied natural gas*, Report of Programme Committee D - TRIENNIUM 2003 ÷ 2006, Algeria, June 2006
3. Deshpande A., Michael J. Economides: *CNG: An Alternative Transport for Natural Gas Instead of LNG,* University of Houston
4. Foss M. M.: *LNG safety and security CEE*, Energy Economics Research, The University of Texas, 2003
5. Gudmundsson J. S.: *Natural gas hydrate problem solver and resource for production and transport*, Gas Hydrates, Tekna, Bergen, October 21-22, 2008
6. Grove T.: The other gas trades: LPG nad CNG, ABS, Intertanko –Houston, 26 march 2007
7. Kanda H.: *Economic study on natural gas transportation with natural gas hydrate (NGH) pellets,* 23rd World Gas Conference, Amsterdam 2006
8. Spano P., Alimonti C.: *CNG Technology*. Society of Petroleum Engineers, Technical Bulletin, March 1/2006,
9. Trzop S: *Bull market for new technologies of natural gas transport and storage* (in Polish). Modern gas industry (Nowoczesne Gazownictwo), 3, (X), 2005
10. *The World Fleet of LNG Carriers*, 8 November 2008.

CONTACT WITH THE AUTHOR

Monika Bortnowska, Ph. D.
Faculty of Marine Technology,
Szczecin University of Technology
Al. Piastów 41
71-065 Szczecin, POLAND
e-mail : mwojciechowska@ps.pl
tel.: (091) 449 47 20

The Ship Handling Research and Training Centre at Ilawa is owned by the Foundation for Safety of Navigation and Environment Protection, which is a joint venture between the Gdynia Maritime University, the Gdansk University of Technology and the City of Ilawa.

Two main fields of activity of the Foundation are:

⮞ Training on ship handling. Since 1980 more than 2500 ship masters and pilots from 35 countries were trained at Iława Centre. The Foundation for Safety of Navigation and Environment Protection, being non-profit organisation is reinvesting all spare funds in new facilities and each year to the existing facilities new models and new training areas were added. Existing training models each year are also modernised, that's why at present the Centre represents a modern facility perfectly capable to perform training on ship handling of shipmasters, pilots and tug masters.

⮞ Research on ship's manoeuvrability. Many experimental and theoretical research programmes covering different problems of manoeuvrability (including human effect, harbour and waterway design) are successfully realised at the Centre.

The Foundation possesses ISO 9001 quality certificate.

Why training on ship handling?

The safe handling of ships depends on many factors - on ship's manoeuvring characteristics, human factor (operator experience and skill, his behaviour in stressed situation, etc.), actual environmental conditions, and degree of water area restriction.

Results of analysis of CRG (collisions, rammings and groundings) casualties show that in one third of all the human error is involved, and the same amount of CRG casualties is attributed to the poor controllability of ships. Training on ship handling is largely recommended by IMO as one of the most effective method for improving the safety at sea. The goal of the above training is to gain theoretical and practical knowledge on ship handling in a wide number of different situations met in practice at sea.

For further information please contact:
The Foundation for Safety of Navigation and Environment Protection

Head office:
36, Chrzanowskiego Street
80-278 GDAŃSK, POLAND
tel./fax: +48 (0) 58 341 59 19

Ship Handling Centre:
14-200 IŁAWA-KAMIONKA, POLAND
tel./fax: +48 (0) 89 648 74 90
e-mail: office@ilawashiphandling.com.pl
e-mail: office@portilawa.com

GDANSK UNIVERSITY OF TECHNOLOGY

is the oldest and largest scientific and technological academic institution in the Pomeranian region. The history of Gdansk University of Technology is marked by two basic dates, namely: October 6, 1904 and May 24, 1945.

The first date is connected with the beginning of the technical education at academic level in Gdansk. The second date is connected with establishing of Gdansk University of Technology, Polish state academic university. Gdansk University of Technology employ 2,500 staff, 1,200 whom are academics. The number of students approximates 20,000, most of them studying full-time. Their career choices vary from Architecture to Business and Management, from Mathematics and Computer Science to Biotechnology and Environmental Engineering, from Applied Chemistry to Geodesics and Transport, from Ocean Engineering to Mechanical Engineering and Ship Technology, from Civil Engineering to Telecommunication, Electrical and Control Engineering. Their life goals, however, are much the same - to meet the challenge of the changing world. The educational opportunities offered by our faculties are much wider than those of other Polish Technical universities, and the scientific research areas include all of 21st Century technology. We are one of the best schools in Poland and one of the best known schools in Europe – one that educates specialists excelling in the programming technology and computer methods used in solving complicated scientific, engineering, organizational and economic problems.

THE FACULTY OF OCEAN ENGINEERING AND SHIP TECHNOLOGY

The Faculty of Ocean Engineering and Ship Technology (FOEST) as the only faculty in Poland since the beginning of 1945 has continuously been educating engineers and doctors in the field of Naval Architecture and Marine Technology.

The educational and training activities of FOEST are supported by cooperation with Polish and foreign universities, membership in different international organizations and associations, as well as participation in scientific conferences and symposia. Hosting young scientists and students from different countries is also a usual practice in FOEST.

The activities of Faculty departments are related to: mechanics and strength of structures, hydromechanics, manufacturing, materials and system quality, power plants, equipment and systems of automatic control, mostly in shipbuilding, marine engineering and energetic systems.

FOEST is a member of such organizations like WEGEMT; The Association of Polish Maritime Industries and the co-operation between Nordic Maritime Universities and Det Norske Veritas. The intensive teaching is complemented and supported by extensive research activities, the core of which is performed in close collaboration between FOEST staff and industry. We take great care to ensure that the applied research meet both the long term and short term needs of Polish maritime industry. FOEST collaborates with almost all Polish shipyards. Close links are maintained with other research organizations and research institutions supporting the Polish maritime industry, such as Ship Design and Research Centre and Polish Register of Shipping, where several members of the Faculty are also members of the Technical Board.

The Faculty of Ocean Engineering and Ship Technology is a unique academic structure, which possesses numerous highly qualified and experienced staff in all above mentioned specific research areas. Moreover, the staff is used to effective co-operation and exchange of ideas between specialists of different detailed areas. This enables a more integrated and comprehensive treatment of research and practical problems encountered in such a complicated field of activity as naval architecture, shipbuilding and marine engineering.

The staff of the Faculty has strong international links worldwide, being members or cooperating with international organizations like International Maritime Organization IMO, International Towing Tank Conference ITTC, International Ship and Offshore Structures Congress ISSC, International Conference on Practical Design of Ship and other floating Structures PRADS just to name a few.

GDANSK UNIVERSITY OF TECHNOLOGY
Faculty of Ocean Engineering and Ship Technology
11/12 Narutowicza Street, 80-952 Gdansk, Poland
Tel (+48) 58 347 1548 ; Fax (+48) 58 341 4712
e-mail: sekoce@pg.gda.pl

www.oce.pg.gda.pl